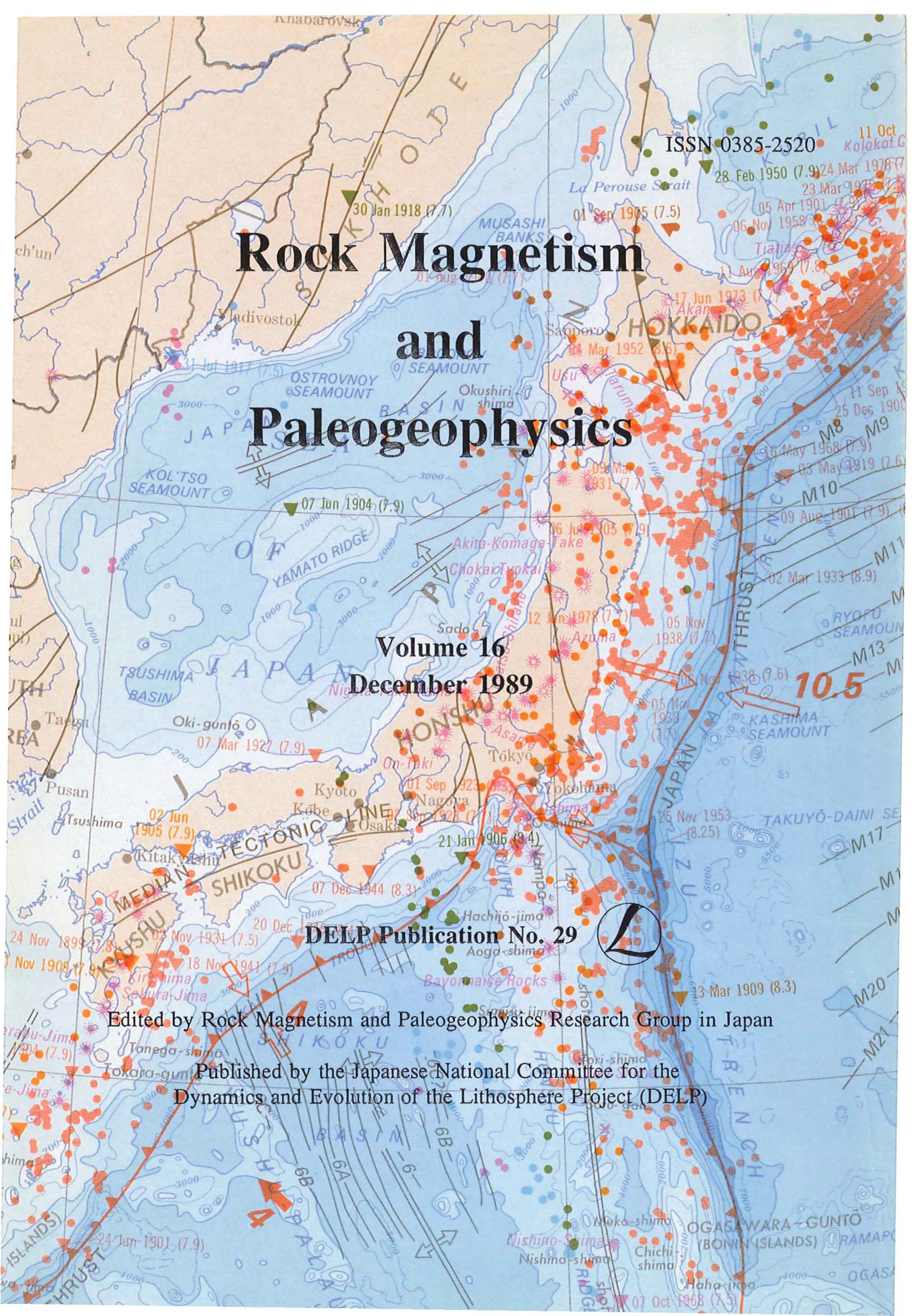

ISSN 0385-2520

Rock Magnetism and Paleogeophysics

Volume 16
December 1989

DELP Publication No. 29

Edited by Rock Magnetism and Paleogeophysics Research Group in Japan

Published by the Japanese National Committee for the Dynamics and Evolution of the Lithosphere Project (DELP)

ISSN 0385-2520

Rock Magnetism
and
Paleogeophysics

Volume 16
December 1989

DELP Publication No. 29

Edited by Rock Magnetism and Paleogeophysics Research Group in Japan

Published by the Japanese National Committee for the
Dynamics and Evolution of the Lithosphere Project (DELP)

まえがき

本書は岩石磁気学・古地磁気学研究グループの1989年度の年次研究報告書であり,「国際リソスフェア探査開発計画 (Dynamics and Evolution of the Lithosphere Project, DELP)」の成果報告 (DELP Publication) 第29号として刊行されるものである. DELP計画は本年度をもって5年間のプログラムが終了する. 我々の研究グループは課題5「日本列島の構造発達」に参加し, 日本列島及びその周辺のテクトニックな発展の歴史を解明しようと努力を続けてきた. これらやその他の研究のいくつかが本研究報告に収められている.

岩石磁気学・古地磁気学研究グループでは, 以前から Annual Report として英文の報文集を刊行してきた (Annual Progress Report of the Rock Magnetism (Paleogeophysics) Research Group in Japan, 1963, 1964, 1965, 1969; Rock Magnetism and Paleogeophysics, 1973-present). 本書は Annual Report の第16巻である. これらの報文集は図書館などからの寄贈要請も多く, 諸外国の関連分野の研究者によってかなり広く利用されている. このような経過からこの報文集もすべて英文によって編集された. 日本国内の方々には幾分不自由をおかけすることになると思うが, 以上の事情によることをご理解いただきたい. なお, 本書はあくまでも extended abstract 集であり, ここに収録された研究はいずれ正式の論文として発表されることになる. 投稿中のものや投稿予定のはっきりしているものについては, 各報文の最後にそのことが示されているので, 引用される場合にはできるだけ正式の論文を参照していただくようお願いしたい.

DELP計画の終了に伴い, 私自身も年次報告書の編集はこれを最後にすることにした. この Annual Report を始めたころには, 国内で立派な研究がなされていてもそれがなかなか国際的に認知されないという問題があり, 本書は国際的な広報に相当な役目を果たしたと思う. しかし最近では, 我々のグループの研究成果はどんどん国際誌に発表されるようになり, この方面での必要性は以前にくらべてずっと少なくなっている. しかし, 一方で20年近くをかけて国際的に定着した Annual Report をここで捨ててしまうのは惜しいという考えもある. 本書の刊行を継続するかどうかは, 1990年内に研究グループ内で検討の上で決定されよう. なお, 編集者を退任するに当たり, これまでの全巻についての索引を作成し本書に収めた.

本書の刊行については, 文部省国際共同研究等経費「リソスフェア探査開発計画 (DELP)」(代表者：秋本俊一) より援助を受けた. ここに記して感謝の意を表する.

1989年12月

河野　長
岩石磁気学・古地磁気学研究グループ

PREFACE

This volume is the annual progress report of the Rock Magnetism and Paleogeophysics Research Group in Japan for the year 1989. We have published annual reports with a title *Annual Progress Report of the Rock Magnetism (Paleogeophysics) Research Groups in Japan* in 1963, 1964, 1965, and 1967. Since 1973, the title changed to *Rock Magnetism and Paleogeophysics* and the reports were published annually (except 1976).

As the previous reports were so, this volume contains a collection of summaries, extended abstracts or brief notes of the research works carried out in our group this year. Many of the reports contain materials which may undergo a significant change or may be revised as the research activity continues. In this respect, readers are warned to regard them as tentative, and are also requested to refer from a complete paper if such is published as a final result. (Names of journals appear at the end of individual articles if they are in press, submitted, or in preparation for submission to some scientific journals).

This is the last year of the DELP Program and also the last year for me to serve as the editor of this annual report. When I began in 1973, I did not think that I will be continuing to do so for more than five years. However, the volumes served as good media to inform the foreign colleagues what we are up to in Japan. We have had large number of quotations from outside Japan. At present, there are divided opinions in our group regarding the future of the annual report. As many of the works nowadays are published in international journals without much delay, some think that we do not need such media any more. On the other hand, there are also opinions that the information channel cultivated in the last 16 years became too valuable to abandon so lightly. The future, therefore, depends on the decision of our group to be made within 1990, and also on the responses received from the colleagues overseas who are receiving them. I would like to take this opportunity to thank the authors for contributing the abstracts for the past volumes, and to the readers in general who encouraged us for this publication. As a token of thanks from the outgoing editor to the authors and readers of *Rock Magnetism and Paleogeophysics*, I have prepared a permuted index for Volumes 1 to 16 inclusive.

This volume is published with a financial aid from Ministry of Education, Science and Culture for the Dynamics and Evolution of the Lithosphere Project (DELP). It is Publication No. 29 of the Japanese DELP Program.

Tokyo
December 1989

Masaru Kono
Editor

Rock Magnetism and Paleogeophysics
Research Group in Japan

Rock Magnetism and Paleogeophysics, Volume 16

Table of Contents

1990．3．28

Annual Report 執筆者各位

Rock Magnetism and Paleogeophysics 第16巻が出来上がりましたのでお届けいたします．まえがきにも書きましたように，私はＤＥＬＰ計画の終了に伴いこの Annual Report の 編集からも手を引かせていただくことにしました．この機会にこれまでの全巻の索引をつくり，著者全員に第16巻をお送りしようと考えたのですが，その数は何と250人以上もあって部数が足りません．やむを得ず，第16巻の著者及び第１巻以来通算３編以上の報文のある方々にしぼらせていただきました．勿論まだ残部がありますので，更に必要な方はお申し出下さい．

私自身は編集をやめますが，この Annual Report 自体が存続するかどうかは，岩石磁気・古地磁気グループでの検討をへて今年中に決定される予定です．

長い間の御協力有り難うございました．

東京工業大学理学部

河野　長

ABRUPT JUMP IN THE MAGNETIC TOTAL FORCE AT THE BLAST BY GUN POWDER -INTERPRETATION BY REMANENT MAGNETIZATION

Hideo SAKAI[1], Hiroyuki ODA[1], Takesi NAKAYAMA[2] and Hikaru DOI[2]

1 Department of Earth Sciences, Faculty of Science, Toyama University, Gofuku 3190, Toyama, 930, Japan
2 Kamitakara Geophysical Observatory, Disaster Prevention Research Institute, Kyoto University, Kamitakara, Gifu, 506-13, Japan

Piezo remanent magnetization (PRM) may exist commonly at the stress concentrated region. Nagata and Kinoshita (1965) showed when the piezo remanence of the order of 10^{-4} bar^{-1} is induced in the sequence underground, the magnetic total force at the surface may change in the magnitude of 1 to 10 nT. When the shock is imposed to the rocks in a quite short period, the remanent magnetization similar to PRM may be acquired. Nagata (1971) named it as the SRM (shock remanent magnetization).

In 1986, October 22, the cooperative research with the artificial earthquake was made at the Ohtaki village in Nagano Prefecture (Figure 1). The main purpose of the project (The joint group of seismological research in western Nagano Prefecture, 1988) was to investigate the crustal structure around this area in detail. At this project, we made the observatory experiments of the magnetic total force in order to identify what kind of change in the magnetic force will be induced by the artificial earthquake. The results may be useful for the discussion of the stress-induced magnetization.

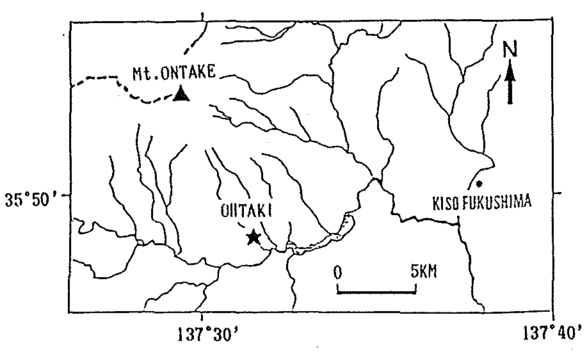

Fig. 1. Map of the area where the artificial earthquake experiment was made. The star mark shows the blast point.

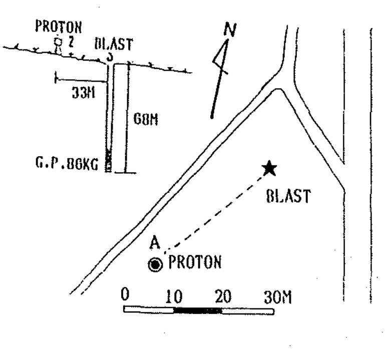

Fig. 2. Map around the blast point (star mark). Double circle represents the position of the proton sensor.

The artificial earthquake was produced by the blast of 86 Kg gun powder placed at the depth of 68 m below ground (point A of Figure 2). The magnetic total force was measured by a proton precession magnetometer (Barringer model GM 122) which was modified to record the data on the printer. We set it 33 m from the blast point. The sensor of the magnetometer was positioned on the aluminum pole of 2 m in height. We supported the aluminum pole firmly so as to restrain the movement of the sensor at the blast. The magnetic total force was measured from twenty minutes before the blast time until three hours after. The data were sampled at 6 second intervals. The apparatus was run with battery power.

Figure 3 shows the change of the magnetic total force around the blast time. The jump of the magnetic force up to 3 nT was observed at the blast. The general trend in the fluctuation of magnetic force before and after the blast was concordant with that of the Amo stationary observatory 50 Km north-westward from Ohtaki district. The proton sensor was fixed rigorously and the magnetic gradient was less than 1 nT within a 15 cm radius from the sensor. Therefore, we could not consider that the movement of the sensor at the blast have caused the observed change in the magnetic force. We concluded that the jump of the magnetic force was induced by the change of magnetic properties underground at the blast.

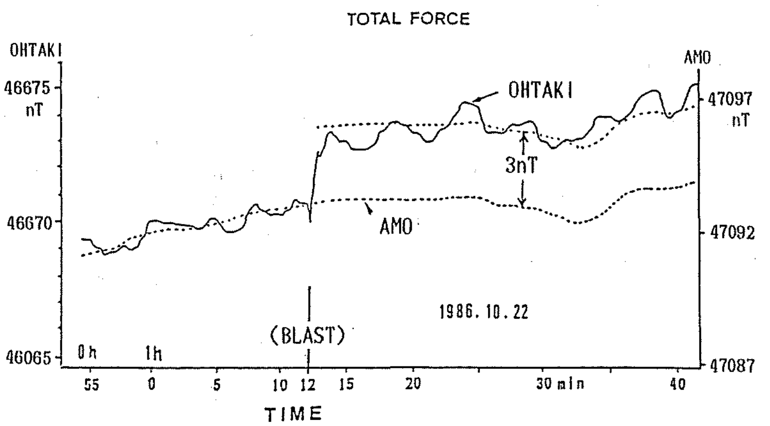

Fig. 3. Variation of the total magnetic force observed around the blast time (1:12 am). Dotted line shows the data recorded at Amo station.

The increment in the magnetic force at the blast did not decrease during the period of 30 minutes after the shot time (Figure 3). According to the succeeding observation, the increment did not decrease after 1 hour from the blast time.

One of the possible cause for this irreversible change in the magnetic force is the effect of iron casing around the blast point. The iron casing of the diameter of 120 mm was placed at the depth from 1.2 to 400 m in order to set the gun powder. Figure 4 shows the contours map of the magnetic force around the blast point observed 1 month after the blast time. It suggests that the iron casing has the effective role for the distribution of the magnetic force around the blast point. At the blast, the casing may have been deformed and/or heated to the high temperatures and the susceptibility (μ) of the iron casing may have changed. This change may have distorted the distribution of the magnetic force and caused the observed increase of the magnetic force.

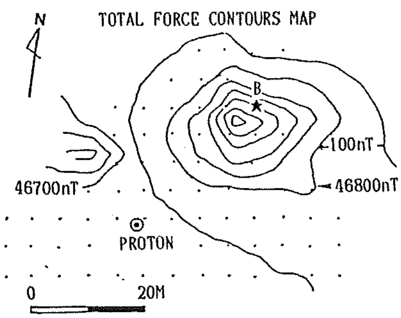

Fig. 4. Contours map of the magnetic force around the blast point observed at the time 1 month after the blast.

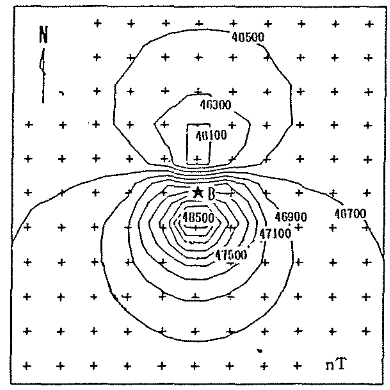

Fig. 5 Calculated distribution of the total magnetic force when the iron casing was placed vertically at the blast point. We assumed the casing (μ=200) of the diameter 120 mm was set at the depth from 1.3 to 400m.

Figure 5 shows the calculated distribution of the magnetic force when the iron casing (μ=200) is placed at the blast point. The distribution of the magnetic force shows the minimum at the north of blast point and maximum at the south. The observed distribution in Figure 4 deflected from the north-south trend in the calculated distribution. It indicates that the magnetization underground around this region also contribute to the distribution of magentic force. The sequence around the blast region consists of andesites and sedimentary rocks. NRMs of the drilled core (sedimentary rocks) at the blast point were measured. They showed the reversed polarity with the intensity of 10^{-3} mA^2 / kg. When the reversed NRM was decreased or broken according to the acqusition of PRM and/or SRM at the blast, the magnetic force at the surface may increase. That is, the induced NRM change in the underground sequence is also resposible for the observed irreversible change in the magnetic force. The further study of the magnetoelectric effect at the artificial earthquake is necessary to know the detrails.

REFERENCES

Nagata, T. (1971) Pure Appl. Geophys., 89, 159.
Nagata, T. and H. Kinoshita (1965) J. Geomag. Geoelectr., 17, 121.
The Joint group of seismological research in western Nagano Prefecture (1988) The 1986 Joint Seismological Research in western Nagano Prefecture -Technical report-, 340.

STUDY OF CRUSTAL STRUCTURE IN THE SOUTH BOSO PENINSULA INFERRED FROM MAGNETIC ANOMALIES

Toshiya FUJIWARA[1], Sumio OGURA[1], Hajimu KINOSHITA[1]
and Rie MORIJIRI[2]

1.Chiba University, Yayoi-cho, Chiba 260
2.Geological Survey of Japan, Tsukuba, Ibaraki 305

We have been conducting land magnetic survey using proton preccession magnetometer in the south Boso Peninsula from 1985 to 1989. In addition to these data, one track magnetic data was acquired in the Tokyo Bay east side of Boso Peninsula by DELP 1987 cruise (Isezaki et al.,1989). So we could construct a detailed magnetic anomaly map in this area (Fig.1, Fig.2).

Data is reduced by IGRF 1985 model referring Kano-zan Geodetic Station, Geographical Institute (about 20km north of surveyed area) to subtract Sq variations. Reduced data is refined by applying upward continuation tecnique to a level of 1500ft(about 460m). H in Fig.3 mark means relative high anomaly and L mark is low anomaly.

Magnetic basement map (Fig.5) is obtained by a two-layer model inversion using pseudo-gravity and reduction to the pole (Okuma et al.,1989) (Fig.4). Magnetization is assumed to be uniform with magnetization intensity of 2 A/m and parallel to the ambient geomagnetic field vector.

Map of Fig.5 is probably explained by steeply decline basement from south to north and vertically magnetized bodies. Fig.5 shows that basement curves down to 2km deep and its horizodnital N-S spread is about 5km. The basement seems to be shallower in the northern part of surveyed area. This matter as mentioned above is maybe more understandable rather fig.4 map than fig.5 map because Fig.5's calculation mesh is still rough. Fig.5's map is obtained basically by downward continuation of fig.4. Location of steep change of basement give a dense contour lines. Low magnetic anomalies is caused by declining of basement and high magnetic anomaly reveals by vertically magnetized bodies.

Location of vertically magnetized bodies match to area of outcrop of Mineoka Ophiolites belt. (They are marked by open triangle in Fig.1) Tectonic setting of the Mineoka Ophiolites have been studied by several authors. Ogawa and Taniguchi (1987) discussed emplacement process of these rocks associated with the obduction of plate. Previous study of simulation which explains gravity and magnetic anomaly in this area is given in a form of a slab dipping toward south by Tonouchi (1981). Our present result does not seem to support this idea positively.

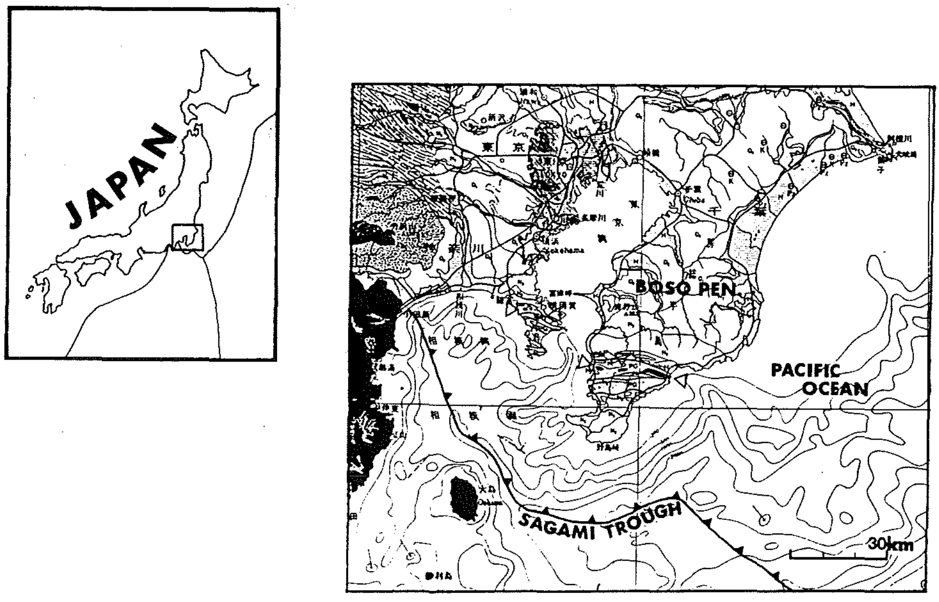

Fig.1 Schematic map of surveyed area.

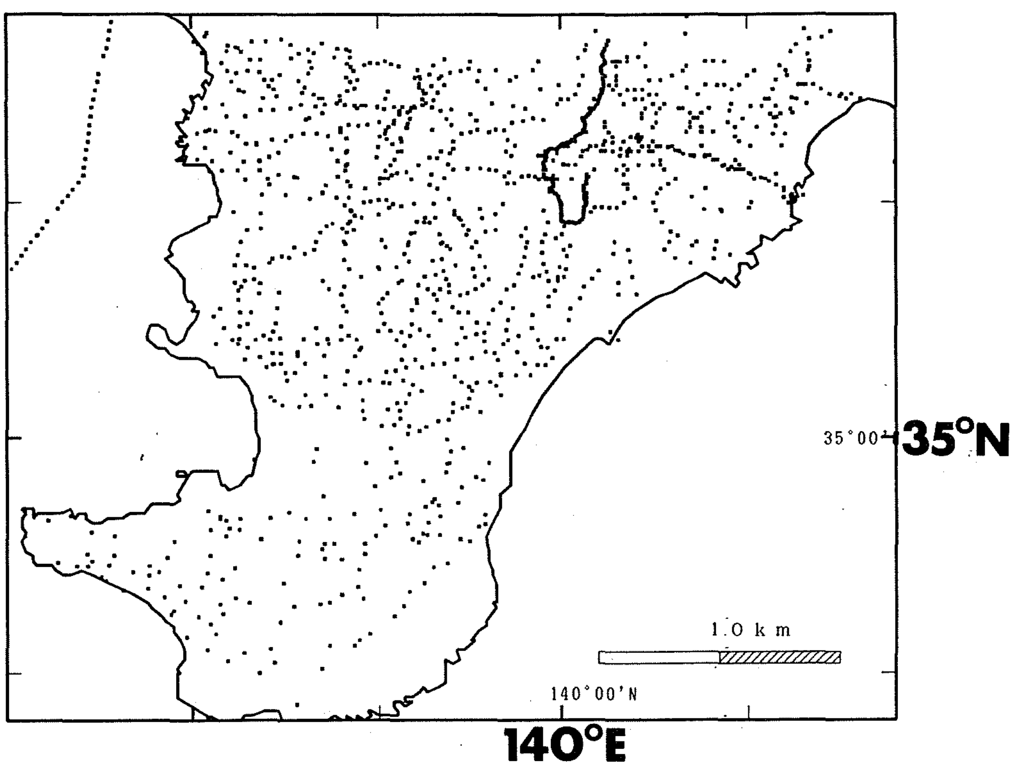

Fig.2 Surveyed area with data points.

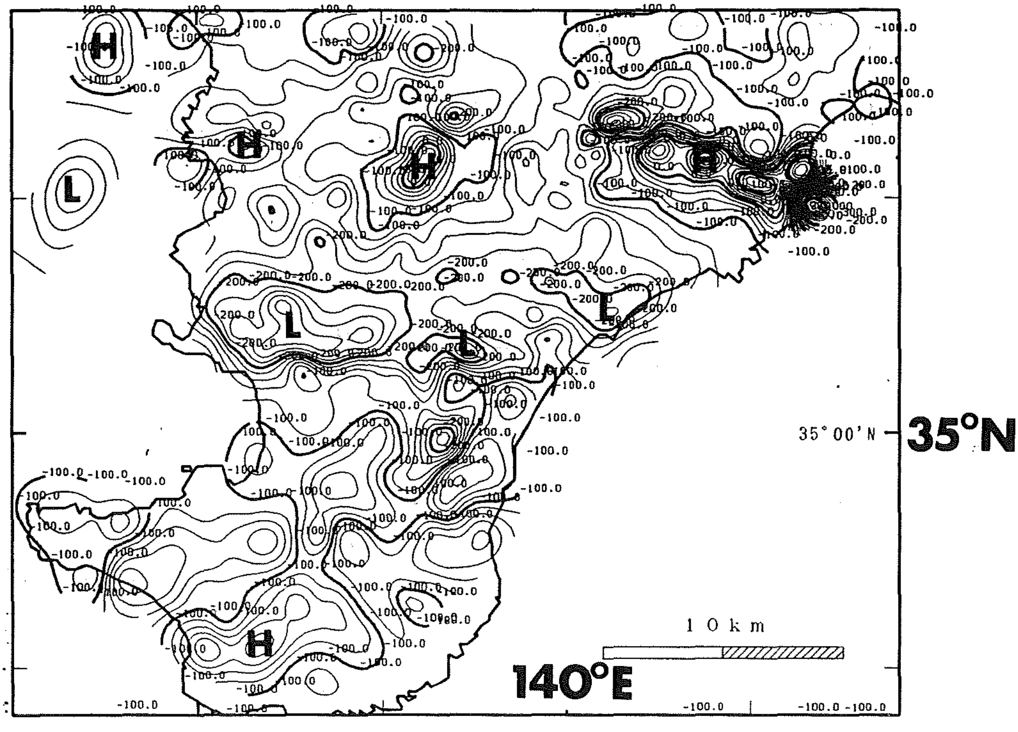

Fig.3 Magnetic anomaly map, contour interval is 20 nT.

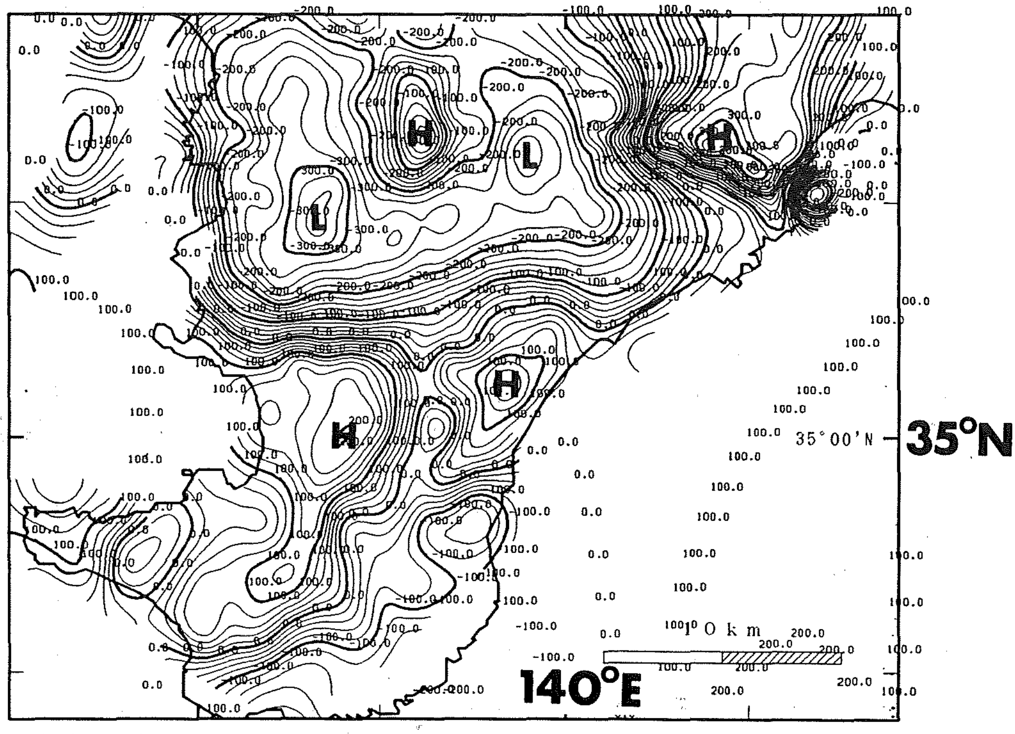

Fig.4 Pseudo-gravity map, contour interval is 20*10^6 nT*m. When magnetic anomaly transform to pseudo-gravity anomaly, top of magnetized body correspond to point of anomaly's peak.

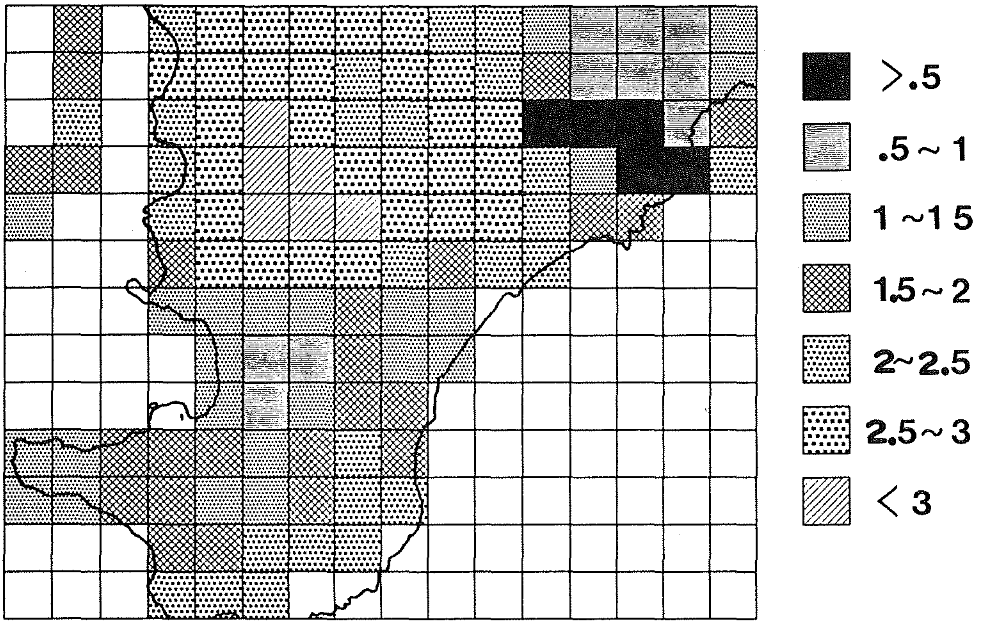

Fig.5 Magnetic basement map inferred from Fig.4, unit is depth below surface in km.

References

Isezaki et al. (1989) Bull. Earthquake Res. Inst., Univ. Tokyo., 64, 179-222

Kinoshita,H et al. (1987) Rock Magnetism and Paleogeophysics., 14, 97

Ogawa,Y and H.Taniguchi (1987) Science Reports Department of Geology Kyushu Univ.(in Japanese with English abst.), 15, 1-23

Okuma,S et al. (1989) Butsuri-tansa.(in Japanese with English abst.), 42, 82-96

Tonouchi,S (1981) Ph.D Thesis, Univ Tokyo.

COMPUTER ALGEGRA FOR AUTOMATICALLY SOLVING KINEMATIC DYNAMO PROBLEMS

Masaru KONO
Department of Applied Physics, Tokyo Institute of Technology
Ookayama 2-12-1, Meguro-ku, Tokyo 152, Japan

1. Introduction

Since the classical paper of Bullard and Gellman (1954), a number of solutions was found for kinematic dynamo problems in which velocity field was assumed to be composed of a small number of toroidal and poloidal low-order spherical harmonics. They include T_1 and S_2^{2c} combination of Bullard and Gellman (1954), T_1, S_2^{2c} and S_2^{2s} of Lilley (1970), T_n and S_n of Gubbins (1973), S_2^{2c} and T_2^{2c} of Pekeris et al. (1973), and T_1, S_2, S_2^{2c} and T_3^{2s} of Kumar and Roberts (1975). After the middle of the 1970's, the focus of interest of dynamo theorists seems to have shifted to turbulent dynamos and hydromagnetic or dynamic treatments, but the importance of the Bullard-Gellman approach does not decrease even today. Kinematic dynamos are useful in understanding the interaction between the velocity and magnetic fields. The expansion into poloidal and toroidal modes is applicable to any solenoidal vector fields, and is useful not only in kinematic problems but also in dynamic or hydromagnetic problems. Behaviors of kinematic dynamos have not been satisfactorily explored yet, as shown by the small number of cases for which existence of solutions was searched. Moreover, the Bullard-Gellman scheme can be extended to solve the time dependent behavior of the dynamo, so that it can form a basis for more general treatments. Therefore, it is very useful if this analysis is carried out for more extensive combination of velocity fields.

The reason why the programming of dynamo problem was so difficult in the previous studies is that the the equations obtained from the induction equation using toroidal-poloidal expansion (Bullard-Gellman type equations) are quite different depending on the velocity fields chosen. If a new combination of velocity modes is considered, the program should be developed almost from the scratch because the equations contain terms completely different from the ones for the previous choice of velocity fields. It was the essential part of the previous studies of kinematic dynamos to derive the correct equations for the particular velocity field. The program developed in this study performs this procedure automatically, and the possibility of program error was thus eliminated. The method of calculation is essentially that given by Bullard and Gellman (1954) themselves, except that the present program handles general functional form rather than numbers appropriate for each specific case.

With this approach, kinematic dynamo problems can be handled with the same program and with the same procedures for different combinations of velocity harmonics. The velocity field for a kinematic dynamo problem can be characterized by the modes such as T_1 and S_2^{2c}, and the shape of the radial function each mode takes. For the present program, the only parameters needed besides the ones specifying the velocity field are the field we are interested in (usually the dipole term, S_1), the maximum degree to which the magnetic field is expanded, and the number of division of radial distance when the differential equations are approximated by the difference form. No change is necessary when different velocity harmonics are employed, or when the calculation is carried out to a different degree or using a different division number.

2. Method of Analysis

The procedure developed below follows very closely the scheme given by Bullard and Gellman (1954). We shall only briefly outline the mathematical treatment as is necessary for understanding the computer program developed later. The normalized form of the induction equation

$$\frac{\partial \mathbf{B}}{\partial t}=R_m \mathrm{curl}(\mathbf{v}\times\mathbf{B})+\nabla^2\mathbf{B} \tag{1}$$

describes the behavior of the magnetic field **B** in the presence of a velocity field **v**. In this equation, R_m is the magnetic Reynolds number characterizing the relative importance of the induction term (curl(**v**×**B**)) against the diffusion term ($\nabla^2\mathbf{B}$). Since both the magnetic field and the velocity field satisfies the divergence-free condition, they can be expressed as sums of toroidal and poloidal vectors, which can then be expanded using spherical harmonics (cf., Chandrasekhar, 1961). For example, the magnetic field can be expressed as

$$\mathbf{B}=\sum_\beta(\mathbf{T}_\beta+\mathbf{S}_\beta)=\sum_\beta\left\{\mathrm{curl}[T_\beta(r)Y_\beta(\theta,\phi)\frac{\mathbf{r}}{r}]+\mathrm{curl}^2[S_\beta(r)Y_\beta(\theta,\phi)\frac{\mathbf{r}}{r}]\right\} \tag{2}$$

where (r, θ, ϕ) are spherical coordinates, $\mathbf{T}_\beta$ and $\mathbf{S}_\beta$ are the toroidal and poloidal vectors of degree l and order m, and $T_\beta(r)$ and $S_\beta(r)$ are their defining scalar functions. (Following Bullard and Gellman (1954), Greek letters such as β represents, collectively, degree l, order m, and either sin or cos of ϕ-dependence of a spherical harmonic function if it appears as a suffix, and simply the degree l if used by itself.) $Y_\beta(\theta,\phi)$ are spherical harmonic functions of unnormalized form. Because of the solenoidal nature, the velocity field can also be expanded similar to (2). In this paper, the suffix α is exclusively used to specify the velocity field, to make the distinction from magnetic field harmonics, which are represented by either β or γ. A notation U_α, U_β, etc. will be employed if either toroidal or poloidal fields is implied. Inserting the toroidal-poloidal expansion into the induction equation (1), and then we integrate the equation over the surface of a sphere of radius r after multiplying by a toroidal (poloidal) function $\mathbf{T}'_\gamma$ ($\mathbf{S}'_\gamma$) which has the same shape as (2) except that the radial function is unity for every value of r. Because of the orthogonality of toroidal and poloidal fields of different degree and order, the results are simplified as

$$r^2\frac{\partial T_\gamma}{\partial t}-r^2\frac{\partial^2 T_\gamma}{\partial r^2}+\gamma(\gamma+1)T_\gamma=-R_m\sum_\alpha\sum_\beta[(T_\alpha T_\beta T_\gamma)+(T_\alpha S_\beta T_\gamma)+(S_\alpha T_\beta T_\gamma)+(S_\alpha S_\beta T_\gamma)] \tag{3}$$

$$r^2\frac{\partial S_\gamma}{\partial t}-r^2\frac{\partial^2 S_\gamma}{\partial r^2}+\gamma(\gamma+1)S_\gamma=-R_m\sum_\alpha\sum_\beta[(T_\alpha S_\beta S_\gamma)+(S_\alpha T_\beta S_\gamma)+(S_\alpha S_\beta S_\gamma)] \tag{4}$$

In these equations, $(U_\alpha U_\beta U_\gamma)$ on the right hand side are the interaction terms representing generation of the magnetic field U_γ by the action of the velocity U_α on the magnetic field U_β.

$$(U_\alpha U_\beta T_\gamma)=-\frac{K_\gamma}{N_\gamma}\iint \mathbf{U}_\gamma'\mathrm{curl}(\mathbf{U}_\alpha\times\mathbf{U}_\beta)\sin\theta d\theta d\phi \tag{5}$$

where K_γ is r^4 or $r^6/\gamma(\gamma+1)$, when $\mathbf{U}_\gamma'$ is $\mathbf{T}_\gamma'$ or $\mathbf{S}_\gamma'$, respectively, and N_γ is the normalizing factore for the spherical harmonic. Equations (3) and (4) determine the behavior of the various modes T_γ and S_γ.

Two different approaches are possible for solving these equations. One is to seek for a steady state solution by eliminating the time derivatives and form an eigenvalue problem for R_m, which was the method employed by Bullard and Gellman (1954). Another is to assume a solution which depends on time as e^{pt}. In this case, $\partial/\partial t$ in (3) and (4) is replaced by p, and we obtain an eigenvalue problem for p, with R_m appearing as a parameter.

3. Programming

The following shows how to implement the above procedure in a computer program. For the programming language, C was used in the first half of the program where algebraic analysis of the induction equation is carried out, and Fortran was employed in the latter half of the program where actual numerical calculations are carried out. This choice was made because C is well suited to carry out logical operations using character variables, while numerical calculations can best be done using Fortran subroutines in mathematical libraries available at most computer centers.

Identification of the Interaction Chain

The first task in the expansion of induction equation is to find which magnetic field is induced by the given velocity field. As the interaction terms $(U_\alpha U_\beta U_\gamma)$ depend either on Gaunt integrals $K_{\alpha\beta\gamma}$ (when the number of the toroidal terms in U is 0 or 2) or on Elsasser integrals $L_{\alpha\beta\gamma}$ (when it is 1 or 3), the search can be implemented by using the selection rules of the Gaunt and Elsasser integrals.

Programming selection rules is quite simple. We start by choosing for the trial function a harmonic U_β which we are interested in (S_1, for example). All the harmonics U_γ with degrees less than or equal to the preassigned maximum degree are tried to see if it can be induced by the combination of the velocity U_α and magnetic field U_β. If $(U_\alpha U_\beta U_\gamma)$ satisfies the selection rules and if U_γ was not used as trial function before, we place the particular U_γ in the waiting list. After the search for one U_β is over, the next one is taken from the waiting list, and the search continues in the same manner, until the waiting list is exhausted.

There are rare cases in which the Gaunt or Elsasser integral vanishes for a combination of harmonics satisfying the selection rules. However, as we need the values of these integrals in any case for constructing the differential equations, appearance of such zeros for the integrals does not cause any trouble. The Gaunt or Elsasser integral is evaluated when the selection rules are satisfied, and the term is discarded if the particular integral vanishes.

The Gaunt and Elsasser Integrals

As mentioned earlier, we need the values of the Gaunt and Elsasser integrals appearing in the interaction terms $(U_\alpha U_\beta U_\gamma)$. For both integrals, the integration by ϕ between 0 and 2π gives $\pi/2$ times the number of occurrence of zero in the expressions $i \pm j \pm k$.

The Gaunt integral can be evaluated by the the method presented by Gaunt (1929). The part in $K_{\alpha\beta\gamma}$ related only to θ $(G_{l\,m\,n}^{i\,j\,k})$ can be written as

$$\int_{-1}^{1} P_l^i(x) P_m^j(x) P_n^k(x) \mathrm{d}x = \frac{2(-1)^{s-m-k}(m+j)!(n+k)!(2s-2n)!s!}{(m-j)!(s-l)!(s-m)!(s-n)!(2s+1)!} \sum_t \frac{(-1)^t (l+i+t)!(m+n-i-t)!}{(l-i-t)!(m-n+i+t)!(n-k-t)!t!} \tag{6}$$

where $2s=l+m+n$, and the summation by t spans integers for which all the factors of factorials are nonnegative. By applying the recurrence formula of Legendre function, we can show that the integral $E_{l\,m\,n}^{i\,j\,k}$ (the part of Elsasser integral related only to θ) can be represented by the use of $G_{l\,m\,n}^{i\,j\,k}$ integrals.

$$E_{l\,m\,n}^{i\,j\,k} = \frac{1}{2}(m+j)\left[(m+j-1)G_{l\,m-1\,n}^{i\,j-1\,k+1} - (n-k)G_{l\,m-1\,n}^{i\,j\,k}\right] - \frac{1}{2}(n+k)\left[(n+k-1)G_{l\,m\,n-1}^{i\,j+1\,k-1} - (m-j)G_{l\,m\,n-1}^{i\,j\,k}\right] \tag{7}$$

Thus the calculation of integrals is reduced to simple summation of terms by (6) or (7). One thing which needs special care in the calculation of the Gaunt and Elsasser integrals is that the numerators and denominators in (6) tend to be quite large and the signs of terms alternate. Thus, if ordinary method is employed in this calculation, error may become unexpectedly large due to the loss of significant digits. The values of $G_{l\,m\,n}^{i\,j\,k}$ and $E_{l\,m\,n}^{i\,j\,k}$ are always rational numbers as shown by (6) and (7). Using this property, each term of (6) are expressed as products of prime numbers in the present program. This procedure is somewhat cumbersome, but by this method the calculations can be carried out in an error-free way.

The values of these integrals were sometimes given in a tabular form, but since its calculation is straightforward as shown above, it is much easier to calculate them when they are needed in the program than to use tabulated numbers.

Evaluation of Interaction Terms

The next step is the formation of the differential equations governing the behaviors of individual harmonics. The interaction terms $(U_\alpha U_\beta U_\gamma)$ in (3) and (4) can be represented by the Gaunt or Elsasser integrals, α, β, γ, and a normalization factor. The expressions are fairly easy and are given by Bullard and Gellman (1954).

The only point we should take care is that the velocity and magnetic field functions in the interaction terms are not necessarily of the form of U_α or U_β, but also their first and second r-derivatives and those divided by r. We have to treat these functions symbolically rather than numerically to keep the generality of the scheme. In the present program, the coefficients of interaction terms are stored separately for each combination of one of U_α, U_α/r, $\partial U_\alpha/\partial r$, $\partial U_\alpha/r\partial r$, $\partial^2 U_\alpha/\partial r^2$ and one of U_β, $\partial U_\beta/\partial r$, $\partial^2 U_\beta/\partial r^2$.

The results of this evaluation are machine readable form of the expanded equation (3) and (4), with correct coefficients for each interaction term. Therefore, this output can be displayed in such a way as is understandable to human thinking.

Reduction of Differential Equation into Difference Form

Since we are studying only the kinematic problem, any forms of the velocity function needed in calculation of (3) or (4) ($\partial U_\alpha/\partial r$, etc.) can be evaluated exactly, as the velocity radial function U_α is given. The differential form of the magnetic field, on the other hand, should be replaced by approximate difference forms. If the range from r = 0 to 1 is divided into M equal parts, and if the value of particular function U_β at the kth grid point is written as $U_{\beta,k}$, the equations (3) and (4) can be written at each grid point by applying the following replacements; $U_\beta = U_{\beta,k}$, $\partial U_\beta/\partial r = M\delta'$, and $\partial^2 U_\beta/\partial r^2 = M^2\delta''$, where δ' and δ'' are the first and second central differences of U_β at point $r_k = k/M$. In the computer program, the easiest way to realize this procedure is to prepare a blank square matrix of necessary dimensions, and to add submatrices formed for the interaction term $(U_\alpha U_\beta U_\gamma)$ (appropriately weighted by the factors obtained earlier) in which differential terms are replaced by the above forms.

Boundary Conditions

The boundary conditions satisfied by the magnetic field harmonics are that they are not singular at the origin, that the poloidal field connects smoothly with the field outside the core which can be derived from a scalar potential, and that the toroidal field is completely contained in the core. Therefore,

$$S_\beta = T_\beta = O(r^{\beta+1}) \text{ at } r=0, \qquad \partial S_\beta/\partial r + \beta S_\beta = T_\beta = 0 \text{ at } r=1 \tag{8}$$

For a toroidal component, the radial function $T_\beta(r)$ vanishes at both r = 0 and 1, so that values at only $(M-1)$ points need to be determined. For a poloidal component, the value at r = 0 also vanishes but the value at r = 1 should be determined by the boundary condition (8). The expressions of derivatives (20) at r=1 gives a relation between $S_{\beta,M-1}$, $S_{\beta,M}$, $S_{\beta,M+1}$, which are values of S_β at r = 1 and its neighboring points. The latter ($S_{\beta,M+1}$) is of course fictitious point outside of the sphere, but through the boundary condition (8), it can be replaced by $S_{\beta,M-1}$ and $S_{\beta,M}$.

Formation of the Matrix Equation and Diagonalization

The matrix formed from the right hand side of the equations (3) and (4) are composed of submatrices of $M_\gamma \times M_\beta$, where M_γ and M_β are either M or $M-1$ depending on the boundary conditions satisfied by U_γ and U_β. These submatrices are placed in the big matrix containing all the equations (3) and (4). The second and third terms on the left hand side of (3) and (4), representing the diffusion of the magnetic field, can also be formulated by the same method and the boundary conditions can be applied as shown above. The diffusion term thus forms a tri-diagonal matrix. The time derivatives in (3) and (4) on the other hand, form a diagonal matrix, which is composed of simply the values of r^2 (or $(k/M)^2$, numerically). A matrix equation is derived by these replacements.

Solving the Eigenvalue Problem

The eigenvalues R_m or p and the eigenvector of the matrix obtained above can be solved by using standard library routines. In the present case, Fortran subroutines in MATH/LIBRARY of IMSL (IMSL, 1987) were used in the computation. In the stationary solution, the smallest real eigenvalue is the one we are seeking. On the other hand, time-dependent case is solved by taking R_m as a parameter. The real part of p usually increases as the magnetic Reynolds number is increased. The value of R_m at which the real part of p changes from negative to positive indicates the onset of instability. If the imaginary part of p is zero, the solution coincides with the steady state solution. If the imaginary part is not zero, the instability takes the form of oscillation with increasing amplitude.

4. Application to the Bullard-Gellman Velocity Field

The programs were developed on Sun-3 and Sun-4 Workstations, and transferred to ETA-10 super computer, both of which run on Unix operating system. The program was first applied to the case of T_1 and S_2^{2c} combination which was repeatedly studied since Bullard and Gellman (1954). That this program works correctly is shown by the fact that correct expansion for Bullard-Gellman velocities are obtained for degrees 2, 3, 4 (Bullard and Gellman, 1954), and 5 (Gibson and Roberts, 1969; with correction in Pekeris et al., 1973). It was also confirmed for the least positive eigenvalues that the same values can be obtained by both stationary and time-dependent formulations.

Table 1 lists the smallest eigenvalues obtained by various authors for different combinations of the degree of harmonics and division in radius. Apparently, large difference in eigenvalues is noticed in a number of cases with the same truncation level and division number. However, on closer look, it appears that the values reported by Gibson and Roberts (1969) are in most cases very different from the values reported by others. The present results are in good agreement with the data of Bullard and Gellman (1954) and of Lilley (1970). The difference between the eigenvalues of these three authors never exceeds 0.5 %. The eigenvalues of Pekeris et al. (1973) are reported to have been obtained by "finite differences, with an interval h of 0.01 or less". The coincidence between the present eigenvalues and the ones given by Pekeris et al. (1973) is also satisfactory. We can conclude from these comparisons that the present program works satisfactorily for a wide range of trancation levels (L) and division in radius (M). Among the earlier results reported for the Bullard-Gellman velocity field, the ones by Gibson and Roberts (1969) are apparently in error.

Figure 1 shows the change of the real part of the eigenvalue p with the change of magnetic Reynolds number. In the present study, satisfactory coincidence was observed in all the cases between the stationary and time-dependent solutions.

5. Conclusions

Table 1. Eigenvalues for Bullard-Gellman velocity $T_1=5r^2(1-r)$, $S_2^{2c}=r^3(1-r)^2$

Degree	No. of Eqs.	Author(s)	Division in r				
			10	16	20	50	100
2	4	BG54					
		GR69		66.46			
		L70	58.6		64.4		
		PAS73					66.460
		K89	58.38	63.22	64.38	66.13	66.38
3	7	BG54	68.8				
		GR69	83.43	83.09			
		L70	67.6		78.5		
		PAS73					83.207
		K89	68.78	76.60	78.78	82.35	82.90
4	12	GR69	76.02	75.95			
		L70		94.3[1]			
		PAS73					95.834
		K89	168.90	94.05	94.57	95.60	95.76
5	17	GR69	143.2				
		PAS73					1369.2
		K89	459.22	305.08	1414.9	1496.8	1434.7

Notes: BG54, Bullard and Gellman (1954); GR69, Gibson and Roberts (1969); L70, Lilley (1970); PAS73, Pekeris et al. (1973); K89, present study.
[1] Number of division was 17.

Computer programs were developed to treat the induction equation in a general way based on the principle of computer algebra. Expansion of the induction equation leads to many terms with coefficients which should be determined one by one. In such a situation, evaluation of the equation is very time-consuming and prone to error if interaction terms are evaluated in a conventional manner. Present programs avoid this by manipulating the functional forms of various velocity and magnetic field harmonics rather than the values of these functions. Because of mathematically simple structure of poloidal-toroidal expansion and because of the fact that the coefficients are always rational numbers, error-free expansion of equations is possible by the method of computer algebra.

Once the equation is correctly expanded, the rest of the program can form the matrix for eigenvalue problem in a straightforward way. Formulation into difference equations, taking care of boundary conditions, and diagonalization needed for making a standard eigenvalue problem can be carried out without much trouble. Computation was also carried out for the case of Bullard-Gellman velocities and the obtained eigenvalues were compared with the values reported by other authors. The eigenvalues obtained by the present program are in good agreement with the values reported by Bullard and Gellman (1954) and Lilley (1970). Satisfactory agreement was also observed between the present eigenvalues and those of Pekeris et al. (1973), although the details of computation are not known for the latter. On the other hand, data in Gibson and Roberts (1969) are quite different from the present results. It can be concluded that their eigenvalues are in error, because the present results are corroborated by comparison with values obtained by different workers and different programs.

The merit of present approach lies in the fact that the equations for given velocity harmonics can be obtained to any degree without errors. Application of this program to other

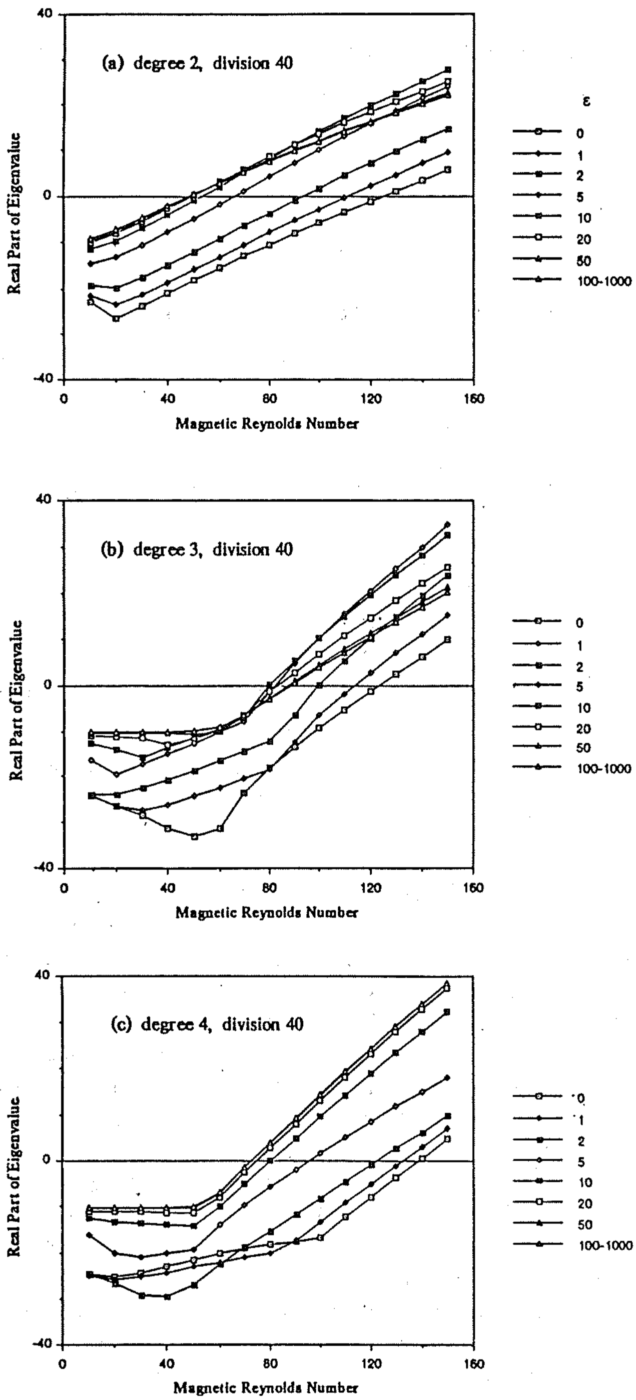

Fig. 1. Change of the largest of the real part of the eigenvalue p for time-dependent solution with the increase of magnetic Reynolds number R_m. The ration of toroidal/poloidal velocities (ε) for each curve is indicated on the right. The number of division in r is 40, and the maximum degrees are (a) 3, (b) 4, and (c) 5.

combination of velocities is now in progress and will be reported elsewhere.

The present approach can also be expanded for the hydromagnetic dynamo with inclusion of Navier-Stokes equation. To do so, the velocity field must also be expanded into a sum of functions U_α, and the equation for the fluid motion can be solved for the unknown values of U_α in the similar way as the Bullard-Gellman formulation (Frazer, 1973). In this approach, we cannot restrict the interaction diagram to a small number of velocity harmonics. If the induction equation is coupled with Navier-Stokes equation, the resulting equations will be quite difficult and conventional approaches will fail just because of their complexity. If Bullard-Gellman expansion is extended to such cases, only algebraic treatment of equations by computer can handle the problem. Otherwise, some different approaches (such as spectral method) are needed to formulate ever increasing complexities. Further, it is planned to incorporate the equation of fluid motion in a way as suggested by Frazer (1973). Such extension of the present program will be useful in studying the behaviors of kinematic and hydromagnetic dynamos.

References

Bullard, E.C. and H. Gellman, Phil. Trans. Roy. Soc. Lond., A247, 213-278, 1954.

Chandrasekhar, S., Hydrodynamic and Hydromagnetic Stability, 652pp., Oxford University Press, London, 1961.

Frazer, M.C., Phys. Earth Planet. Inter., 8, 75-82, 1974.

Gaunt, J.A., Phil. Trans. Roy. Soc. London, A228, 151-196, 1929.

Gibson, R.D. and P.H. Roberts, in The Application of Modern Physics to the Earth and Planetary Interiors, edited by S.K. Runcorn, pp. 577-602, Wiley, London, 1969.

Gubbins, D., Phil. Tran. Roy. Soc. Lond., A274, 493-521, 1973.

IMSL, MATH/LIBRARY User's Manual, Version 1.0, 1149p, Houston, Texas, 1987.

Kumar, S. and P.H. Roberts, Proc. Roy. Soc. Lond., A344, 235-258, 1975.

Lilley, F.E.M, Proc. Roy. Soc. Lond., A316, 153-167, 1970.

Pekeris, C.L., Y. Accad, and B. Shkoller, Phil. Trans. Roy. Soc. Lond., A275, 425-461, 1973.

(in press in Journal of Geomagnetism and Geoelectricity)

OPAQUE MINERALS IN HYDROTHERMAL ALTERATION ZONES AND THEIR RELEVANCE TO ROCK MAGNETISM.

Hirotomo UENO

Department of Geology, College of Liberal Arts,
Kagoshima University, Kagoshima 890

Introduction

It is important to discriminate TRM and CRM, nevertheless it is not easy by usual paleomagneical treatments. The simplest identification with the CRM may be that the remanence is due to ferromagnetic minerals which are crystallized newly or recrystallized from the same minerals during alteration or metamorphism. In this paper opaque minerals, which are inclusive of both primary rock-forming Fe-Ti oxide minerals in igneous rocks, secondary Fe-Ti oxide minerals and new sulfide minerals changed from Fe-Ti oxide minerals, are examined in hydrothermal alteration zones around ore deposits, and remanences characterized by these ore minerals are dealt with.

Continuous sections from fresh to altered within the same igneous rock body are selected for this study.

Volcanic Sulfur Deposits

The opaque minerals in fresh rocks of two pyroxene andesite lava around the Numajiri volcanic sulfur deposits(38° 38'N,140° 15'E) consists of primary magnetite with accessory ilmenite. Advancing alteration, magnetite changes partly to maghemite. In this step the alteration of silicate minerals is slight decomposition of plagioclase and pyroxene. As kaolinite, montmorillonite and jarosite are detected in more altered sites, fine grained Ti rich hematite is formed from maghemite and magnetite. Opaque minerals in highly altered sites consist mainly of Ti poor hematite with accessory with pseudobrookite, and alunite is found in these sites. Finally those opaque minerals change to marcasite (Fig. 1).

The median destructive fields by alternating field demagnetization of samples from fresh and altered sites are 10 to 20 mT and 50 to over 60 mT, respectively. The CRMs due to hematite in altered sites are harder than the TRMs in fresh sites (Ueno and Nedachi, 1985).

The similar occurrences of Fe-Ti oxide minerals in the

Green Tuff alteration zone at the western Gunma and in the geothermal alteration zone at Noya have reported by Sato (1984) and Fujimoto (1987), respectively. But, they have not mentioned sulfide minerals. Therefore, results described here can be applied to the region of Green Tuff alteration and geothermal alteration.

Kuroko Deposits

Generally almost rocks around the Kuroko deposits are altered, but the Torigoe dacite lava around the Kosaka Kuroko deposits (40 ° 19'N,140 ° 46') and the Hatabira dacite of the Tsuchihata Kuroko deposits (39 ° 17'N,140 ° 50'E) have fresh parts.

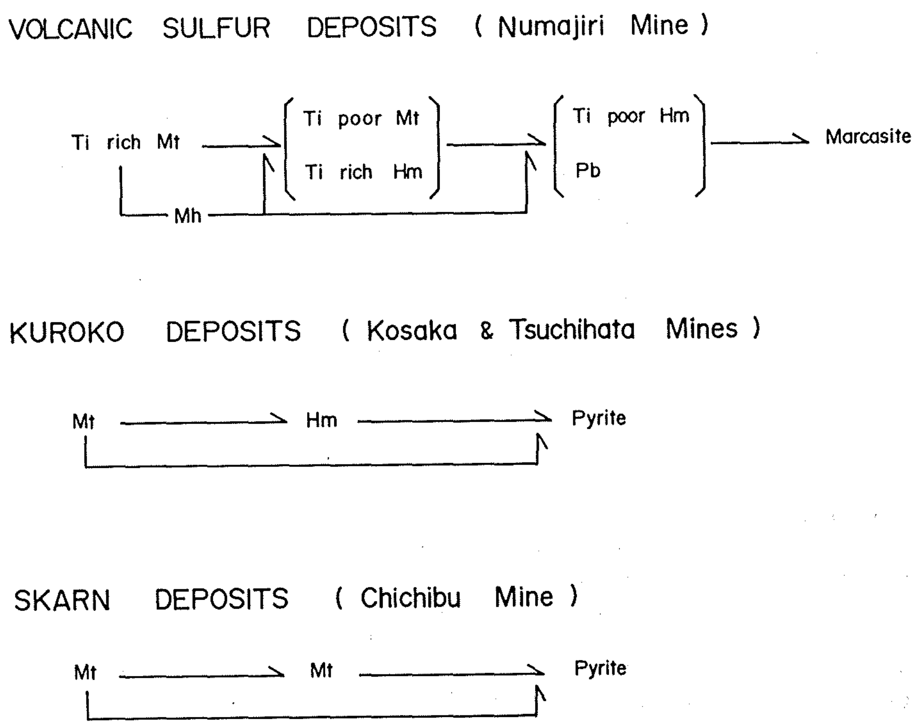

Fig. 1. Opaque minerals in hydrothermal alteration zones.
Mt; magnetite, Mh; maghemite, Hm; hematite,
Pb; pseudobrookite

The Torigoe dacite lava whose thickness in 68 m underlies the Kosaka Kuroko deposits. The bottom and upper one third parts are altered with pale gray or greenish white in color, but the central one third part is fresh with brownish gray in color. The fresh part have relatively fine grained magnetite which is euhedral or subhedral. The most fresh rock include no clay mineral. The altered parts have hematite of needle shape. In this part chlorite and sericite are detected. Finally hematite changes to pyrite. The Hatabira rhyolite dome of the Tsuchihata Kuroko deposits is host rock of the network copper veins which are believed to the Keiko-type ores of the Kuroko deposits. The most fresh rock among collected samples is 300m of the ore body at the near the entrance adit of Level 0, and the rocks become more altered as the distance to the ore body decrease. Even if the most fresh part with brownish gray in color primary magnetite changes partly to hematite along the rim of the grain. As chlorite and sericite increase, hematite replaces almost magnetite. Two perlite zones resulted from rapid cooling of original rock appear in the altered zone. Although clay mineral is mordenite instead of chlorite and sericite in the perlite zone, hematite appears as a continuously changing phase of opaque minerals. Finally hematite changes to pyrite (Fig.1).

Samples from fresh and altered parts have normal and reversed polarity magnetizations, respectively (Ueno, 1982). The median destructive fields of samples from fresh parts are about 10 mT, and those from altered parts are over 60 mT.

Pyrometasomatic Deposits

The Chichibu pyrometasomatic deposits (36°01'N,138°49'E) have genetical relation to quartz diorite. The quartz diorite bodies have undergone the different grade of hydrothermal alteration. The fresh parts of the quartz diorite bodies have euhedral or subhedral magnetite of 150 microns or less in size. As the alteration increases in grade, magnetite ought to be recrystallized as the aggregate of small magnetite of 10 microns in each grain size. The recrystallized magnetite contains less V_2O_3, Al_2O_3 and TiO_2 (Ueno, 1986). The Curie temperatures are 560°C on fresh rock and 580°C on altered rocks. The chemical composition of magnetite is exactly concordant with the Curie temperature, and it seems that recrystallized magnetite become more pure magnetite. Finally those change to pyrite (Fig. 1).

The median destructive fields of samples from fresh sites are 15 to 45 mT. The magnetizations due to recrystallized magnetite have the median destructive fields of 60 or over 60 mT (Ueno, 1987).

The ore deposits described above are of Miocene to Holocene in age. The older deposits may be examined by the same procedure, but the mineral changes in the later stages must be considered. There found no typical igneous body including fresh and altered parts around vein type ore deposits because of overlapping of so called propylitization.

Summary

Opaque minerals in the hydrothermal alteration zone around ore deposits change according to the grade of the alteration. And the changing style of opaque minerals are different in each type ore deposit. That means the opaque minerals are reflecting upon the conditions during alteration. It is clear from the results that volcanic sulfur deposits and Kuroko deposits are higher oxidation state than pyrometasomatic deposits.

As mentioned above it is sure that median destructive fields of the CRM acquired during hydrothermal alteration is high as compared with the original TRM.

References

Fujimoto, K.(1987) Jour. Faculty Sci. Univ. Tokyo, Sec. 2, **21**, 257-282.

Sato, W. (1984) Chikyu Kagaku (Earth Sci.), **33**, 161-181.

Ueno, H. (1982) Sci. Rept. Tohoku Univ., Ser. 2, **15**, 273-280.

Ueno, H., Nedachi, M. (1985) Rock Mag. Paleogeophys., **12**, 66-71.

Ueno, H. (1986) Rock Mag. Paleogeophys., **16**, 60-65.

Ueno, H., Tonouchi, S. (1987) Econ. Geol., **82**, 1723-1731.

THERMAL VARIATION OF INITIAL SUSCEPTIBILITY BY USING AUTOMATIC HIGH-TEMPERATURE SUSCEPTIBILITY METER

Masayuki TORII*, Hirokuni ODA* and Hidetoshi SHIBUYA†

*Department of Geology and Mineralogy, Kyoto University, Kyoto 606.
†Department of Earth Sciences, The University of Osaka Prefecture, Sakai 591.

Thermal demagnetization is a very powerful technique to remove secondary overprintings of remanence either of low-blocking or high-blocking temperature components. However some of the minerals in the rock samples turn magnetically or chemically unstable during thermal cleaning to a few hundred degrees in Celsius. Thermal instability of the magnetic minerals often degrades usefulness of thermal demagnetization and shows a confusing pattern on the vector diagram (Fig. 1). Titanomaghemite, pyrrhotite, and goethite are typical minerals of thermally unstable nature. Main difficulty may come from the fact that those minerals convert to magnetite during the heating experiment. Newly formed magnetite can easily override the primary remanence due to its very large magnetization. Growth of magnetite during the artificial heating is generally prominent for the case of unconsolidated sediments because of the presence of reducing agent, dehydration, and less abundance of primary stable magnetic minerals.

Thermal demagnetization is a very time-consuming procedure and destructive experiment. By these reasons it is practically important to know prior to thermal demagnetization whether the samples can survive the thermal treatment or not. It is also helpful to know the maximum temperatures to be allowed for each particular sample. There are numerous, well-established laboratory techniques for indicating thermal variation of magnetic property during the heating. Thermally sensitive parameters are as follows: Curie temperature, coercivity spectrum of isothermal or anhysteretic remanence, remanent coercivity, rotational hysteresis, initial susceptibility, and so on (e.g., Lowrie and Heller, 1982; Collinson, 1983). The initial susceptibility is one of such parameters and has some advantages for practical use. Firstly the initial susceptibility is sensitive to the portion of finer magnetic particles which may carry stable part of remanence. Secondly measuring thermal change of the initial susceptibility is simple and less time-consuming particularly by using an automatic high- temperature susceptibility meter system.

We employed Bartington M.S.2.W/F system which is a very common commercially developed high-temperature susceptibility meter. It has very sensitive sensor which enable us to measure less magnetic samples such as sediments; the noise level is about 1×10^{-8} in SI

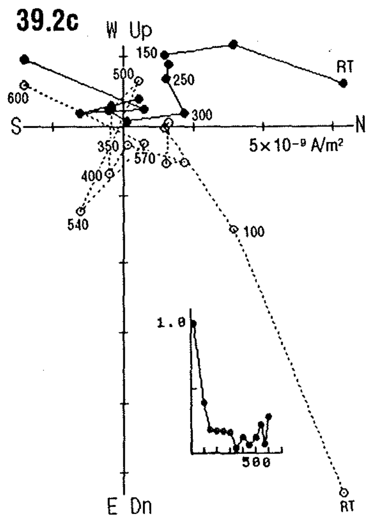

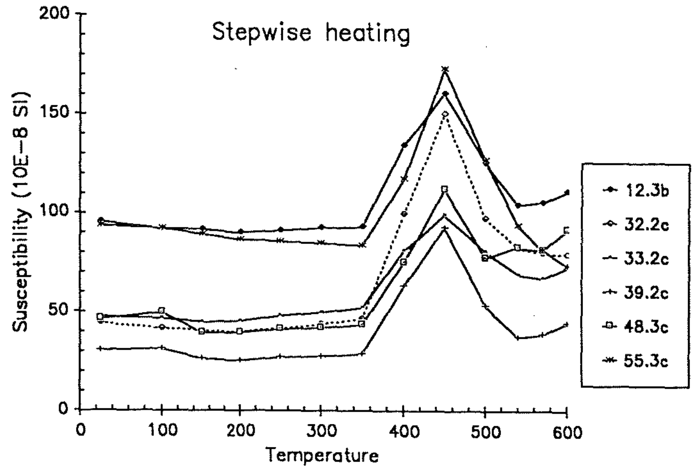

Fig. 1 (left) Unsuccessful thermal demagnetization at the higher temperatures (above 300°C). Sample is a marine siltstone from the Boso peninsula (Pleistocene).

Fig. 2 (right) Initial susceptibility measured after each step of progressive thermal demagnetization for six samples from the Boso peninsula. Initial susceptibility increases above 350°C.

unit. For high-temperature measurement, sample should be prepared as a cylindrical shape of 15 mm in diameter and 25 mm highs. A furnace controller unit is equipped with a RS232C port through which we can transfer read out of susceptibility and temperature. However we could not control susceptibility meter through the RS interface such as to stop heating or to preset maximum temperatures. This one-way communication system forced us to keep watching the thermometer during heating process and to switch the power controller towards cooling at the turning temperatures. We therefore made some improvement to the electric circuit to enable automatic switching of the furnace through RS interface. The adhon circuit is, in practice, very simple one and we do not think necessary to show the circuit diagram in this report. The interfacing program is coded with Turbo Pascal (ver. 5.0), and the diagrams are illustrated by using Microsoft Chart (ver. 3.1).

Thermal change of the initial susceptibility can be observed through measurement of the susceptibility after every steps of progressive thermal demagnetization as shown in Fig. 2. The figure is a case of Pleistocene marine sediment form the Boso peninsula. We can find pronounced increase in susceptibility by heating samples above 350°C. We can, however, know the change only after thermal demagnetization.

Continuous change in the initial susceptibility is observed during heating by using the automatic high-temperature susceptibility meter (Fig. 3). Heating and cooling rate is controlled as 10°C/min. Sudden increase in susceptibility appears at 350°C and 500°C on

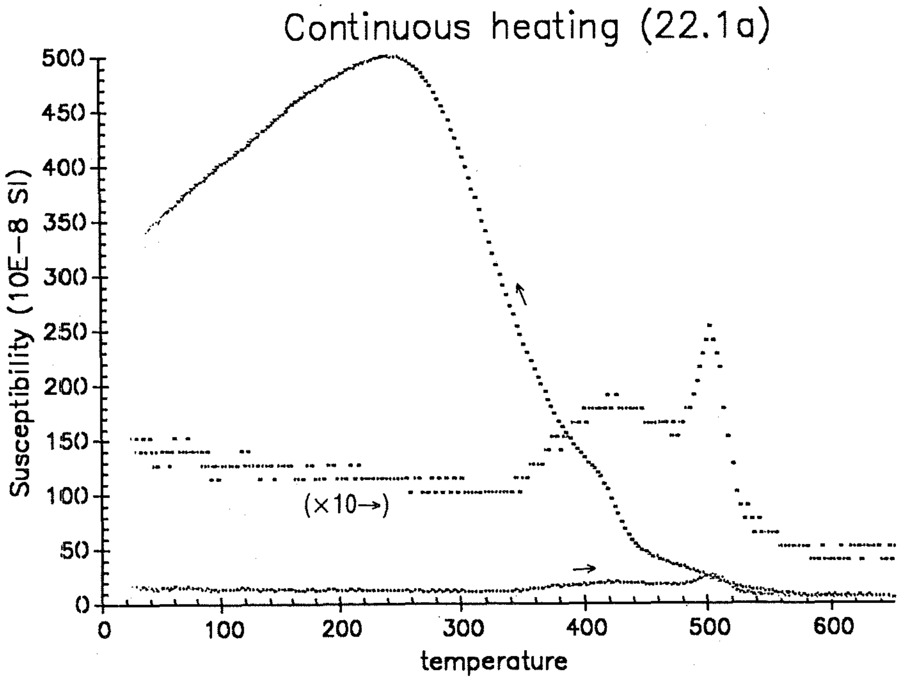

Fig. 3 Variation of initial susceptibility during continuous heating up to 350°C. Heating curve is exaggerated by ten (indicated by × *10*) to show increase of susceptibility. Cooling curve is completely irreversible compared to the heating curve.

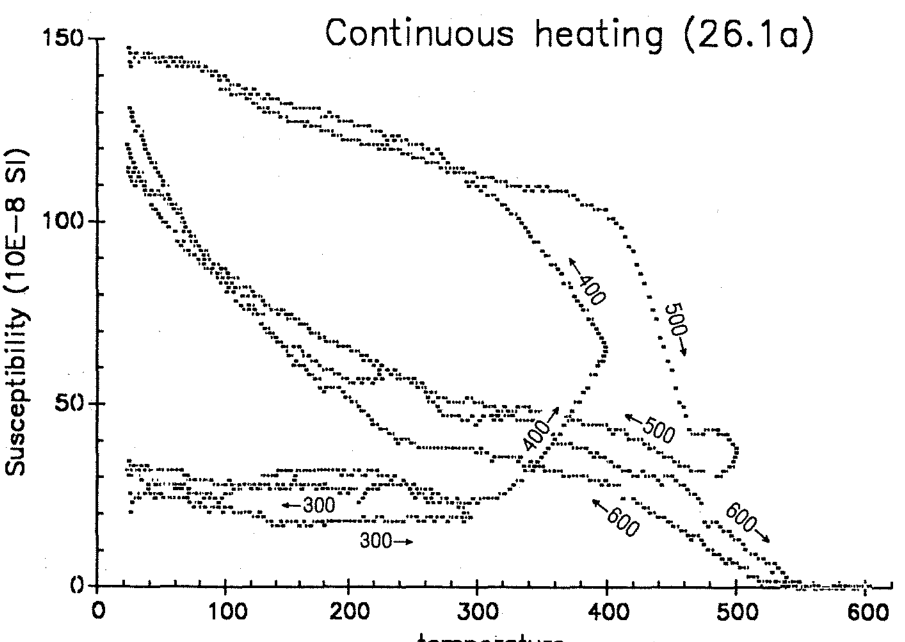

Fig. 4 Stepwise, continuous variation of initial susceptibility recorded by automatic high-temperature susceptibility meter. Irreversible change observed by heating above 300°C.

heating process. Increase in susceptibility is much enhanced on the cooling curve. This sample clearly showed irreversible change of the initial susceptibility at high-temperatures (above 350°C).

Thermal change in susceptibility is more clearly observed with stepwise, continuous heating experiments; to heat up sample to a certain temperature and to cool down to the room temperature, and then to repeat heating/cooling cycles at the higher temperatures (Fig. 4). This progressive experiment is more similar to the actual condition of thermal demagnetization experiment. We can point out the temperatures above which the susceptibility makes irreversible change by heating.

Our tentative conclusion is that we cannot safely carry forward thermal demagnetization above the irreversible point indicated by the continuous high-temperature susceptibility measurement. The high-temperature susceptibility measurement can serve as a time-saving technique in terms of a reconnaissance of thermal demagnetization.

Reference:

Lowrie, W. and F. Heller (1982) Rev. Geophys. Space Phys., **20**, 171.

Collinson, D.W. (1983) Method in Rock Magnetism and Paleomagnetism, (Chapman and Hall, London), 503.

AN AUTOMATIC SPINNER MAGNETOMETER
WITH THERMAL DEMAGNETIZATION EQUIPMENT

Masaru Kono, Masayuki HOSHI[1], Koji YAMAGUCHI[2], and Yosuke NISHI[3]

Department of Applied Physics, Tokyo Institute of Technology
Ookayama 2-12-1, Meguro-ku, Tokyo 152

1. Introduction

Spinner magnetometer is a very useful instrument and widely used in rock magnetism and paleomagnetism. Some of the important steps in its development were the introduction of fluxgate magnetometer with phase sensitive circuit by Foster (1966) and that of the ring-core sensor by Molyneux (1971). In paleomagnetic measurements, it is necessary to replace the sample several times to obtain three components of the magnetization vector. Moreover, measurement of magnetization cannot be considered complete without appropriate magnetic cleaning such as alternating field (AF) or thermal demagnetization. Because the measurement of remanence and demagnetization is very time-consuming, several attempts have been made to automatize either the measurement itself (e.g., Kono et al., 1981), or the entire process of measurement and demagnetization (e.g., Noel and Molyneux, 1975; Niitsuma and Koyama, 1989).

Kono et al. (1981) constructed a spinner magnetometer in which the sample is rotated around two axes simultaneously, and the signal from a single ring-core fluxgate sensor supplies sufficient information about the magnetization of a sample. This was made possible because the vertical component of the magnetic field measured on the surface of a sphere completely determines the potential field outside, as they satisfy the classical Dirichlet condition. Sample replacements were made unnecessary by the rotation of the sample around the two orthogonal axes (vertical and horizontal) by the use of bevel gears. For further automation, this instrument may be combined with alternating field (AF) demagnetization. But it is practically impossible to combine this with thermal demagnetization because of the mechanical complexity.

As sophisticated demagnetization techniques became needed to characterize different components of magnetization, thermal demagnetization seems to have gained importance compared with AF demagnetization, as the latter is often useless for rocks containing very high coercivity components such as hematite. To include thermal demagnetization in an automatic system, it is necessary to make the mechanical parts as simple as possible to avoid damages caused by the heating, or the sample and the moving mechanism should be well separated so that heating does not affect the mechanical components.

We have designed an automated system in which a sample is rotated and translated and the signal is measured by a fluxgate sensor. In contrast to the scheme of Kono et al. (1981), the present magnetometer measures the field over the surface of a cylinder surrounding the sample. In principle, this method gives the complete description of the potential field by a source within a cylinder only when the vertical component is measured over the infinite stretch of the cylinder. In practice, however, the magnetic moment of a sample can be determined to a satisfactory level by measureing the field over a short distance in the axial direction even when it contains a considerable amount of multipole fields, e.g., quadrupole and octapole terms. We incorporated thermal demagnetization as a part of automatic operation, with an electric furnace placed in a three-

---

[1] Now at Sony Corporation, Kita-Shinagawa 6-7, Shinagawa-ku, Tokyo 141.

[2] Now at Kawasaki Steel Corporation, Uchisaiwai-cho 2-2, Chiyoda-ku, Tokyo 100.

[3] Now at Yamatake-Honeywell Electric Corporation, Shibuya 2-12, Shibuya-ky, Tokyo 150.

layer permalloy shield well separated from the sensor. We shall describe below the method of determination of remanence direction and intensity, and also give brief descriptions of the electric circuit and mechanical setup, and some examples obtained by this instrument.

2. Determination of Magnetic Remanence

The magnetic potential of a sample can be expressed by expansion into spherical harmonics

$$W=c\sum_{n=1}^{\infty}\sum_{m=0}^{n}\left(\frac{c}{r}\right)^{n+1}P_n^m(\cos\theta)(a_n^m\cos m\phi+b_n^m\sin m\phi) \tag{1}$$

where c is some length scale included to make the dimension of a_n^m and b_n^m that of the field, (r,θ,ϕ) are spherical coordinates with the origin placed at the center of the sample and the polar axis taken along the sample rotation axis, $P_n^m(\cos\theta)$ are associated Legendre functions, and a_n^m and b_n^m are the Gauss coefficients describing the magnetic moment of the sample. In our case, it is more convenient to use the cylindrical coordinated (s,z,ϕ). The three components of the magnetic field at the surface of a cylinder of radius c can be obtained by partial differentiation of the potential W by these coordinates.

$$B_s=\sum_n\sum_m\sin^{n+1}\theta[(n+1)P_n^m(\cos\theta)-(n-m+1)\cos\theta P_{n+1}^m(\cos\theta)](a_n^m\cos m\phi+b_n^m\sin m\phi) \tag{2}$$

$$B_z=\sum_n\sum_m(n-m+1)\sin^{n+2}\theta P_{n+1}^m(\cos\theta)(a_n^m\cos m\phi+b_n^m\sin m\phi) \tag{3}$$

$$B_\phi=\sum_n\sum_m m\sin^{n+1}\theta P_n^m(\cos\theta)(a_n^m\sin m\phi-b_n^m\cos m\phi) \tag{4}$$

Obviously, axially symmetric terms in the potential (m=0) does not contribute to the field component B_ϕ, so that we cannot obtain any information about them from the measurement of the ϕ-component of the magnetic field. On the other hand, it is possible to determine the potential either from z-component or s-component or from both. If the sample is rotated at a fixed value of z, a non-axisymmetric term ($m\neq0$) produces a signal which is sinusoidal with periods equal to the time for one revolution divided by m. Distinction between terms with different m can therefore be made easily by frequency sensitive analysis such as the fast Fourier transform (FFT). The distinction between the terms with different n can only be made possible through the analysis of the z-dependence of the magnetic field. Unfortunately, the signals corresponding to different n are not orthogonal to each other in contrast to the case of the sampling over the surface of a sphere (Kono et al., 1981). Therefore, the Gauss coefficients a_n^m and b_n^m will change if the level of truncation in n is changed. It should be noted, however, that the components of the magnetic field are either even or odd function of z. Since even and odd functions are orthognal to each other if the interval of measurement is taken to be symmetric about z=0, the presence of the quadrupole term (n=2) does not hinder the precise determination of the dipole term (n=1). The source of largest error in the determination of the dipole term is obviously the octupole term which has similar dependence on z as the dipole term. We found out that the magnetization of the sample can be determined satisfactorily from the measurement of the magnetic field by the fluxgate sensor when the sample is rotated around and translated along an axis at the same time.

3. The Spinner Magnetometer

Figure 1 shows a schematic drawing of the magnetometer-furnace system. The rotation and translation of the sample are carried out by two stepping motors mounted about 50 cm away from the sample. The stepping motors are actuated by the pulses sent from the computer.

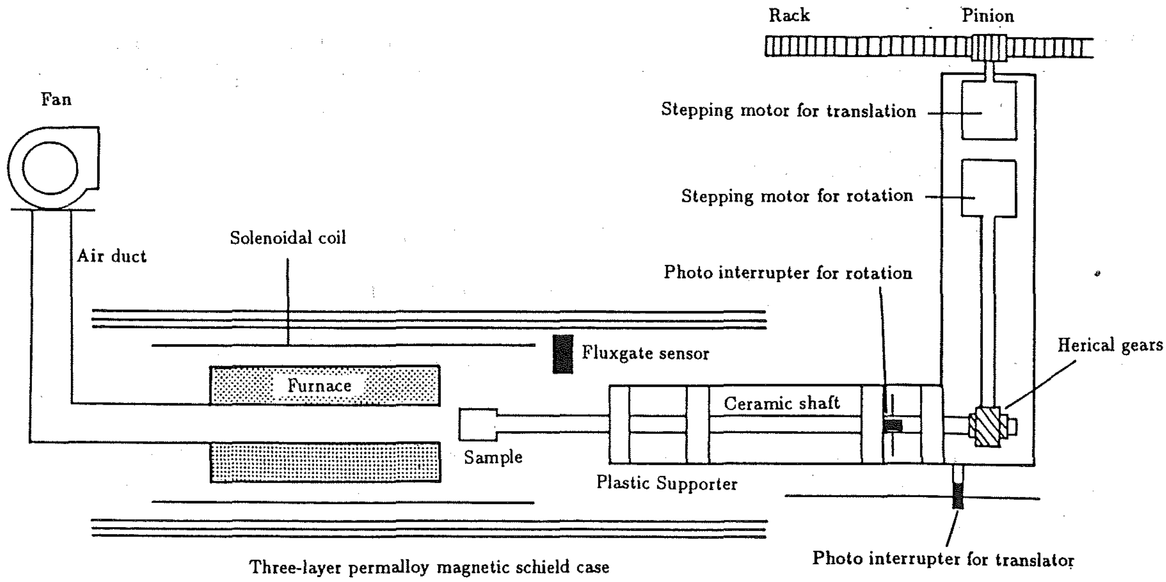

Fig. 1. Schematic diagram of the spinner magnetometer-electric furnace system developed in this study.

Counterclockwise or clockwise rotation of 0.2-3 revs/s, or translation to the left or to the right with a speed of 0.4-5 cm/s, or their combination can be attained through the computer control. A fluxgate sensor of ring-core type is located in the middle of the non-magnetic field inside the three-layer shield. The sensor measures the s-component of the magnetic field in the present setup.

In the measurements, the axisymmetric components of the magnetization (a_n^0) is harder to obtain than the other components because it induces only DC magnetic field and because the magnetometer shows a non-negligible amount of drift. Non-axisymmetric terms give frequency dependent signals and therefore can well be determined. The axisymmetric terms can only be determined from the variation with z. It is necessary to repeat more translation than rotation in order to effectively reduce the noise due to the drift.

Figure 2 shows the wave forms of the axisymmetric component for various stacking numbers when a sample was measured by this magnetometer. This component contains the largest noise as indicated above. Obviously the stacking is quite effective in reducing the measurement noise. The RMS noise is reduced as the inverse square root of the stack number, as it should if the noise is random. In practice, too large stack numbers are not practical as the sampling time becomes too long. Stack numbers less than about 40 is used in actual measurement.

4. Furnace Control

An electric furnace with noninductive winding is placed further away in the shield case, well separated from the fluxgate sensor in order to avoid the heating of the latter. The block diagram of the furnace control circuit is shown in Figure 3. The current to the furnace is controlled through a zero-cross solid-state-relay (SSR). The temperature is monitored by a Pt-Pt13%Rh thermocouple of which voltage is read into the computer through 12-bit AD converter. After the necessary linearization, the temperature shown by the thermocouple is compared with the target temperature.

The computer calculates the necessary output power in terms of proportional action (P),

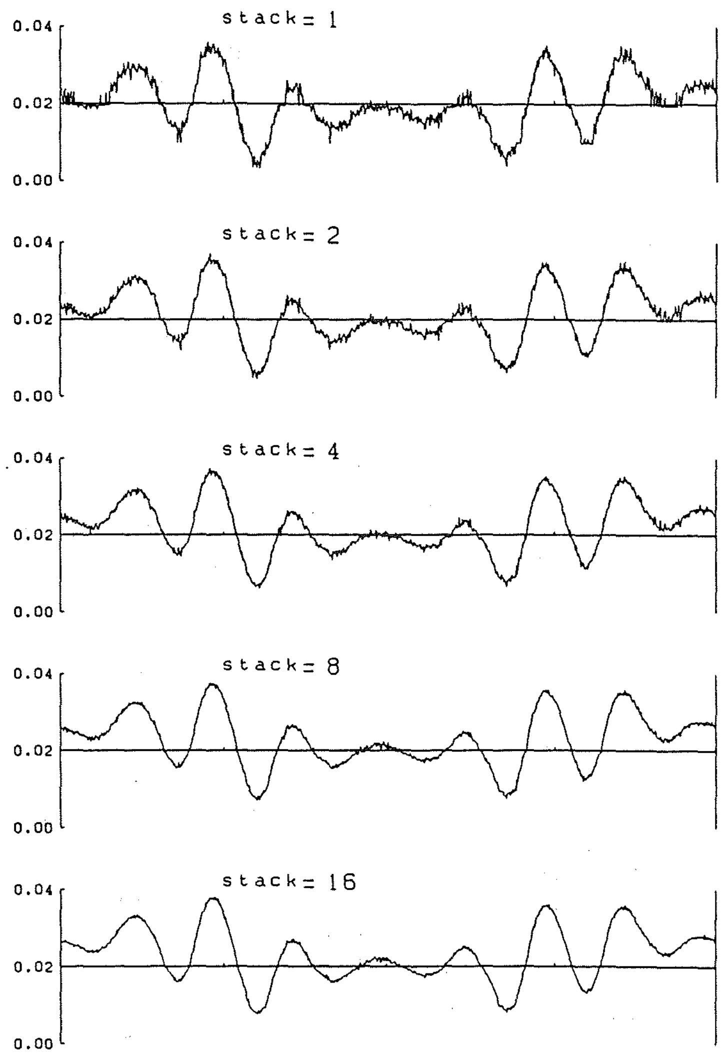

Fig. 2. The axisymmetric component of magnetization measured with various stacking numbers. Note the change in the zero level, which reflects the long-term drift of the DC level of the magnetometer.

integral action (I), and derivative action (D). The output power to the furnace is thus the sum of PID actions. The combination of these three actions improves the performance of the furnace well if the parameters are suitably chosen. In the actual program, we use a formula written in the discrete form

$$P_n = k_p[E_n + \frac{1}{T_i}\sum_{j=m}^{n} E_j + T_d(E_n - E_{n-1})/\delta t] \tag{5}$$

where P_n and E_n are the output and the deviation at the nth step, respectively, and δt is the interval between the steps. The numerical parameters in the above equation (k_p, T_i, T_d) were determined empirically, so as to optimize the performance. This power is applied to the furnace by switching on the mains supply for certain numbers of half cycles in total of 128 cycles of the mains supply and switching off for the rest of period. It was shown that the highest temperature is quite close to the set temperature at every step, and also that the paired heatings show the temperature changes almost identical with each other. This reproducibility is the most important characteristics requied of a furnace used in paleointensity experiments (Thellier and Tehllier, 1959).

5. Discussion and Conclusions

An automatic magnetometer-furnace system was built which can operate a series of thermal demagnetization or magnetization experiments with the computer control. It was shown that, with the combination of rotation and translation of a sample along an axis, it is possible to determine the vector magnetization to a satisfactory level. By this approach, the need to change the sample orientation in measurements was eliminated, and therefore the possibility arise to measure and demagnetize the sample without removing it from the sample holder.

As the needed movements (rotation and translation) are quite simple, the actuators for the movements (stepping motors) and sensors to measure the position (photo-interrupters) can be placed well separated from the sample. This has a merit in reducing the noise caused by these elements, as well as in permitting to construct the sample holder and the shaft with a heat resistant material such as ceramics. Thus, the sample can be translated to the inside of the furnace

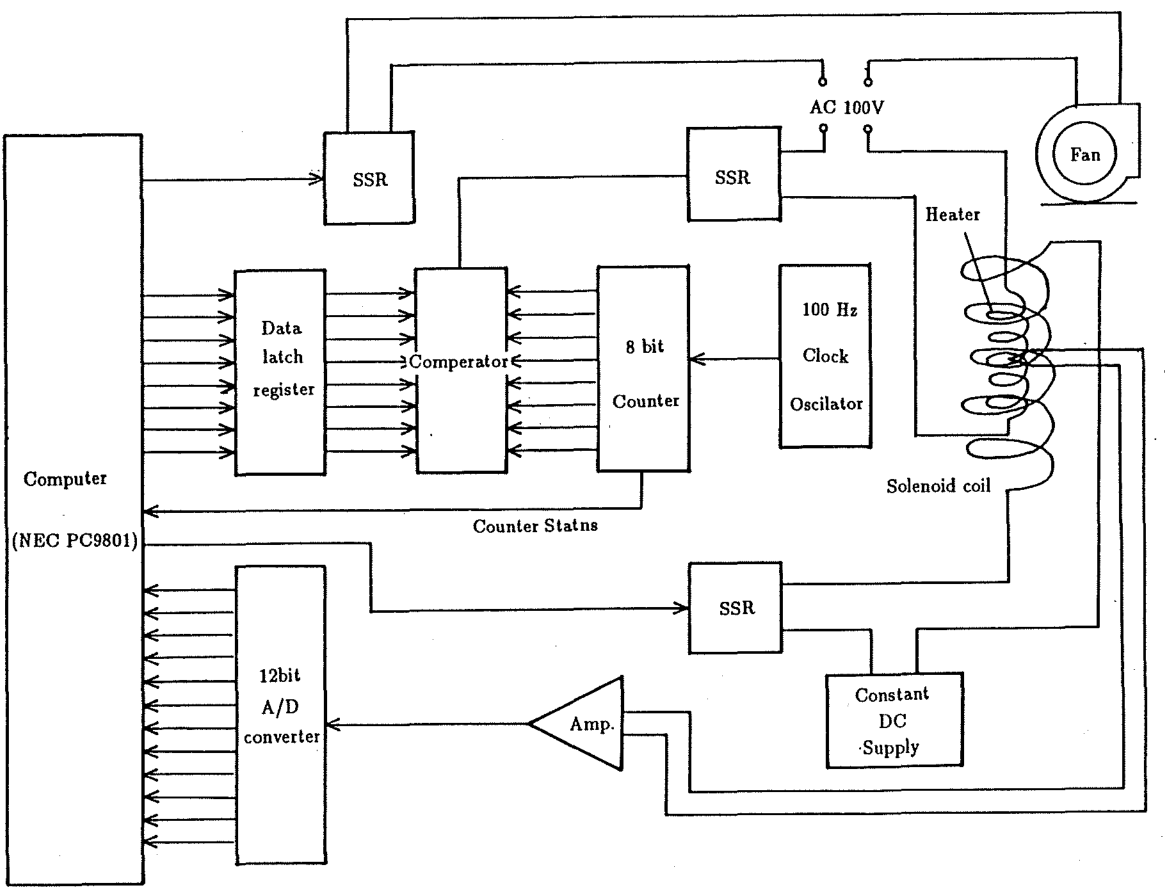

Fig. 3. Block diagram of the electronic circuit controling the temperature of the furnace, applied magnetic field, and electric fan for cooling the sample and the furnace.

and heated to high temperatures, enabling the combination of heat treatment and measurement to be carried out successively.

We used this system for paleointensity experiments and found some improvements over the ones done by using conventional instruments. First of all, because the sample is never removed from the sample holder during the course of an experiment, sample orientation errors are practically eliminated. Secondly, the sample stays inside the three-layer magnetic shield all the time, so that the effect of unwanted magnetic field is small compared with the ordinary experiments. This apparatus may also be useful for thermal demagnetization of viscous samples which acquire large remanences in the laboratory. Thirdly, it is possible to perform demagnetization in a good vacuum to avoid chemical changes by sealing the samples inside a quartz capsule. There is no need to place the entire system in vacuum.

There are still some shortcomings which need improvement. They include raising the sensitivity and reducing the noise level of the sensor, shortening the turn-around time by cooling with water or with compressed air circulation. All of these points are technically feasible. We hope to improve the system with such considerations in a near future.

References

Foster, J.H., Earth Planet. Sci. Lett., 1, 463-466, 1966.
Kono, M., Y. Hamano, T. Nishitani, and T. Tosha, Geophys. J. R. Astr. Soc., 67, 217-227, 1981.
Molyneux, L., Geophys. J. R. Astr. Soc., 24, 349-372, 1971.
Niitsuma, N. and M. Koyama, paper presented at IAGA General Assembly, Exeter, 1989.
Noel, M. and L. Molyneux, Geophys. J. R. Astr. Soc., 43, 1017-1021, 1975.
Thellier, E. and O. Thellier, Ann. Geophys., 15, 285-376, 1959.

(submitted to Journal of Geomagnetism and Geoelectricity)

ARCHEOMAGNETIC INVESTIGATION OF OHDATENO REMAIN IN AKITA PREFECTURE

Tadashi NISHITANI and Chihiro SHIMURA

Institute of Mining Geology, Mining College,
Akita University, Akita 010 Japan

Archeomagnetic investigations were performed at Ohdateno Remain. Ohdateno is in the northern part of Akita prefecture (Fig.1). Figure 2 indicates an arrangement of houses and furnaces. Total 145 specimens were collected in 13 furnaces using a plastic case. An archeological age of this place are interpreted in 10 to 11 century. Chronologically different stages gathered there. SI-14 cuts the area of SI-17 and SI-17 cuts that of SI-18. The sequence of age, therefore, can be interpreted as SI-18, 17 and 14. We tried to specify its orders and studied the relations between archeological ages and archeomagnetic results.

We tried to specify their orders and studied the relations between archeological ages and archeomagnetic results. Three pilot samples from each furnace were demagnetized progressively up to a peak alternating field of 45 mT and an optimum alternating field was determined. Other specimens were demagnetized using above optimum alternating field. Fig.3 shows some results of this treatment.

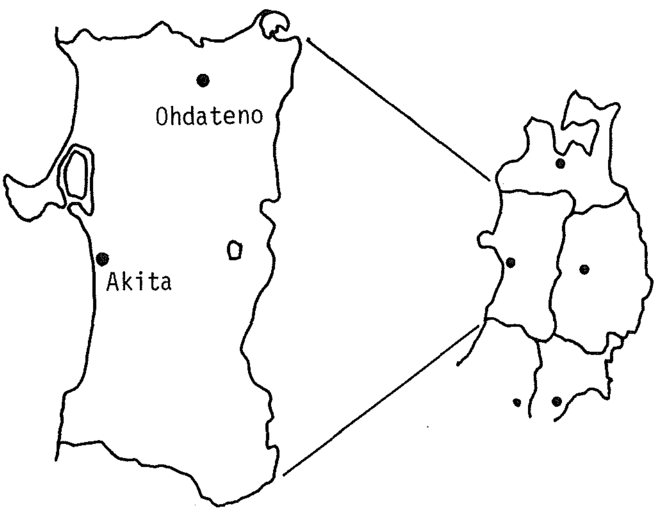

Fig.1 Ohdateno is in the northern part of Akita Prefecture in Japan.

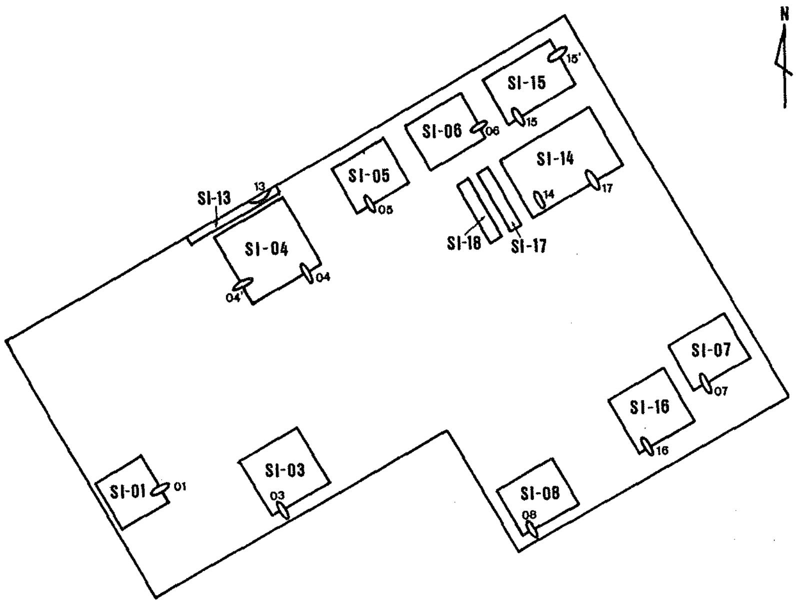

Fig.2 Samples were collected in the furnaces. SI means a house. An oval-shaped mark indicates a furnace. All samples were collected from the furnaces.

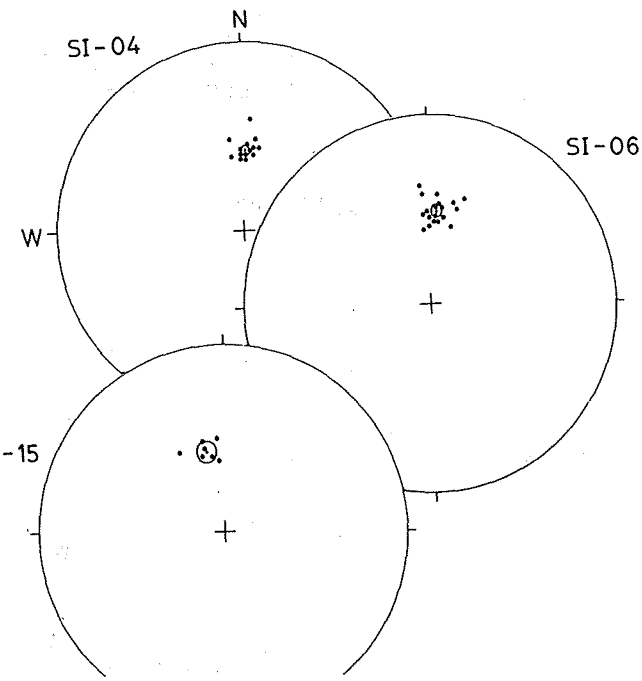

Fig.3 Examples of results obtained after alternating field demagnetization. Mark (+) indicate mean inclinations and declinations. α_{95} confidence circle is also indicated.

Table I summarized the results. Figure 4 showed the mean inclinations and declinations. We applied correction in declination and inclination values, which were determined assuming that the Earth's magnetic field is a dipole field, to the results of Hirooka (1971). It may be concluded that SI-17 and SI-15 are older than others.

Reference

Hirooka, K. (1971) Mem. Fac. Sci., Kyoto Univ., Ser. Geol. Mineral., 38, 167.

Table I Archeomagnetic results of Ohdateno remain.

Sample	N	Dec	Inc	k	α_{95}
SI-15	7	-12.366	54.164	147.853	4.981
SI-06	19	5.682	49.217	105.937	3.276
SI-14	4	2.896	52.124	373.149	4.763
SI-15'	5	5.505	60.501	54.118	10.494
SI-04	14	3.592	54.404	213.753	2.725
SI-04'	5	12.633	51.526	21.046	17.069
SI-03	6	6.259	50.379	260.067	4.162
SI-01	7	1.033	55.417	24.523	12.433
SI-13	3	30.221	54.004	24.304	25.568
SI-07	6	21.113	53.261	92.353	7.008
SI-08	7	11.719	50.310	292.175	3.537
SI-05	10	12.810	53.049	57.225	6.440
SI-17	3	-16.256	49.860	65.121	15.402

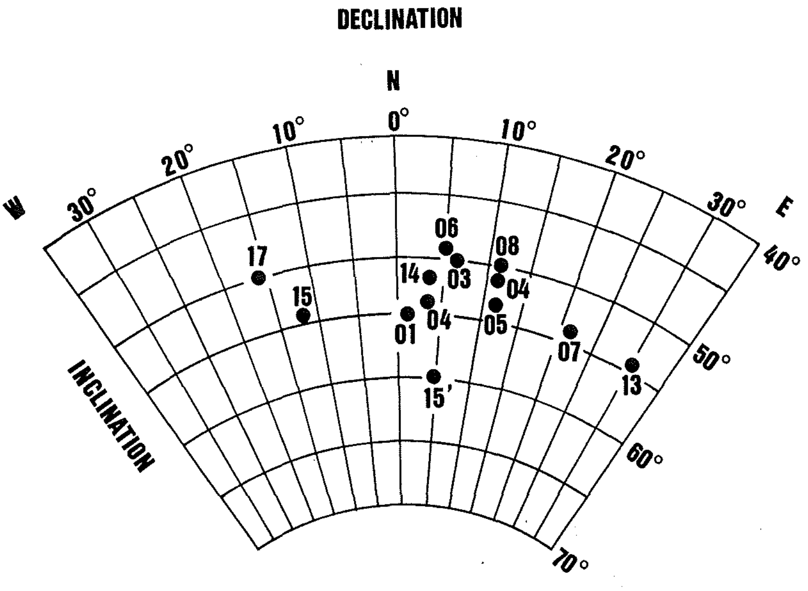

Fig. 4 Results of mean inclinations and declinations.

A GEOMAGNETIC EXCURSION RECORDED IN A STALAGMITE (SPELEOTHEMS) COLLECTED FROM WEST AKIYOSHI PLATEAU, JAPAN

Hayao MORINAGA[1], Ikuko HORIE[2], Haruko MURAYAMA[2], and Katsumi YASKAWA[2]

1. The Graduate School of Science and Technology, Kobe University, Nada, Kobe 657, Japan
2. Faculty of Science, Kobe University, Nada, Kobe 657, Japan

1. Introduction

The existence of the geomagnetic excursion has been demonstrated mainly by paleomagnetism of sediments and partly by paleomagnetism of volcanics. A few problems, however, have been indicated; the possibility that magnetic phenomenon like an excursion is spuriously recorded in unconsolidated sediments because they are easy to distort physically and the lack of 'temporal consistency' and 'spatially consistency' of proposed excursions (Verosub and Banerjee, 1977).

Some excursions detected in sediments and volcanics; Mono Lake excursion (Denham and Cox, 1971) and La Champ excursion (Roperch et al., 1988) may be true phenomena of the geomagnetic field. Some interests are still unclear; their occurrence was global or regional, how was their fine-scale behavior, when they occurred and how long they lasted? This is caused by detection of excursions in unconsolidated sediments whose remanent magnetization seems to be a result of a convolution integral of the geomagnetic field variation and a moment fixing function (Hyodo, 1984), and in volcanics which record only a short-time aspect of the geomagnetic field. It is very important to detect a high-quality record of excursions in continuously growing materials with a high time-resolution.

Speleothems (secondary deposits of limestone cave) continuously grow like sediments. Small amount of magnetic particles are mixed into their growth layers and carry stable remanent magnetizations. Some paleomagnetic studies (Latham et al., 1986; Morinaga et al., 1989) have reported that the remanent magnetization of speleothems is a fossil of the geomagnetic field at deposition of thin growth layers of calcium carbonate and that speleothems are useful for clarifying the past geomagnetic field variation.

We got a stalagmite (one of speleothems) collected from an unnamed limestone cave in West Akiyoshi Plateau, Yamaguchi Prefecture, Japan through a souvenir processing company. When we investigated the magnetic stability and the reliability of the remanent magnetization of the sample, we detected the magnetic recording like a geomagnetic

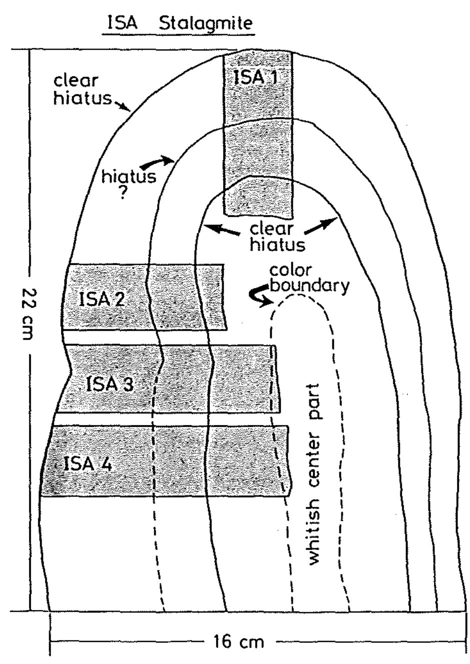

Figure 1 Schematic view of the vertical section of the stalagmite sample, showing three clear growth layers (hiatuses).

excursion.

2. Stalagmite sample and magnetic measurement

The stalagmite had a conical (a hanging bell like) shape, with a diameter less than 16 cm and a height of 22 cm (Figure 1). Three clear growth layers were observed by visual inspection. These clear growth layers may correspond to growth hiatuses. The stalagmite sample was easily divided into blocks at two of three clear growth layers; outer and inner layers. This suggests the existence of considerably long-period growth hiatuses. As the outer (younger) part of a few centimeter thick than the outer clear growth layer had been almost stripped and lost when we got the stalagmite sample, we were able to obtain the geomagnetic information in the corresponding period. The center part of the stalagmite sample is whitish owing to a very small amount of impurities and therefore is not suitable to measure its remanent magnetization. $^{234}U/^{230}Th$ dating method was performed on the sample taken out from the center part.

Four time-equivalent samples were drilled from the stalagmite sample; one of them drilled vertically and three drilled horizontally. Each drilled sample was of 2.5 cm diameter and 6.5～11.5 cm in length. The growth layers of time-equivalent samples had similar patterns, so that simultaneous growth layers could be identified in respective samples from their characteristic patterns. The growth layers' patterns for four samples (ISA-1, -2, -3 and -4) are shown in Figure 2. These four samples were cut by a diamond blade into 96 thin disc subsamples of 2.0～3.0 mm thick in order to measure their remanent magnetizations.

Magnetic measurements were carried out using a cryogenic magnetometer whose sensitivity is 10^{-11} Am^2. Progressive alternating field demagnetization (AFD) was performed on all disc subsamples in order to examine the magnetic stability and to define the characteristic component of their magnetization. During the progressive AFD, only 6 disc subsamples, which had weaker remanent magnetization intensities by one to two orders than normal subsamples, showed no stable component and therefore was not used in latter discussion.

All the rest subsamples had a fairly to rather stable component. The directions of the components changed only slightly during demagnetizing up to 40 mT (partly up to 80 mT) and showed a Fisherian

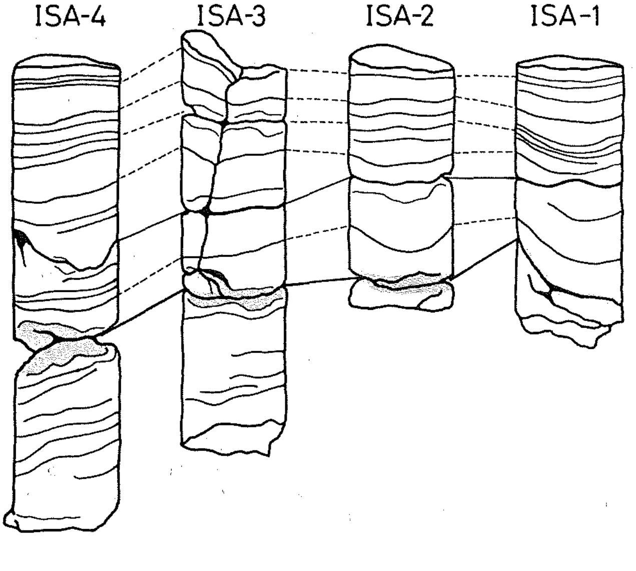

Figure 2 Growth layers observed in four drilled samples. Lines indicate correspondence of simultaneous growth layers and solid lines indicate correspondence of clear growth layers (hiatuses).

distribution on the stereographic net. We determined the AF level range of the Fisherian distribution of the direction on the net by visual inspection and calculated the characteristic direction for each subsample, which was a unit vectorial average of the data after AFD in the AF levels of the range.

3. Results and discussion

The characteristic direction variations along the drilled sample axes were consistent with each other, according to the correspondence of growth layers observed for four drilled samples. Consistency of the paleomagnetic results for a vertically drilled sample with those for three horizontally drilled samples implies that the remanent magnetization of the stalagmite is apparently unaffected by dip of the stalagmite surface. The positions of all subsamples were adjusted to distance from the surface of a 'master' sample (ISA-4) by stretching and compressing the data. All the results of direction (relative declination and inclination) for 90 subsamples are shown in Figure 3. Solid lines in this figure show smoothed variations by the vectorial running-means method of a 5.0 mm length, shifted with a 2.5 mm step. Arrows in this figure indicate the positions of growth hiatuses identified by visual inspection. The intermediate clear growth layer may not correspond to so long-period growth hiatus, because of the smooth change of the direction data at the position.

In the inner (older) part than the clear growth hiatus of 6.5 cm distance from the surface, relative declination rotates by about 180° and

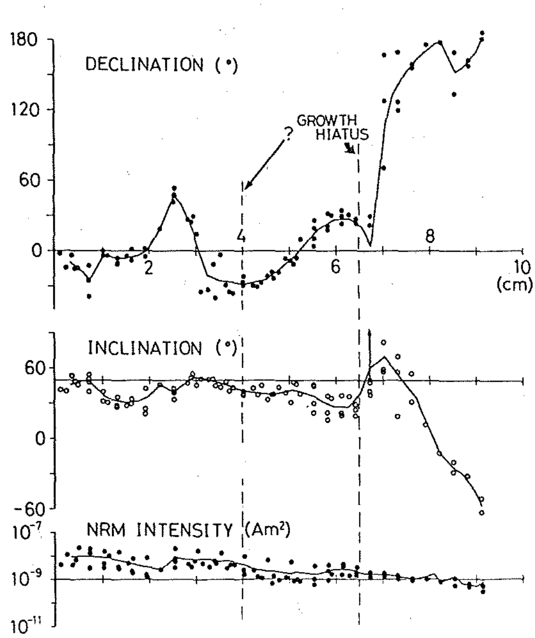

Figure 3 Direction data of 90 subsamples from four drilled sample. In the older (inner) part than the inner growth hiatus, the direction data gradually rotate in an opposite direction.

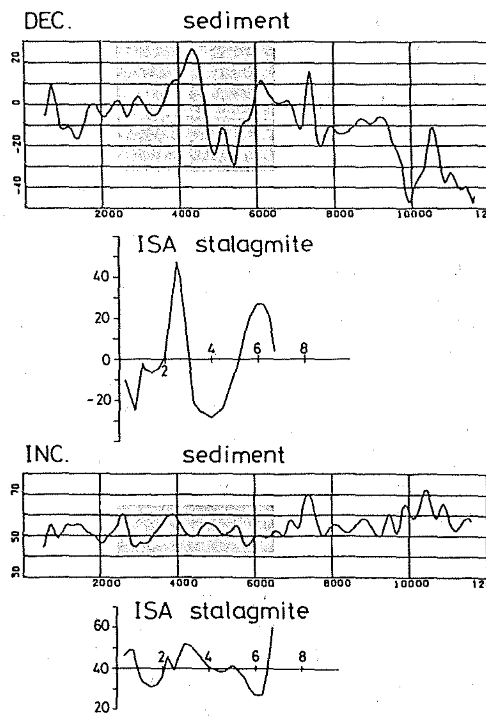

Figure 4 Tentative correlation between the direction variation for the stalagmite described in the present study and that (shaded zone) from paleomagnetism of unconsolidated sediments (M. Hyodo, personal communication).

sign of inclination becomes reversed. This suggests the existence of some geomagnetic reversal recorded in the stalagmite. The direction variation for the outer (younger) part than the position of about 6.5 cm distance from the surface is fairly well correlated with the geomagnetic secular variation record for 4000 years of 6500 to 2500 yr. BP (Figure 4), which has been obtained from paleomagnetism of unconsolidated sediments in Japan (Masayuki Hyodo, personal communication). This fairly good correlation show that the inner growth hiatus was over 6500 yr. BP and that the geomagnetic reversal occurred at the older time before 6500 yr. BP. The inner growth hiatus may correspond possibly to the last glacial period, when ground water scarcely flowed into the limestone cave. The growth layers recording the geomagnetic reversal may correspond possibly to the former interglacial period.

A $^{234}U/^{230}Th$ age for the whitish center part is about 302 (+inf., -123) ka. Because of the low isotopic ratio of $^{230}Th/^{232}Th$ (11.2), which indicates probably a contamination of the dated sample by detritic sediments with the possibility of a source of ^{230}Th different from a disequilibrium source, it is possible that the age is between 300 and 350 ka but the most probably is older. The $^{234}U/^{230}Th$ dating method was performed on the growth layers recording the geomagnetic reversal. However, the analysis of the sample had no good result because of the very low $^{230}Th/^{232}Th$ ratio of 4.5, which indicates the possibility of contamination by detritic Th. Datations were made by CERAK, Centre d'Etudes et de Recherches Appliquees au Karst, Faculte Polytechnique de Mons, rue de Houdain, 9, B-7000 MONS- Belgique.

On the basis of this age, the geomagnetic reversal seems to be an excursion younger than 300 to 350 Ka. Some excursions (or events) have been detected in a sediment core from Lake Biwa; their ages are about 18, 49, 110, 180 and 295 Ka (Nakajima et al., 1973; Yaskawa, 1974; Yaskawa et al., 1973). The detected excursion in the stalagmite may correspond to one of them, although the correspondence can not be defined.

Anyhow, it is very significant to detect a geomagnetic excursion (reversal) in other material different from unconsolidated sediments and volcanics. The geomagnetic reversal is situated at the distance of 7~9 cm from the surface. On the basis that the younger (outer) part than the inner clear growth layer (hiatus) of 6.5 cm distance from the surface may correspond to duration of about 4000 years, duration of the geomagnetic reversal can be calculated to be about 1200 years. The virtual geomagnetic pole during the geomagnetic reversal passed nearly along the meridian on Japan from the South hemisphere to the North hemisphere (Figure 5).

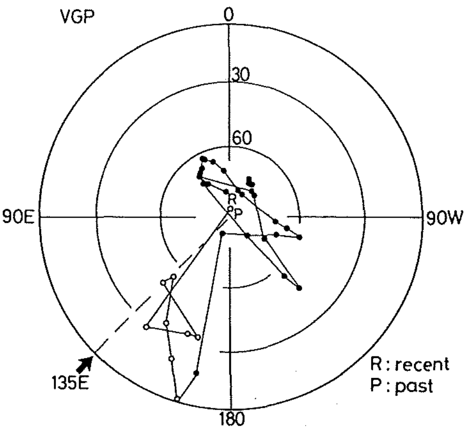

Figure 5 Equal-area plot of the virtual geomagnetic poles from the stalagmite described in the present study.

References

Denham, C.R. and A. Cox (1971) *Earth Planet. Sci. Lett.*, **13**, 181.

Hyodo, M. (1984) *J. Geomag. Geoelectr.*, **36**, 45.

Latham, A.G., H.P. Schwarcz, and D.C. Ford (1986) *Earth Planet. Sci. Lett.*, **79**, 195.

Morinaga, H., H. Inokuchi, and K. Yaskawa (1989) *Geophys. J.*, **96**, 519.

Nakajima, T., K. Yaskawa, N.

Natsuhara, N. Kawai, and S. Horie (1973) *Nature Phys. Sci.*, **244**, 8.
Roperch, P., N. Bonhommet, and S. Levi (1988) *Earth Planet. Sci. Lett.*, **88**, 209.
Verosub, K.L. and S.K. Banerjee (1977) *Rev. geophys. Space Phys.*, **15**, 145.
Yaskawa, K. (1974) *Paleolim. Lake Biwa Japan. Pleist.*, 2, 77.
Yaskawa, K., T. Nakajima, N. Kawai, M. Torii, N. Natsuhara, and S. Horie (1973) *J. Geomag. Geoelectr.*, **25**, 447.

(To be submitted to J. Geomag. Geoelectr.)

PALEOENVIRONMENTAL SECULAR CHANGE IN CH'I-LIN-TS'O, TIBET AS INFERRED FROM PALEOMAGNETISM AND STABLE ISOTOPE ANALYSIS

Chizu ITOTA[1], Hayao MORINAGA[1], Minoru KUSAKABE[2], Fumiyuki MURATA[1], Satoru YAMAGUCHI[3], Nobuhiro ISEZAKI[4], Hiroya GOTO[5], and Katsumi YASKAWA[4]

[1]The Graduate School of Science and Technology, Kobe University, Kobe 657, Japan
[2]Institute for Study of the Earth's Interior, Okayama University, Misasa 682-02, Japan
[3]Teikoku Women's Junior college, Moriguchi Osaka 570, Japan
[4]Department of Earth Sciences, Faculty of Science, Kobe University, Kobe 657, Japan
[5]Faculty of Liberal Arts and Sciences, Kobe University, Kobe 657, Japan

Ch'i-Lin-Ts'o (Siling Co) is a closed lake in Tibet, China. In August 1988, bottom sediments were collected from Ch'i-Lin-Ts'o using a pneumatical piston corer with an aim to obtain useful information of paleoenvironmental secular change in Tibet.

Three cores were collected; CH8801, CH8802 and CH8803. Two cores were long (3m) and one was short (1m). CH8803 core was longer one and the sediments were composed of black to grayish white clay. CH8801 core was longer, too, but the sediments were coarser than those of CH8803 core (sand to silt). In this paper we report the results of paleomagnetic study and stable isotope analysis carried out for CH8803 core.

PALEOMAGNETIC STUDY

Ninty-nine sequential paleomagnetic samples were collected from one side of replicated cores in $2.2\times 2.2\times 2.2$ cm^3 non magnetic polycarbonate boxes. Natural remanent magnetization (NRM) of the samples were measured with a ScT cryogenic magnetometer. The majority part of samples has NRM intensities ranged from 10^{-7} to 10^{-6} Am^2/kg. The rest part of samples has more intense NRMs (Fig.1).

Twenty-seven pilot samples were subjected to a stepwise alternating field (AF) cleaning, at levels of 3, 6, 9, 12, 15, 20, 25, 30, 35, 40, 45, 50, 55 and 60 mT (Fig.2). At lower AF levels, directions of

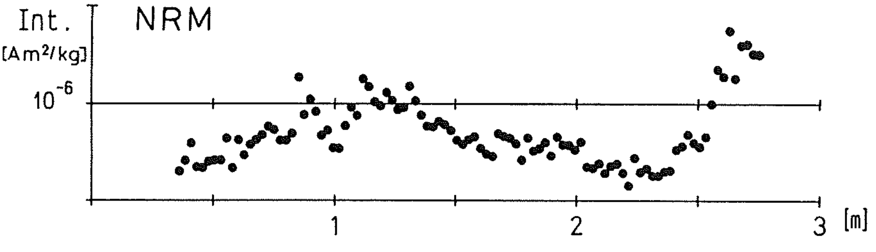

Figure 1. NRM intensity in log scale as a function of depth in meter measured from the top of the core tube.

remanent magnetization are considerably stable. At higher AF levels, the directions are scattered. Stable components of remanent magnetization are obtained between 3-6 to 9-30 mT AF levels for each sample.

All the rest samples were subjected to a stepwise AF cleaning at levels of 3, 6, 9, 12, 15, 20, 25 and 30 mT. Directional deviations between adjacent samples are fairly large. Running mean curves of the directions after AF cleaning below 12 mT AF level seem to represent the same variation pattern with each other (Fig.3(a)). Above 12 mT level the variation patterns are different from each other (Fig.3 (b)). These deferences would be attributed to instability of each sample's remanent magnetization after high AF levels' cleanings. Average direction for each sample was calculated using remanent magnetizations measured after AF cleanings ranged from 6 mT to 12 mT (Fig.3(c)).

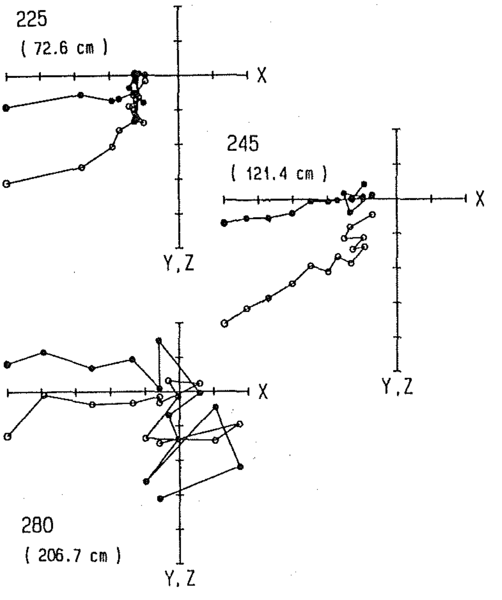

Figure 2. Typical orthogonal vector component diagrams for stepwise AF cleaning. Closed circles represent end point of remanence vector projected on to a plane perpendicular to core axis (X-Y plane). Open circles projected on to a vertical plane (X-Z plane).

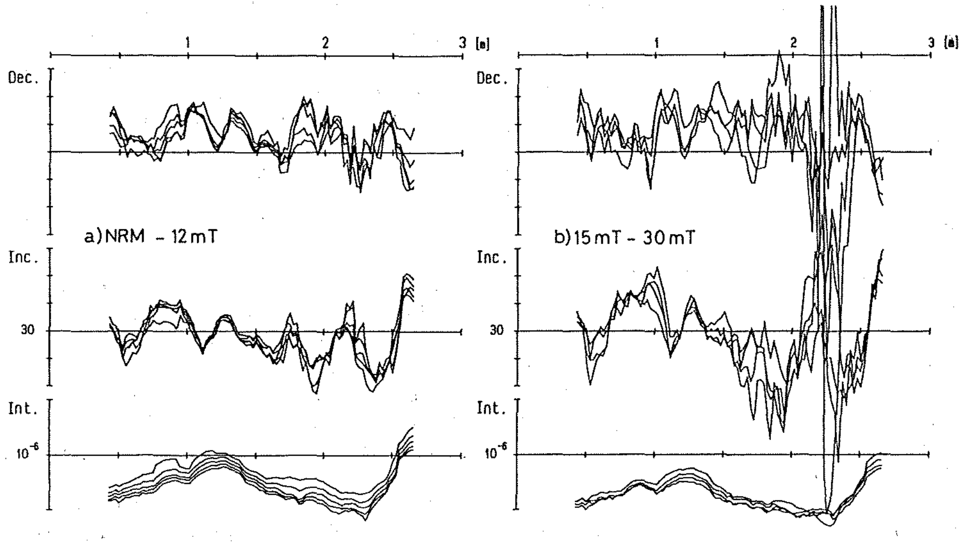

Figure 3. Change in relative declination, relative inclination and intensity after AF cleaning at levels of (a)0, 3, 6, 9 and 12mT; (b)15, 20, 25 and 30mT, smoothed with a seven-point running mean, corresponding to a 15cm averaging interval. Declination and inclination axis are marked every ten degrees.

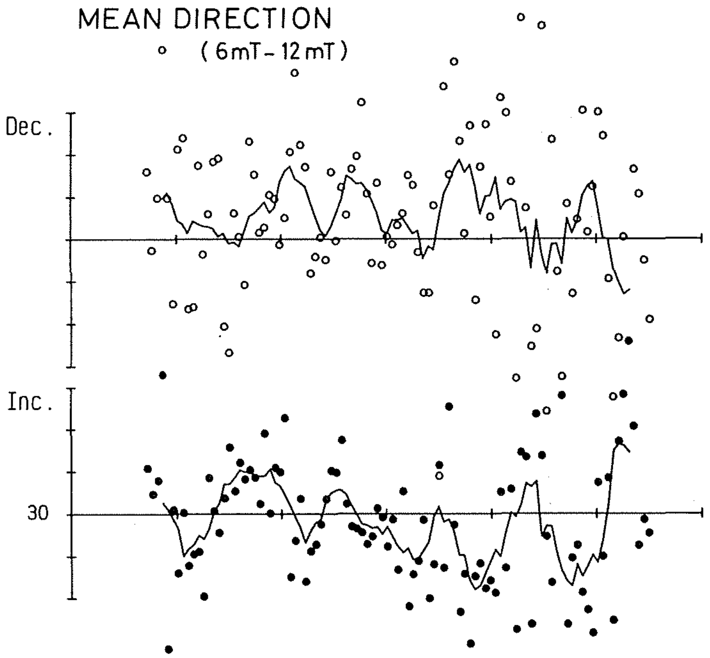

Figure 4. Relative declination and inclination as a function of depth. Mean direction are unit vectorial average for AF data ranged from 6mT to 12mT. Open circles represent relative declination values and closed circles represent relative inclination values. Solid lines denote seven-point running mean.

Average directions are still highly dispersed through the core. Sample cases had arranged unidirectionally through transportation from sampling site to our laboratory and through storage at the laboratory. If samples had remagnetized between sampling and magnetic measurement, resultant viscous components must have the same effect on the remanent direction. Scattered directions cannot be attributed to this sort of remagnetization. This dispersed pattern would reflect paleogeomagnetic secular variation itself. The directions might have been scattered, of course, by random magnetic noises acquired at and after deposition of the sediments, and/or by sampling and measurement errors. Some averaging technique such as sample mean and running mean can diminish such random noises.

STABLE ISOTOPE

$^{13}C/^{12}C$ and $^{18}O/^{16}O$ ratios in $CaCO_3$ deposited from supersaturated water are depend on their ratios in the mother water and its temperature. Standardized $^{13}C/^{12}C$ ratio ($\delta^{13}C$) and standardized $^{18}O/^{16}O$ ratio ($\delta^{18}O$) are good indicators of paleoenvironment.

The stable isotope analysis was performed on using the same samples used for paleomagnetic measurement. Only even numbered samples were used for this analysis. The results of $\delta^{13}C_{PDB}$, $\delta^{18}O_{SMOW}$ and CO_2 gas recovery rate are plotted in figure 4.

CO_2 gas recovery rates reflect the volume of $CaCO_3$ contained in sediment. Variation of the recovery rates contrast with the NRM intensity variation. This fact supports the idea that the NRM intensity reflect the concentration of magnetic minerals.

On the basis of changes of $\delta^{13}C$, $\delta^{18}O$ and CO_2 gas recovery rate, CH8803 core was divided into three sections.

First section (I) is correspond to depth level ranged from bottom of the core to 2 m. This section is characterized by rapid decrease of $\delta^{18}O$, increasing $\delta^{13}C$ and unstable recovery rate. Instability of the

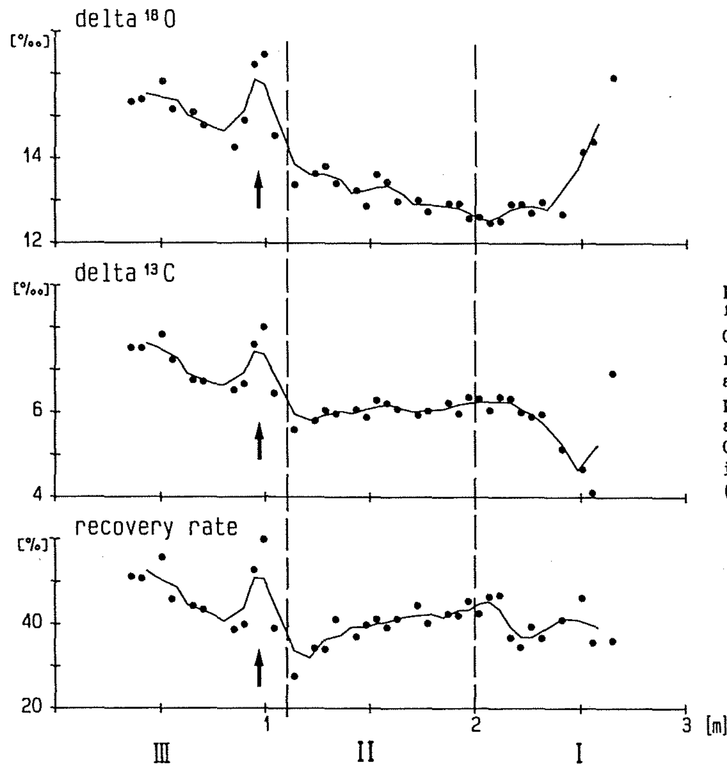

Figure 5. $\delta^{18}O$ and $\delta^{13}C$ profiles of total CO_2 and CO_2 gas recovery rate profiles. The average curves (five-point running mean) are also shown (solid line). CH8803 core was divided into three sections (dashed line).

recovery rate might reflect the disturbance of lake water volume caused by inflow of sediments and water, and heavy rain fall.

Second section (II) is correspond to depth level ranged from 2 m to 1.1 m. This section can be regarded as the period of stable environment. There are slight increase in $\delta^{13}C$ and slight decrease in $\delta^{18}O$. During this epoch the environment around Ch'i-Lin-Ts'o would have been controlled under steady state.

Third section (III) is correspond to depth level upper than 1.1 m. In this section variations of three variables agree with each other. Increasing $\delta^{13}C$ and $\delta^{18}O$ indicate that supply of light water (low $\delta^{13}C$ and $\delta^{18}O$; i.e. rain) generally decreased and/or evaporation of light water and degas of light CO_2 generally flourished in this period, though in short time inflow of water and rain fall increased and therefore lake water was diluted isotopically (indicated by arrows in figure 5). It may suggest the existence of the dry environment more lately in Tibet.

(to be submitted to Earth Planet. Sci. Lett.)

PALEOINTENSITY AT THE 75,000 YEARS B.P.

Hideo SAKAI
Department of Earth Sciences, Faculty of Science
Toyama University, Toyama 930

The paleointensity of the paleolithic age was obtained at the Douara site (34°38.5'N, 38°27.5'E) in Syria. The oriented samples were collected from the baked earths in the fireplace at the Douara cave (Akazawa and Sakaguchi, 1987). The mean NRM direction shows the Declination of 11.8° and Inclination of 53.5°. The paleointensities were estimated by the Thellier's method. The results in Table 1 indicate that the geomagnetic intesity was about 65% of the present. The age of this Douara site was determined by three methods. The age by both C14 method and TL method shows that this site is older than 50 thousands years B.P. Fission track age by Nishimura (1979) suggested the age of 75,000 years B.P.

Table 1. Results of the paleointensity experiments by the Thellier's method.

Specimens with the same integral number were cut from the same block sample of baked earth. F: determined past geomagnetic intensity; Fb: standard error of intensity; T1 and T2: temperature interval where NRM-TRM relation is linear; N: the number of points in this temperature interval; C.C: coefficient of correlation of the points.

Specimen NO.	T1 – T2 (°C)	N	C.C	F* (μT)	Fb (μT)
1.1	0 320	7	0.997	28.7	1.0
1.2	60 380	6	0.991	34.1	2.3
1.3	0 320	7	0.996	32.8	1.2
2.1	60 320	5	0.993	24.0	1.6
2.2	undetermined				
3.1	0 260	6	0.992	23.0	1.4
3.2	0 380	7	0.997	28.8	1.0
3.3	0 320	7	0.993	26.9	1.4
4.1	0 430	9	0.996	36.2	1.2
4.2	0 380	7	0.979	29.6	2.8
4.3	0 430	8	0.994	29.2	0.9
5.1	0 150	4	0.951	38.4	8.8
5.2	undetermined				
6.1	0 150	4	0.997	39.9	2.3
6.2	undetermined				
7.1	0 210	5	0.998	22.7	2.0
7.2	0 210	5	0.958	35.8	6.2
8.1	0 430	9	0.991	23.5	1.2
8.2	0 320	6	0.936	26.8	4.5

Averaged past-geomagnetic intensity
$F=29.4\pm4.1\ \mu T$
* Data with N(>7) and C.C(>0.99) were used for the calculation.

Figure 1 shows the paleointensity obtained from the Douara site and the previously summarized data by McElhinny and Senanayake (1986). The large intensity around 30 thousands B.P. is considered to be caused by the lake Mungo excursion (Barbetti and McElhinny, 1976). Figure 1 indicates, besides the large intensity around Mungo event, the weak intensity is dominant from 75,000 to 20,000 B.P. Barbetti and Flude (1979) calculated the effect of the paleointensities on the radiocarbon age by the method of Lingenfelter and Ramaty (1970). They suggested if the paleointensity before 50,000 B.P. is as weak as that of 50,000 B.P., the age between 50,000 and 20,000 B.P. estimated by C14 method may be few thousands years younger than the absolute age. The low intensity at 75,000 years B.P. suggests this possibility. The preliminary data from the volcanic rocks in Hokuriku district (Ogawa and Sakai, in prep.) show that the paleointesity around 120 thousands B.P. was similar to the present value, which indicates the dominant low intensity has possibly existed from the age older than 75,000 years B.P.

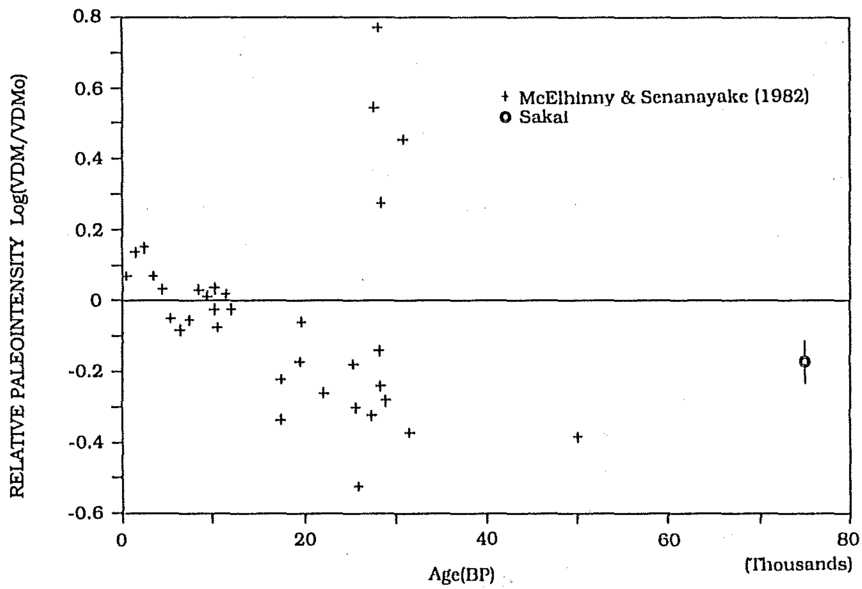

Figure 1. The paleointensity obtained from the Douara site and the paleointensities summarized by McElhinny and Senanayake (1982). The age of Douara site was estimated by Nishimura (1979).

References

Akazawa, T. and Y. Sakaguchi (1987) Paleolithic site of the Douara cave and paleogeography of Palmyra basin in Syria, part IV: 1984 excavations (University of Tokyo Press), 166.

Barbetti, M. and K. Flude (1979) Nature, 279, 202.

Barbetti, M. and M.W. McElhinny (1976) Philos. Trans. R. Soc. Lond. A, 281, 515.

Lingenfelter, R.E. and R. Ramaty (1970) Radiocarbon variations and absolute chronology; ed. Olsson, I.U. (Almquist and Wiksell), 513.

McElhinny, M.W. and W.E. Senanayake (1982) J. Geomag. Geoelectr., 34, 39.

Nishimura, S. (1979) Univ. Mus., Univ. of Tokyo, Bull., 16, 235.

PALEOMAGNETIC STUDY ON MIYAKO-JIMA ISLAND IN THE SOUTH RYUKYU ARC

Masako MIKI[1] and Yo-ichiro OTOFUJI[2]

1. The Graduate School of Science and Technology, Kobe University, Kobe 657, Japan
2. Department of Earth Sciences, Faculty of Science, Kobe University, Kobe 657, Japan

Paleomagnetic direction of Ishigaki-jima Island in the south Ryukyu arc shows that the area has undergone clockwise tectonic rotation since 10 Ma (Miki et al., 1989). The paleomagnetic study were carried out on Miyako-jima Island north-east of Ishigaki-jima Island, in an attempt to compare the paleomagnetic directions of the two islands.

Samples were collected from the Shimajiri Group (Fig. 1), for which the age of about 4 Ma were reported (Kuramoto and Konishi, 1989). The samples consist of fine clay from 20 sites and tuff from one site. Three

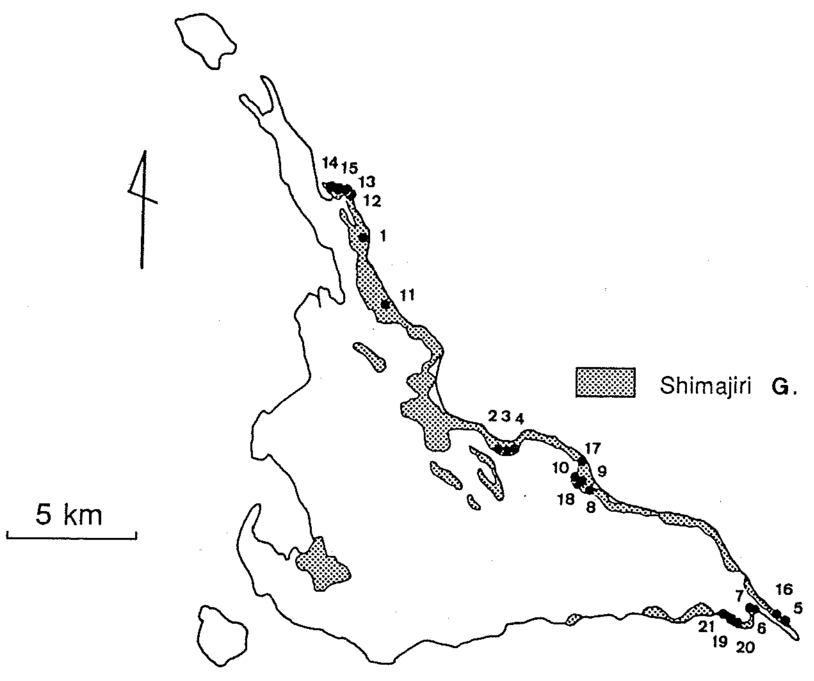

Fig.1 Map showing the distribution of the Shimajiri Group on Miyako-jima Island. Solid circles are sampling localities.

or four oriented large block samples were collected by hand sampling from each clay site. About ten 2.5 cm cubic specimens were cut from each block sample. Specimens were coated with acrylic fiber. Ten block samples were collected from the tuff site, and two or three 2.5 cm core specimens were cut from each block sample.

The stability of remanent magnetization was examined through progressive demagnetization of both alternating field and thermal technique. The orthogonal demagnetization plot shows well defined single magnetization component are resolved by both demagnetization methods (Fig.2). The component was taken by the principal component analysis by Kirschvink (1980).

Reliable paleomagnetic directions were obtained from 12 sites (Fig.3). Both normal and reversed polarity were observed. The mean direction after tilt correction is D = -1.5°, I = 27.0° and α_{95} = 12.5°. The direction shows no deflection from northward, contrasting with the clockwise deflection in the Eocene and 10 Ma paleomagnetic direction of Ishigaki-jima Island.

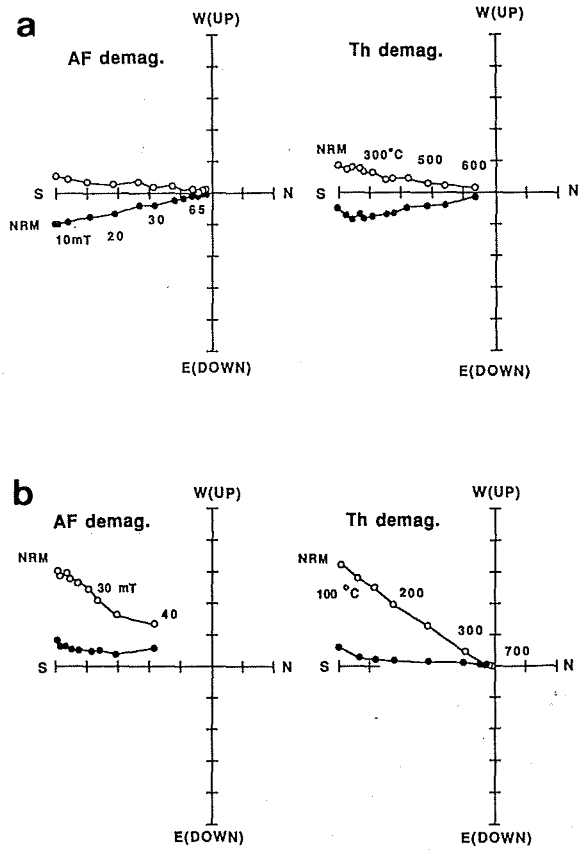

Fig.2 Typical examples of the orthogonal projection plots for NRM stability examinations. a: demagnetization path for a tuff sample. b: demagnetization path for a clay sample. Open (solid) symbols show the magnetic vectors projection on the vertical (horizontal) plane. Th demag = thermal demagnetization. AF demag = alternating field demagnetization.

The geomorphological data shows, that there are no such large fault as cut the Ryukyu arc between Miyako-jima Island and Ishigaki-jima Island (Hamamoto et al., 1979). Miyako-jima Island and Ishigaki-jima Island appears to be contained in one rigid block. The paleomagnetic results indicate that Miyako-jima Island has not rotated since 4 Ma. We concluded that 1) Miyako-jima Island has been subjected to the clockwise rotation together

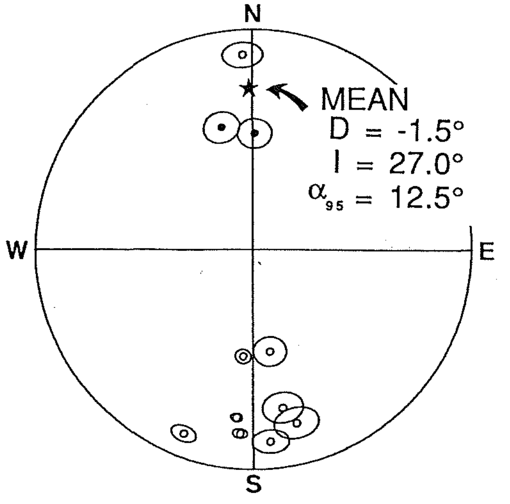

Fig.3 Site mean paleomagnetic directions with 95 % confidence circles from the Shimajiri Group on Miyako-jima Island. Projections are equal area, solid (open) symbols on the lower (upper) hemisphere. Star: mean direction.

with Ishigaki-jima Island as a rigid block since 10 Ma, 2) the rotation of south Ryukyu arc finished before 4 Ma.

References

Hamamoto, F., M. Sakurai and M. Nagano (1979) Report of Hydrographic Researches, 14, 1-38.

Kirschvink, J.L. (1980) Geophys. J. R. Astr. Soc., 62, 699-718.

Kuramoto, S and K. Konishi (1989) Tectonophysics, 163, 75-91.

Miki, M., T. Matsuda and Y. Otofuji (1989) Tectonophysics, in press.

PALEOMAGNETIC STUDY ON THE CENTRAL RYUKYU ARC
- KINEMATIC HISTORY OF THE RYUKYU ARC -

Masako MIKI[1], Shinya KONDO[2] and Yo-ichiro OTOFUJI[2]

1. The Graduate School of Science and Technology, Kobe University, Kobe 657, Japan
2. Department of Earth Sciences, Faculty of Science, Kobe University, Kobe 657, Japan

Paleomagnetic and Geochronological study were carried out on Tertiary rocks from Okinawa-jima Island and Kume-jima Island of the central Ryukyu arc, in an attempt to see the kinematic history of the Ryukyu arc. The south Ryukyu arc has been rotated clockwisely since 10 Ma (Miki et al.,1989). In this study, we determined the relative tectonic movement of the central Ryukyu with respect to the south Ryukyu arc.

More than 200 samples were collected from 21 sites. The samples consist of dike rocks (3 sites) and Miocene sedimentary rocks (1 site) from Okinawa-jima Island, and lava flows of the Aradake Formation (12 sites) and lava flows of the Uegusukudake Formation (5 sites) from Kume-jima Island.

The K-Ar whole rock dating was attempt on lava flows from Kume-jima Island. The amount of radiometric argon was measured using the method of Nagao and Itaya (1988). We obtained the age of 17.0 ± 0.4 Ma and 17.9 ± 0.4 Ma from the Aradake Formation, and the age of 2.2 ± 0.1 Ma from the Uegusukudake Formation.

Stability of remanent magnetization was examined through progressive demagnetization of both alternating field and thermal technique. The stable high temperature component was defined as a linear segment decaying

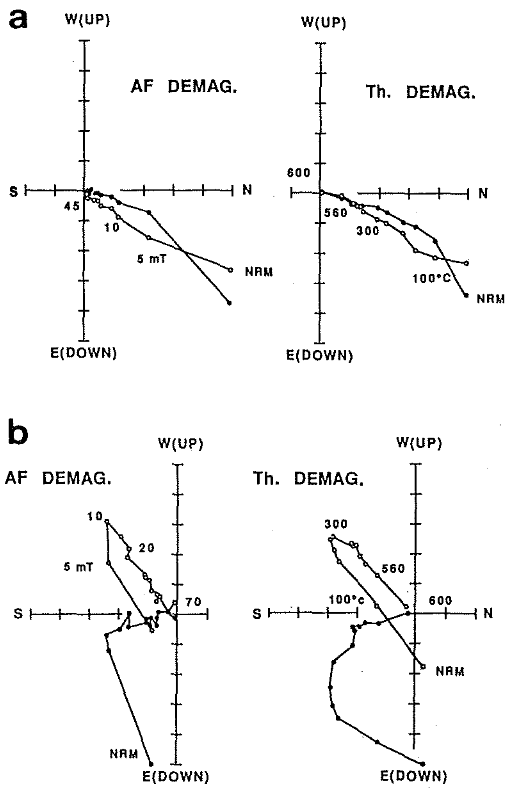

Fig.1 Typical examples of orthogonal projection plots for progressive demagnetization experiments. a:Lava flows of the Aradake Formation; b:lava flows of the Uegusukudake Formation. Th demag = thermal demagnetization. AF demag = alternating field demagnetization. Open (solid) symbols show the magnetic vectors projection on the vertical (horizontal) plane.

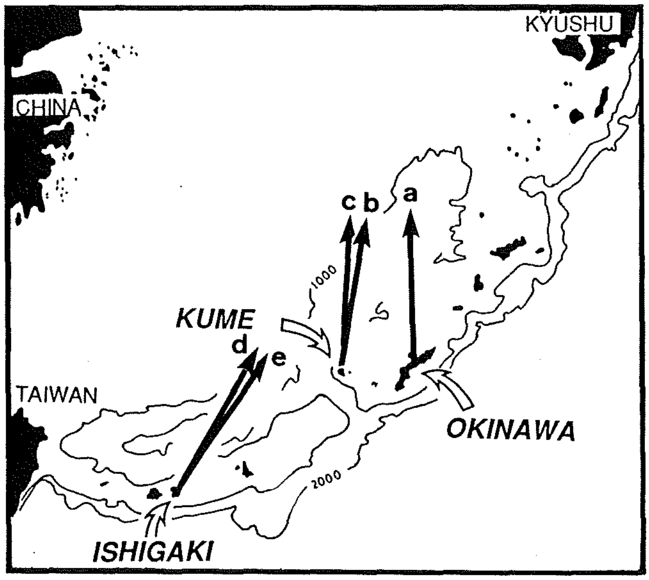

Fig.2 Declinations of the paleomagnetic directions for the Ryukyu arc. (a) Direction of a dike of 11 Ma from Okinawa-jima Island; (b) mean direction of the 17 Ma Aradake Formation; (c) mean direction of the 2 Ma Uegusukudake Formation. (d) Mean direction for the Eocene volcanics; (e) direction of a dike of 10 Ma (Miki et al., 1989).

toward the origin on the orthogonal plot (Fig. 1). The high temperature components were taken by the principal component analysis by Kirschvink (1980).

Reliable paleomagnetic directions were obtained from fourteen sites; D=-9.6°, I=48.5° from a dike rock with the age of 11 Ma (Daishi et al., 1982) on Okinawa-jima Island, D=8.5°, I=39.7°, α_{95}=9.8° from nine sites of the Aradake Formation and D=-1°, I=40.5°, α_{95}=33.6° from four sites of the Uegusukudake Formation on Kume-jima Island. These directions are almost same as the present axial dipole field direction.

These results indicate that the central part of the Ryukyu arc has undergone little rotation or translation since 17 Ma. Comparison with the paleomagnetic direction of the south Ryukyu arc (Fig. 2) suggests that the central Ryukyu arc has behaved as the different block from the south Ryukyu arc since 10 Ma.

References

Daishi, M. and M. Hayashi (1982) Geological Studies of The Ryukyu Islands, 6, 5-10.

Kirschvink, J.L. (1980) Geophys. J. R. Astr. Soc., 62, 699-718.

Miki, M., T. Matsuda and Y. Otofuji (1989) Tectonophysics, in press.

Nagao, K. and T. Itaya (1988) Mem. Geol. Soc. Japan, 29, 5-21.

FAST DRIFTING OF SOUTHWEST JAPAN
INFERRED FROM PALEOMAGNETISM AND K-Ar DATING

YO-ICHIRO OTOFUJI*, TETSUMARU ITAYA**
AND
TAKAAKI MATSUDA***

* Department of Earth sciences, Faculty of Science, Kobe University, Kobe 657, Japan
** Hiruzen Research Institute Okayama Branch, Okayama University of Science, Okayama 700, Japan
*** Department of Geology, Himeji Institute of Technology, Himeji 671-22, Japan

Miocene volcanic rocks have been sampled from the San'in district in the central part of Southwest Japan, in an attempt to evaluate the drifting velocity of Southwest Japan. Twenty nine localities have reliable data of both paleomagnetic direction and K-Ar dating. A declination value of 40.6° is observed in the Kawai Formation of 16.1 ± 1.4 Ma, whereas a northerly direction (D=1.8°) is in the Omori Formation of 14.3 ± 0.6 Ma. The Matsue Formation of 11.3 ± 0.3 Ma shows northerly declinations. These data indicate that Southwest Japan rotated clockwise 40° between 16.1 ± 1.4 Ma and 14.3 ± 0.6 Ma. Compared with the amount of rotation of Southwest Japan estimated on the basis of the Cretaceous paleomagnetic data (Otofuji and Matsuda, 1987), more than 80 % of the clockwise rotation of Southwest Japan occurred later than 16.1 Ma (Fig. 1).

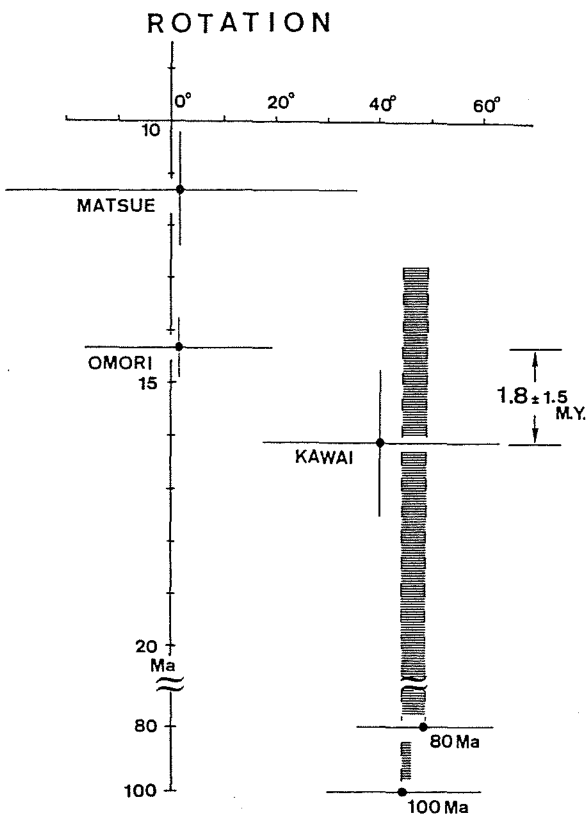

Fig. 1. Rotation with respect to eastern part of Eurasia versus age for geologic unit in the San'in district of Southwest Japan. The rotation error bars are the $\Delta R = \sin^{-1}(\sin \alpha_{95}/\cos(I))$ where I and α_{95} are inclination and radius of 95 % confidence about the mean direction. The age error bars are the 95 % confidence limit. Shaded rotation zone is amount of clockwise rotation of Southwest Japan with respect to eastern part of Eurasia estimated on the basis of the Cretaceous (80-100 Ma) paleomagnetic data (Otofuji and Matsuda, 1987).

The large rotational motion of 40° has spanned as little as 1.8 ± 1.5 Myr. The angular velocity of Southwest Japan about the rotation pivot of 129°E, 34°N reached 22°/Myr at about 15 Ma. We thus conclude that the eastern part of Southwest Japan moved at a rate of 23 cm/year. The high drifting velocity implies that the low viscous asthenosphere of the order of $10^{17} \sim 10^{19}$ Poise prevailed beneath the area of the Southwest Japan-Japan Sea system at about 15 Ma.

REFERENCES

Otofuji, Y. and Matsuda, T. (1987), Earth planet. Sci. Lett., 85, 289.

(submitted to Earth Planet. Sci. Lett.)

PALEOMAGNETIC STUDY AND FISSION-TRACK DATING IN YANAGAWA AND TAKADATE AREA, NORTHEAST JAPAN

Hirokuni ODA*, Masayuki TORII* and Akira HAYASHIDA**

*Department of Geology and Mineralogy, Kyoto University, Kyoto 606, Japan
**Laboratory of Earth Sciences, Doshisha University, Kyoto 606, Japan

Paleomagnetic study and fission track dating were carried out on the Miocene sediments and volcanic rocks in the Yanagawa and the Takadate areas, Northeast Japan. These areas are situated in the northern margin of the Abukuma massif which mainly consists of the Mesozoic granitic rocks. The Abukuma massif is bordered by two large tectonic faults. One is the Futaba fault on the eastern margin and the other is the Tanakura fault on the southwestern margin (Fig. 1).

In these areas, basalt, andesite and rhyolite lava flows and pyroclastic layers unconformably overlie the granitic basement and there are some intrusive rocks (Fig. 2). The Ryozen volcanic rocks are widely distributed in the Yanagawa area. Three K-Ar dates were reported for these rocks as 14.1, 15.0, and 21.7 Ma (Kimura, 1988). In the Takadate area, volcanic rocks of the Takadate Formation are distributed. K-Ar ages obtained from these rocks are 12.6, 15.2, 20.7, and 22.0 Ma (Uto et al., 1989).

The volcanic rocks are covered by the sedimentary rocks which contain large amount of volcanic material. In the Yanagawa area, the Yanagawa Formation cover the Ryozen volcanic rocks. The Yanagawa Formation consists of tuffaceous sands and silt. The sediments of the Yanagawa Formation is subdivided into three members (Suzuki and Wako, 1987). The lower member is the Hirosegawa Member which consists of coarse sand stone with many shell fossils. The middle part of the Yanagawa Formation is called the Isazawa Member which bears planktonic foraminifera and calcareous nannofossils. The upper part, the Ubagafutokoro Member, consists of pumiceous silt and sand stone. The Hirosegawa Member is correlated to Blow's N8 zone and the Isazawa Member to N9~N10 by Suzuki and Wako (1987). In Takadate area the Moniwa Formation which mainly composed of conglomerate covers the Takadate Formation unconformably. The Moniwa Formation bears N8 planktonic foraminifera fossil. The Moniwa Formation is covered with the Hatatate Formation. The Hatatate Formation mainly consists of tuffaceous fossiliferous silt (Kitamura et al., 1986). The lower most part of the Hatatate Formation is correlated to N9 and the middle part to N16 (Oda and Sakai, 1977).

We collected about ten hand-samples for paleomagnetic study from each site.

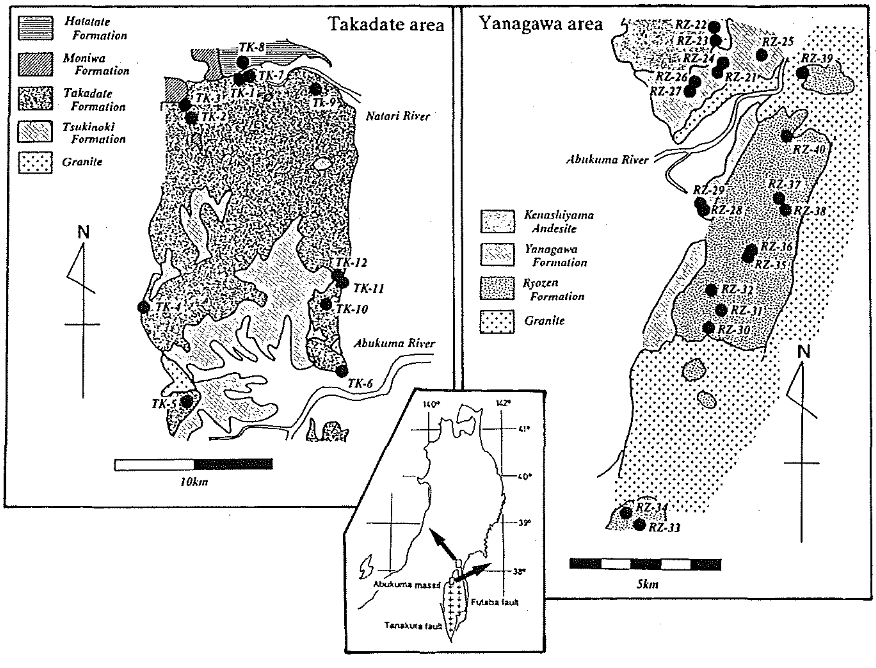

Fig. 1 Sample sites of the Yanagawa area (right) and the Takadate area (left). Base map is from Suzuki and Wako (1987) and Kitamura et al. (1986).

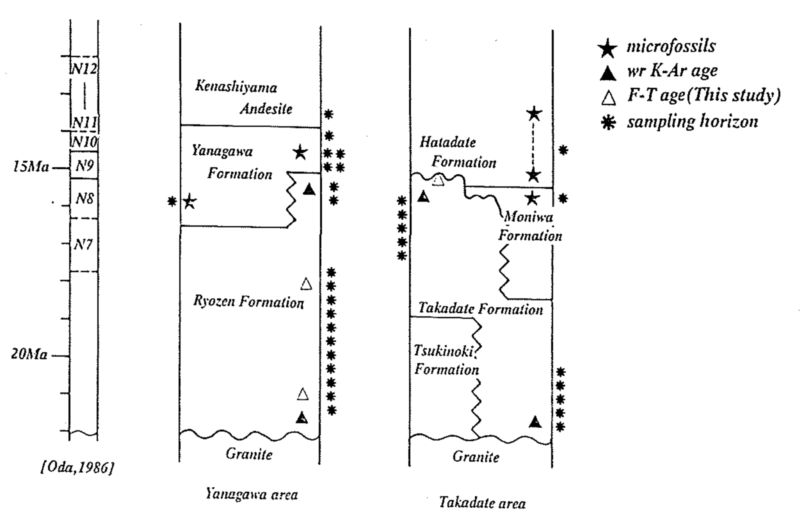

Fig. 2 Geologic columnar sections of the studied areas. Asterisks indicate sample sites. Star represents datum of the biostratigraphic control by microfossils (Suzuki and Wako, 1987; Oda and Sakai, 1978). Open and Solid triangles denote fission- track dates by the present authors and whole rock K-Ar dates (Kimura, 1988; Uto et al., 1989).

Samples for fission-track dating were collected to determine the ages of acidic volcanic rocks from three sites. Natural remanent magnetizations are measured using a cryogenic magnetometer (ScT C-112) and a spinner magnetometer (Schonstedt SSM-1A). Both alternating field demagnetization (AFD) and thermal demagnetization (ThD) were performed progressively on two or three pilot specimens from each site. We could obtain stable remanent magnetizations from the volcanic rocks. Some of the sediments also yielded stable components. The stability of the remanent magnetizations are confirmed on the orthogonal projections diagrams (Fig. 3). Tilt corrections are carried out only on the magnetic directions from the sediments. We rejected some sites which showed instability against progressive demagnetization process. We selected sites that gave stable magnetic components and whose AFD and ThD results agree well with each other.

Fission-track dating was carried out by external detector method (ETD) on zircon crystals using internal surface and calibrated by zeta-value (Table 1).

Paleomagnetic directions obtained from volcanic rocks indicate both clockwise and counter-clockwise deflection as shown in Fig. 4. The overlying sedimentary rocks, however, exclusively show clockwise deflected directions after untilting (Fig. 4). We think that the remanence of the sediments are reliable because of their stable and strong magnetization. The age of the clockwise deflected sediments are assumed to be N8 in terms of calcareous microfossils. Most of the reliable mean direction point clockwise from the present axial dipole field throughout the studied area except some sites from the Ryozen volcanic rocks (Fig. 4). This apparent inconsistency may be attributed to unsuccessful tilt correction for the volcanic rocks. However most of the remanence of the sedimentary rocks are of viscous nature. This fact may indicate another possibility to explain the clockwise deflection due to the viscous magnetization.

Otofuji et al. (1985) reported that Northeast Japan had rotated counter-clockwise about 50° between 20 Ma to 12 Ma as a result of the opening of the Japan Sea. Taking account the ages (N8) and the clockwise directions from the studied area, the areas rotated clockwise relative to the main part of the Northeast Japan. We interpreted this inconstant rotation to the fault movement along the Futaba fault whose maine tectonic phase has been estimated to be middle Cretaceous (Tsuneishi, 1978). If the Futaba fault was reactivated as a right lateral strike slip fault, the Yanagawa and Takadate areas could be rotated clockwise through mechanism called "ball bearing" (Beck, 1980) as shown in Fig. 5. Tsuneishi (1978) suggested that there were four tectonic stages in the movement of the Futaba Fault. His second stage (early Miocene) of the fault movement possibly brought about the block rotation of the studied areas. The second stage movement is characterized by the normal fault caused by the EW-trending tensional forces. However he could not find any line of evidence to indicate large-scale lateral motion of the Futaba Fault during middle Miocene. Otofuji et al. (1985) reported a

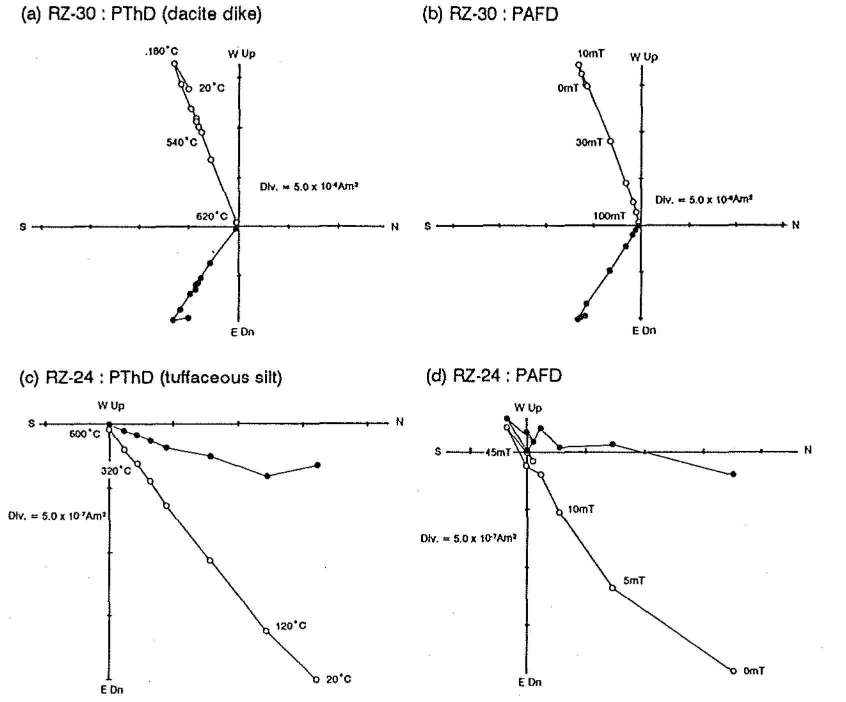

Fig. 3 Typical examples of progressive thermal demagnetization and progressive alternating field demagnetization, projected on the vector orthogonal diagrams. (a) and (b) show thermal and alternating field demagnetizations from the volcanic rocks, respectively. (c) and (d) show thermal and alternating field demagnetizations from the sedimentary rocks, respectively.

Sample name	N	spontaneous track density ($\times 10^6 cm^{-3}$)	indused track density ($\times 10^6 cm^{-3}$)	dosimeter glass track density ($\times 10^4 cm^{-3}$)	age(1σ) (Ma)	P(χ^2) (%)
BM4II	10	1.17	1.82	14.84	16.2±0.7	88
FCTZR6	6	5.72	5.50	14.84	26.3±1.3	2
RZ-34	8	3.51	2.67	8.82	19.8±0.9	9
RZ-30	7	2.61	2.10	8.82	18.7±1.1	1
TK-3	3	2.83	3.85	8.82	13.8±1.0	12

Table 1. BM4II and FCTZR6 are age standard samples. N is number of zircon grains measured. NBS-SRM612 is used for dosimeter glass. P(Kai^2) is probability of obtaining the observed value. We used 342.1 as zeta-value(Tagami, 1987).

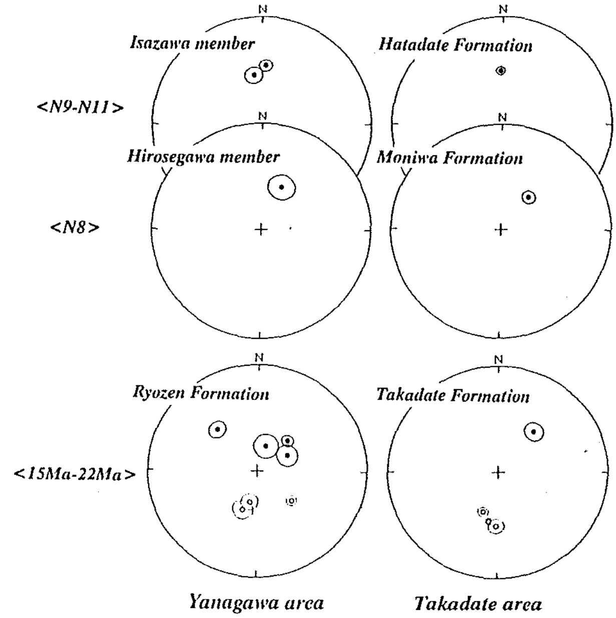

Fig. 4 Site-mean directions are illustrated on equal area projections. Directions from the sedimentary sites are untilted. Paleomagnetic directions are arranged from bottom to top in terms of their geologic age; bottom (15 - 22 Ma), middle (N8), and top (N9 - N11). Right side of the figure indicate the data from the Takadate area, and left from the Yanagawa area.

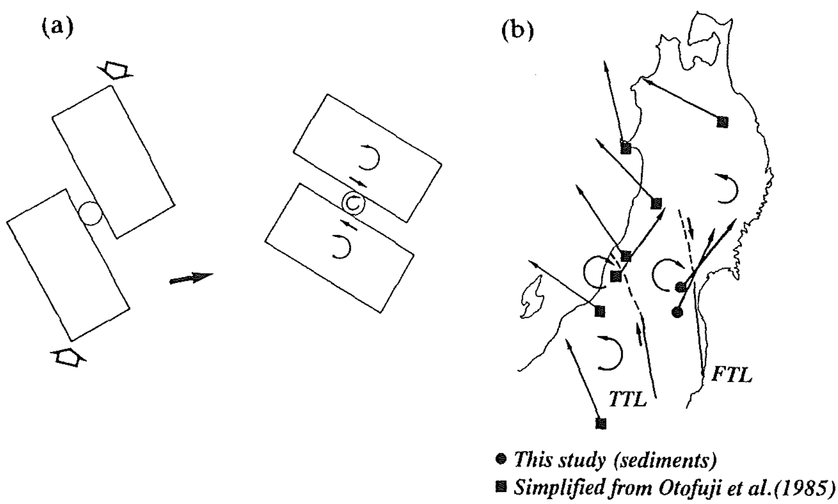

Fig. 5 "Ball-bearing" rotation of the crustal block. (a) Model showing "ball-bearing" rotation of a small block sandwicthed between two large fault-bounded blocks in a sense of Beck (1976). (b) Right lateral motion along the Futaba fault can explain clockwise rotation of the studied areas. Solid circles show the paleomagnetic directions from the sediments of the present study. Solid squares indicate paleomagnetic directions from Northeast Japan simplified from Otofuji et al. (1985).

couple of stable remanent magnetizations of clockwise deflected directions from the western Asahi mountain area. They explained those anomalous direction to the movement of the Tanakura fault which was activated by the opening of the Japan Sea. The anomalous paleomagnetic directions may reflect local-scale tectonics which cannot be detected by the previous geological studies. Detailed paleomagnetic study will reveal actual process of the crustal movement accompanied with the large-scale tectonic movement such as the opening of the Japan Sea.

References

Beck M.E. (1976) : Am. Jour. Sci., **276**, 694-712.

Kimura,K. (1988) : Rep. Tech. Res. Center, **15**, 14-17.

Kitamura,N., T.Ishii, A.Sangawa, H.Nakagawa (1986) : Geology of the Sendai district, Geol. Surv. Japan, 134p

Oda,M., T.Sakai (1977) : Prof. K.Fujioka Memorial Volume, Univ. Touhoku, 441-456.

Oda,M. (1986) : Prof. N.Kitamura Memorial Volume, Univ. Touhoku, 297- 312

Otofuji,Y., T.Matsuda, and S.Nohda (1985) : Earth Planet. Sci. Lett., **75**, 265-277.

Suzuki,K., R.Wako (1987) : Sci. Rep., Univ. Fukushima, Fac. Education, **40**, 33-48

Tagami,T. (1987) : Nucl. Tracks Radiat. Meas., **13**, 127-130.

Tsuneishi,Y. (1978) : Bull. Earthq. Res. Inst., Univ. Tokyo, **53**, 173-242.

Uto,K., K.Shibata and S.Uchiumi (1989) : Jour. Geol. Soc. Japan, **95**, 865-872.

PRELIMINARY RESULTS FROM PALEOMAGNETISM ON APPARENT POLAR WANDER PATH FOR THE SOUTH CHINA BLOCK

Yasuhisa ADACHI[1], Hayao MORINAGA[1], Yu Yan LIU[2], Guo Zhu FANG[2] and Katsumi YASKAWA[3]

1) The Graduate School of Science and Technology, Kobe University
1-1, Rokkodai-cho, Nada-ku, Kobe 657, Japan
2) China University of Geosciences (WUHAN)
Yujiashan, Wuhan, Hubei, People's republic of China
3) Department of Earth Sciences, Faculty of Science, Kobe University,
1-1, Rokkodai-cho, Nada-ku, Kobe 657, Japan

China is composed of several distinct continental fragments separated by accretionary fold belts (Zhang et al., 1984). Paleomagnetic study has been performed on sedimentary rocks from the Quaternary to the Precambrian formations to establish an apparent polar wander (APW) path for South China block. At the present, paleomagnetic data are few (McElhinny et al., 1981; Chan et al., 1984; Lin et al., 1985; Kent et al., 1986), specially for Paleozoic and Proterozoic, to establish the APW path for the South China block.

Oriented hand samples were collected from Wuchang (30.2°N, 114.3°E) and Jingshan (31.2°N, 113.1°E) counties in Hubei province (Fig.1). The sampling sites were distributed in formations of all the periods or eras from the Quaternary to the Middle Proterozoic respectively (84 samples from 17 sites)(Table 1). The lithofacies of the samples are mainly limestones and sandstones, only the Quaternary samples are unconsolidated clay sediments.

Remanent magnetizations of all specimens were measured with superconducting quantum interference device (SQUID). Natural remanent magnetization (NRM) of most specimens was stable and the intensities distributed

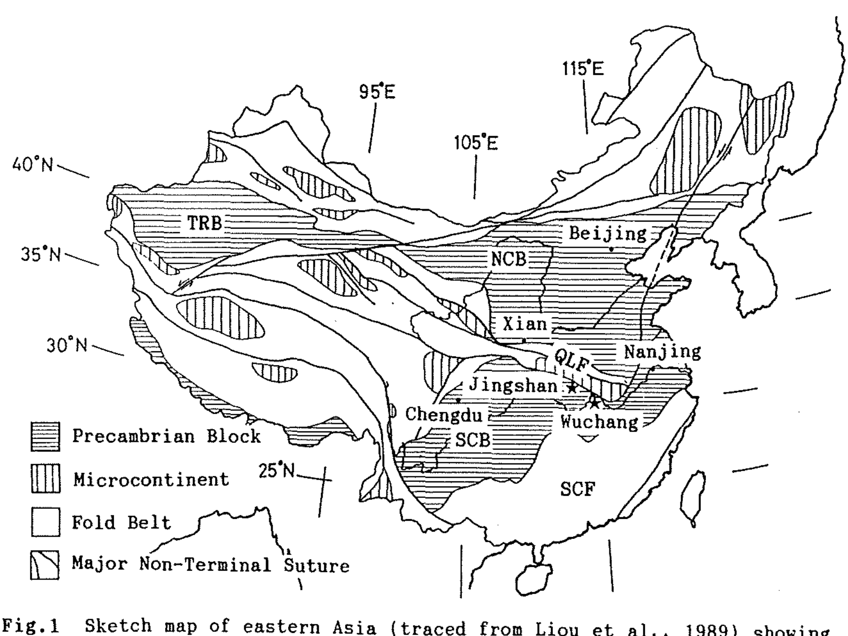

Fig.1 Sketch map of eastern Asia (traced from Liou et al., 1989) showing major tectonic units and paleomagnetic sampling localities (star symbols). SCB, South China block; NCB, North China block; TRB, Tarim block; QLF, Qinling fold belt; SCF, South China fold belt.

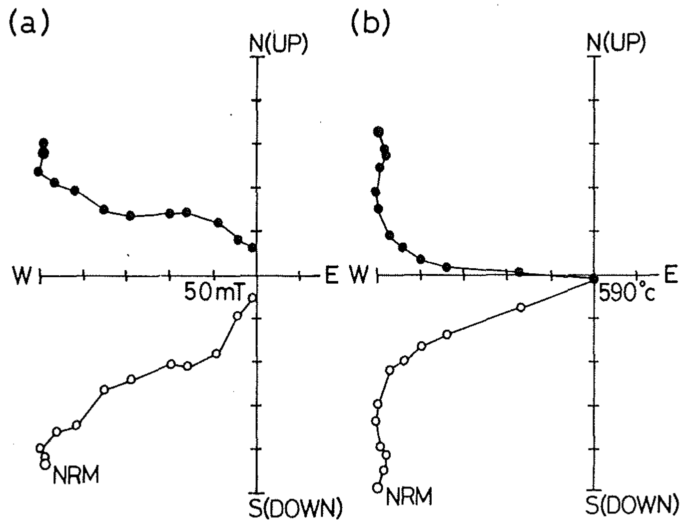

Fig.2 Vector plots of a), alternating magnetic field (AF) demagnetization method and b), thermal (TH) demagnetization treatment of samples (Middle Proterozoic dolomite) from Jingshan area. Open circles plotted on vertical planes and filled circles plotted on horizontal planes in geographic coordinates.

from 8.49×10^{-2} A/m (Quaternary sediment) to 1.48×10^{-4} A/m (Late Proterozoic sandy shale). Each characteristic component was obtained through thermal demagnetization treatment rather than alternating magnetic field demagnetization method (Fig.2). All the specimens were demagnetized

Table 1 Characteristic site-mean directions for Quaternary to Middle Proterozoic rocks in Wuchang and Jingshan of the South China block

Era	Period	Site	Sa	Sp	In situ				Tilt corrected				VGPs	
					Dec.	Inc.	k	α_{95}	Dec.	Inc.	k	α_{95}	Lat.(°N)	Long.(°E)
	Quaternary	1~12	12	12	-2.2	47.3	10.0	15.2	-2.2	47.3	10.0	15.2	86.7	328.4
Cenozoic	Tertiary	108	5	7	19.7	63.3	32.8	13.6	23.6	71.1	33.0	13.5	60.5	140.4
	Cretaceous	109	4	6	-167.3	-34.6	20.2	21.0	-168.5	-41.0	19.9	21.1	77.2	237.4
	Jurassic	019	5	10	4.1	47.8	11.3	20.9	1.5	-15.2	2.7	50.7		
Mesozoic	Triassic	105	5	8	-1.6	57.6	13.3	17.2	-84.1	0.8	2.9	42.8		
	Permian	106	5	9	-3.9	42.0	60.6	7.2	-96.9	-6.8	24.7	11.4		
		206	4	4	-3.7	54.6	55.2	16.8	10.9	11.1	64.6	15.5		
	Carboniferous	115	4	7	-5.5	48.0	85.5	7.3	-104.9	6.5	89.2	6.5		
	Devonian	107	5	5	11.9	36.4	48.8	13.3	-103.8	-22.8	48.5	13.3	17.8	199.8
	Silurian	103	4	7	8.9	56.8	92.1	7.0	-100.2	48.0	72.7	7.9		
	Ordovician	102	5	7	9.2	49.1	81.0	7.5	-75.1	55.0	58.2	8.9		
	late Cambrian	101	4	6	46.6	51.8	20.6	20.8	-134.9	67.3	38.5	15.0	0.6	86.1
Paleozoic	early Cambrian	112	5	8	-2.7	24.3	5.7	27.8	-43.2	30.9	5.3	30.9	48.2	13.0
		113	4	8	11.6	55.5	121.3	5.5	-69.2	75.5	51.7	8.5		
	late	111	4	6	-174.5	-33.6	122.7	11.2	135.3	-6.6	160.8	9.8	39.6	358.7
		211	5	7	13.7	46.6	131.3	5.9	27.8	42.1	106.0	6.5		
Proterozoic	middle	110	4	6	-71.4	15.5	26.5	15.1	-60.0	10.7	17.3	18.9	28.3	11.5

Sa is the number of samples per site, from which Sp, the number of specimens were measured. k is Fisher precision parameter of site-mean direction. α_{95} is radius of cone of 95% confidence on within-site and overall means. VGPs are virtual geomagnetic poles calculated for site-means after tilting corrections.

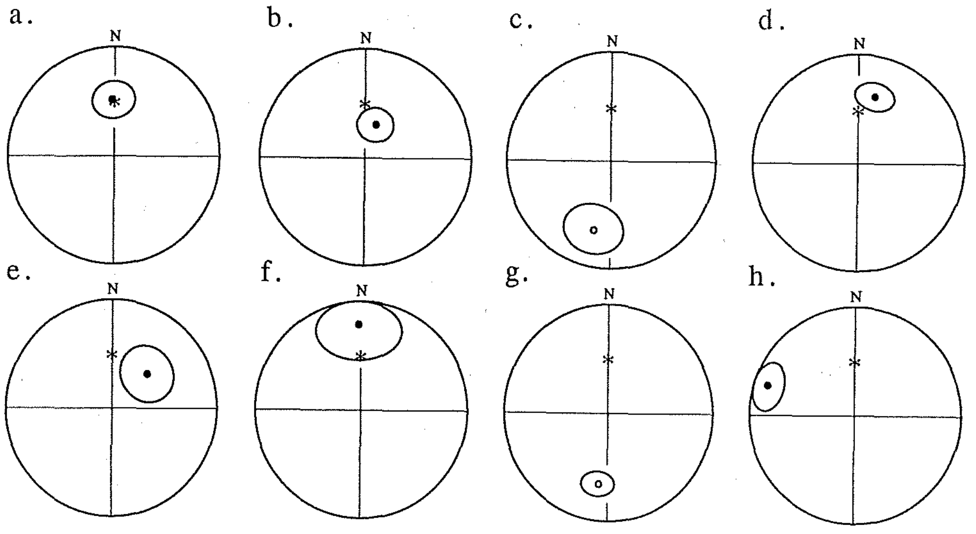

Fig.3 Site-mean characteristic directions before tilting corrections. Filled and open circles on lower and upper hemisphere, respectively, and ellipses are 95% confidence circles of equal-area projections. Asterisk symbol is the direction of the geocentric dipole field for sampling locality. a, Quaternary (Q); b, Tertiary (E); c, Cretaceous (K); d, Devonian (D); e, Late Cambrian (Cm); f, Early Cambrian (Z); g, Late Proterozoic (Pt_3); h, Middle Proterozoic (Pt_2).

through progressive thermal treatment and the characteristic component of remanent magnetization for each site was separated using multivariate technique of Kirschvink (1980). The site-mean paleomagnetic directions for thermally demagnetized results are shown in Table 1. The high temperature component was adopted for the site for rocks showing the characteristic multi-component because of little possibility of secondary viscous magnetization. The characteristic component for each site was accepted as reliable provided the following criteria were satisfied: a remanent magnetization is stable with respect to progressive thermal demagnetization and a site-mean direction before tilting correction is different from the direction of the geocentric dipole field, suggesting that the direction of remanent magnetization is not attributed at least to recent secondary magnetization.

Eight sites were found to have a reliable primary magnetic component through thermal demagnetization and selection using above mentioned criteria. Paleomagnetic directions of these sites before tilting correction are plotted with associated circles 95% confidence in Fig.3. These sites are from the formations of Quaternary (Q), Tertiary (E), Cretaceous (K), Devonian (D), Late Cambrian (Cm), Early Cambrian (Z), Late (Pt_3) and Middle Proterozoic (Pt_2). It is very significant that paleomagnetic data for Paleozoic and Proterozoic were successfully obtained from present study.

Virtual geomagnetic poles (VGPs) calculated from the data after tiling correction were shown in Fig.4. These pole positions were compared with those previously reported for the South China block. Kent et al. (1986) reported the Cretaceous paleomagnetic pole (80.8°N, 296.8°E, α_{95} =7.7°) from western Sichuan (26.5°N, 102.3°E) and another one (76.3°N, 172.6°E, α_{95}=10.3°) from Nanjing area (32°N, 119°E). These paleomagnetic poles were shown in Fig.4 by triangular symbols. Our Cretaceous pole position is located between the two poles of Kent et al. (1986) and is not significantly different at the 95% confidence level.

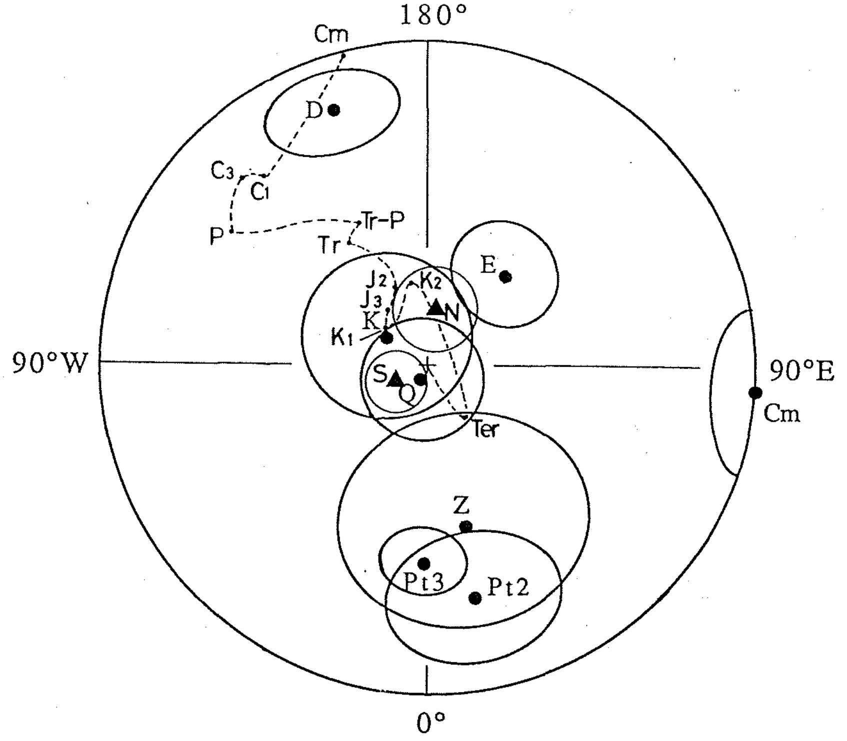

Fig.4 VGPs for the Quaternary to Middle Proterozoic rocks with associated circle of 95% confidence. Poles shown by triangular symbols are reported by Kent et al. (1986), N, Nanjing area; S, Western Sichuan. A dotted line is APW path for the South China block demonstrated by Lin et al. (1985). Ter, Tertiary; K_2, Upper Cretaceous; K_1, Lower Cretaceous; J_3, Upper Jurassic; J_2, Middle Jurassic; Tr, Triassic; P, Permian; C_3, Upper Carboniferous; C_1, Lower Carboniferous; Cm, Cambrian.

Lin et al. (1985) demonstrated the Phanerozoic polar wander path for the South China block from paleomagnetic of several formations in Zhejing, Guizhou, Yunnan and Hubei provinces. The polar wander curve was described in Fig.4 by a dotted line. The paleomagnetic pole for Cretaceous rocks we obtained for Hubei province (77.2°N, 237.4°, α_{95}=21.1°) agrees well with lower Cretaceous one (76.2°N, 225.7°, α_{95}=4.8°) of Lin et al. (1985). A shape of APW path since Devonian from present study is similar to that of Lin et al.(1985). The inconsistency on the Cambrian pole position may have been caused by that Jingshan area had been subjected to the tectonic deformation by Qinling orogenic movement because Jingshan is close to the Qinling orogenic belt.

REFERENCES

Chan, L.S., C.Y.Wang and X.Y.Wu (1984) *Geophys.Res.Lett.*, **11**, No.11, 1157.

Kent, D.V., G.Xu, K.Huang, W.Y.Zhang and N.D.Opdyke (1986) *Earth Planet.Sci.Lett.*, **79**, 179.

Kirschvink, J.L. (1980) *Geophys.J.R.astr.Soc.*, **62**, 699.

Liou, J.G., X.Wang and R.G.Coleman (1989) *Tectonics*, **8**, No.3, 609.

Lin, J.L., M.Fuller and W.Y.Zhang (1985) *Nature*, **313**, No.7, 444.

McElhinny, M.W., B.J.J.Embleton, X.H.Ma and Z.K.Zhang (1981) *Nature*, **293**, No.17, 212.

Zhang, Z.M., J.G.Liou and R.G.Coleman (1984) *Bull.Geol.Soc.Am.*, **95**, 295.

(To be submitted to Nature.)

NATURAL REMANENT MAGNETIZATION OF SOME ROCKS FROM SURTHERN SRI LANKA

Minoru FUNAKI[1], Masaru YOSHIDA[2] and P.W. VITANAGE[3]

1: National Institute of Polar Research, 9-10, Kaga 1-chome Itabashi-ku, Tokyo 173, Japan
2: Department of Geosciences, Osaka City University,3-138 sugimoto 3-chome, Sugiyoshi-ku, Osaka 558, Japan
3: Department of Geology, University of Peradeniya, Peradeniya, Sri Lanka

1. Introduction

Recently geological and geochronological knowledges of Sri Lanka have been accumurated in focused on reconstruction with East Antarctica. The general reconstruction model has been proposed that Sri Lanka was situated in Gondwana in the offing of Lützow-Holm Bay connected with the east Gunners Bank in Enderby Land, East Antarctica (e.g. Collerson and Sheraton, 1986: Yoshida and Funaki, 1987). Structural, petrological and metamorphic grade are similar between the Highland Group of Sri Lanka and the granulite facies portion of Lutzow-Holm Complex and between the eastern Vijayan Complex of Sri Lanka and the Yamato Belgica Complex of eastern Queen Maud Land (Yoshida and Funaki, 1987). This model is also supported by the geochronological evidences (e.g. Grew and Manton, 1979).

However, very poor paleomagnetic study has been done for Sri Lanka up to present. Funaki et al. (1989) carried out paleomagnetic reconnaissance of Precambrian and Jurassic rocks of Sri Lanka using the samples collected for geological studies. The results indicated that the dominant NRM directions of the Highland Group form two clusters at I=61.2°, D=260.4°, α_{95}=5.8° (cluster A) and I=68.7°, D=349.0° and α_{95}=6.9°(cluster B). Many samples of the Vijayan Complex showed relative low inclination without clear cluster around the present geomagnetic field direction of Sri Lanka. Jurassic dolerite dyke rocks showed the mean NRM direction of I=24.6°, D=67.5° and α_{95}=24.6° (cluster C), although number of sample was only 2.

The VGP positions obtained from the cluster A (latitude (Lat)=2.3°N, longitude (Lon)=34.1°E) and cluster C (Lat=24.0°N, Lon=159.5°E) were consistent with those of Cambro-Ordovician and Jurassic VGPs from East Antarctica after rotation of Sri Lanka based on the model proposed by Barron et al.,1978.

We obtained a total of 95 paleomagnetic samples from southern Sri Lanka. The rock types are granite (Tonigala granite) and granitic rock from Tonigala region, dolerite, biotite gneiss and pegmatite from Gallodai region, granite (pink granite) and migmatite from Kandy region, charnockite from Mahiyangaran region and gneissose granite and hornblende gneiss from Ambarangoda region. The samples of biotite gneiss were collected systematically taking distance into consideration of the dolerite dike at Gallodai region.

2. Basic magnetic properties

Representative 3 samples from each formation were selected for AF demagnetization test up to 50mT. The stable NRM components were recognized in Tonigala granite, pink granite, Gallodai dolerite, migmatite, gneissose granite, pegmatite and biotite gneiss. The samples of hornblende gneiss have either stable NRM or unstable one. However only unstable NRM was recognized for charnockite and granitic rock from Tonigala region. Figure 1 shows Zjiderveld projection of Gallodai dolerite, having a larger soft magnetic component, which is demagnetized completely up to 20mT, associated with the hard NRM component. The optimum demagnetized field intensities were decided

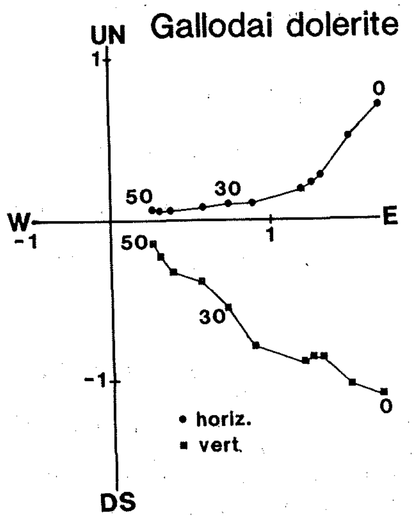

Fig. 1
AF demagnetization of Gallodai dolerite.

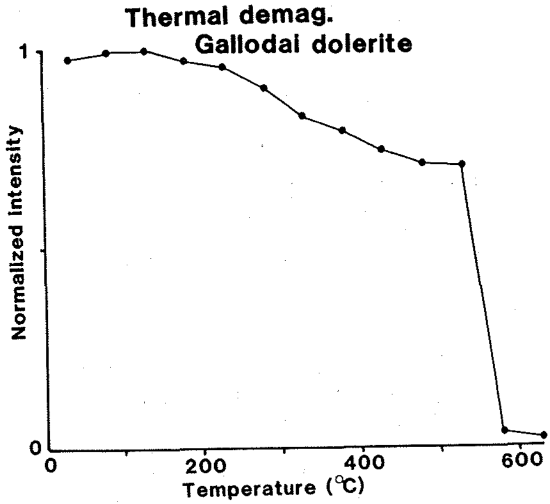

Fig. 2
Thermal demagnetization of Gallodai dolerite.

to 30mT for every sample, except 35mT for pink granite, based on the results of the Zjiderveld projections.

Thermal demagnetization test was carried out for the samples to have stable NRM components in air from room temperature to 630°C at intervals of 50°C. The samples were supplied after being AF demagnetized to the optimum field. Unblocking temperatures (TBs) of NRM were observed between 530° and 580°C for Tonigala and pink granites, although demagnetization curves were zigzag compared with those of the AF demagnetization. The unstable magnetization is estimated due to oxidation of magnetic minerals and breaking off of small parts of the samples during heat treatments. A clearly defined TBs of NRM were obtained at 580°C and 330°C for Gallodai dolerite, as shown in Fig. 2. They are the TBs of the hard NRM component, because the sample was already AF demagnetized to 30mT. Significant directional change of NRM was not observed before and after the TB at 330°C. The TBs of NRM for gneiss rocks and migmatite were distributed between 330° to 580°C, although it is occasionally different TBs among same formations.

Thermomagnetic (Js-T) curves of the 1st and the 2nd run cycles in Fig. 3 were obtained for the samples of Tonigala granite, pink granite and Gallodai dolerite from room temperature to 650°C by a magnetic balance under 0.4T external magnetic field in 10^{-2}Pa atmosphere. The Js-T curves of Tonigala granite is completely reversible with Curie point at 580°C indicating single phase of almost pure magnetite. By the microscopical observation, magnetite grains smaller than 200μm in diameter were observed in the sample. That of pink granite is irreversible in the 1st run cycle; magnetization increases after the cooling maintaining same Curie point. This phenomenon suggests that small amount of magnetite was produced by the heating. In this sample magnetite grains smaller than 250μm in diameter with ilmenite exolutions were observed by the microscope. Very small amount of hematite was observed along the grain boundary and cracks of the magnetite grains. The increased magnetization after the 1st run cycle is caused by reduction of this hematite. The samples of Gallodai dolerite showed irreversible Js-T Curves having Curie point at 575°C in the 1st run cycle. After the cycle the magnetization decreased about 83% compared with original one. The 2nd run is

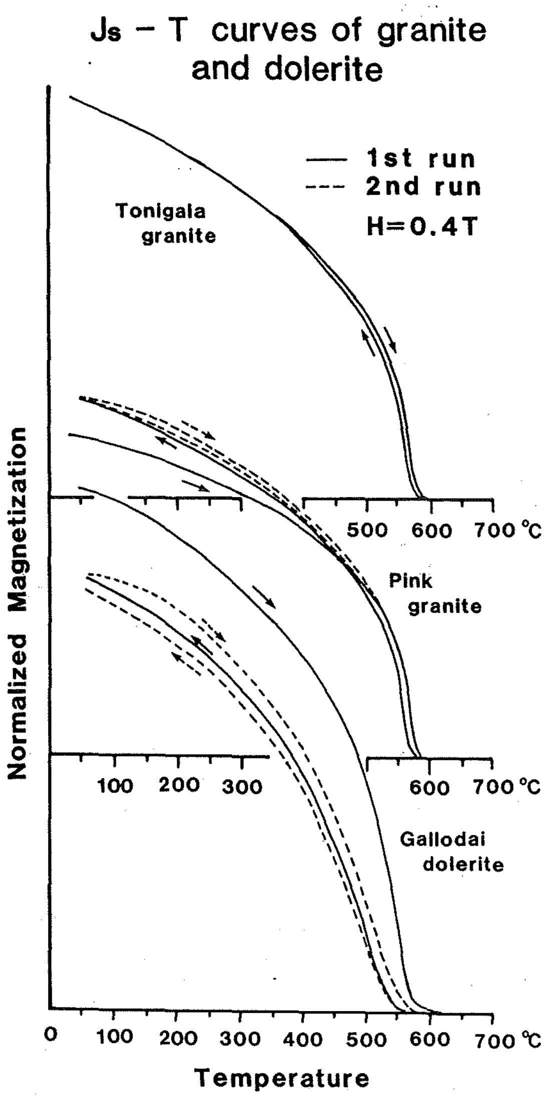

Fig. 3.
Thermomagnetic curves of Tonigala granite, pink granite and Gallodai dolerite. solid lines: the 1st run cycle, dotted line: the 2nd run cycle.

reversible and consistent with the 1st run cooling curve, maintaining same Curie point. Microscopical observation suggested that the magnetic grains smaller than 100μm in diameter were heavily oxidized; maghemite and/or titanomaghemite veins were spread into the magnetite grains.

3. NRM direction

Every sample having stable NRM components was AF demagnetized by 3 steps; the respective optimum field and both of lower and higher 5mT than that field. When α_{95} showed the minimum value, mean NRM directions were adopted for representative NRM direction of its formation. Reasonably good clusters were obtained from Tonigala granite, pink granite and Gallodai dolerite. The mean NRM intensity (R), inclination (I), declination (D), precision (K) and α_{95} are listed in Table 1 and NRM directions with α_{95} values are illustrated in Fig. 4. The NRM directions of hornblende gneiss and gneissose granite clustered unclearly around the present geomagnetic field direction at present Sri Lanka, probably resulting VRM. Biotite gneiss

NRM distributions after AF demag. to 30 or 35mT

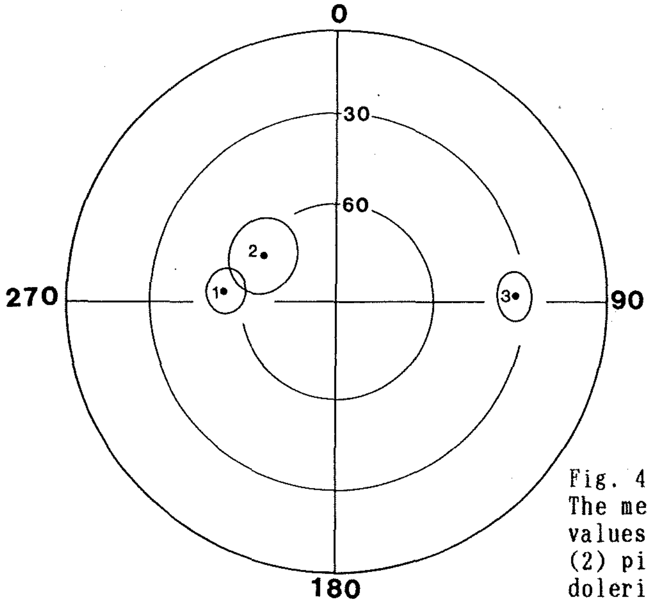

Fig. 4
The mean NRM directions and α_{95} values of (1) Tonigala granite, (2) pink granite and (3) Gallodai dolerite.

and pegmatite within 10m from the dolerite dyke showed almost parallel NRM direction to that of dolerite dyke. It may suggest that biotite gneiss was remagnetized by heating of the dyke intrusion. However, the NRM directions of migmatite scattered widely through the both hemisphere, although individual samples have stable NRM components.

4. Discussion

Tonigala granite has almost pure magnetite grains estimated from the Js-T curves. Since its NRM is very stable against AF and thermal demagnetization, the NRM is believable paleomagnetically. The NRM of pink granite is also stable, but a part of the magnetite grains were oxidized to hematite. Hematite may be produced by the weathering in present judging from its formation on the garins. As the amount of hematite is very small compared with magnetite, the original NRM may not be so disturbed by the hematite magnetization. On the other hand, a part of the NRM of Gallodai dolerite is carried by maghemite and/or titanomaghemite, associated with the magnetization resulting magnetiet. Biotite gneiss remagnetized evidently by the dolerite intrusion showed the NRM direction toward that of Gallodai dolerite. It indicates that the NRM direction of Gallodai dolerite did not be disturbed by the formation of maghemite and/or titanomaghemite. From these estimations the NRM of Tonigala granite, pink granite and Gallodai dolerite can be believed.

Geochronological ages have been obtained from Tonigala granite (for instance 986±28ma by Rb/St of total rock (Crawford and Oliver, 1969) and 558±14ma by U/Pb of zircon (Hölzl and Köhler, 1987)). The ages may indicate the times intruded at middle Proterozoic and metamorphosed at Cambrian respectively. A Cambrian age (580±7ma; U/Pb in zircon) has been reported from a similar rock with pink granite around Kandy region (Kroner et al., 1987). Many data from 460 to 520ma (late Cambrian to middle Ordovician) by Rb/Sr age have been reported from whole Sri Lanka. Since the age determined by U/Pb method shows older age than that of Rb/Sr one generally, it can be

Table 1. Paleomagnetic results of Sri Lanka and some previous results for East Antarctica

No	site	dem	N	I	D	K	α_{95}	Lat	Lon	Lat*	Lon*
1	Tonigala	0	13	31.6	230.3	10	18.5				
	granite	30		55.5	275.2	45	6.2	6.1S	28.0E	10.7S	21.6E
2	pink	0	13	40.9	358.9	3	33.5				
	granite	35		63.8	301.9	15	11.0	27.1N	38.5E	23.2S	55.5E
3	Gallodai	0	17	31.2	74.7	7	14.5				
	dolerite	30		33.6	88.3	32	6.4	8.5N	152.9E	45.2S	152.0W
4	biotite	0	5	34.3	151.3	2	73.5				
	gneiss	30		17.7	76.2	45	11.5	14.7N	162.9E	35.8S	160.9W
5	Ongul I.	10	80	59.1	336.8	14	4.5	20.2S	20.7E		
6	Wright V.	15	26	-69.4	237.6	137	2.4	45.3S	152.0W		

* after rotation: rotation Lat=5.3°S, Lon=23.8°E and ω=-100.5

understood that wide areas of Sri Lanka were metamorphosed at late Cambrian to middle Ordovician. These areas might be magnetized or remagnetized at that period.

The NRM directions of Tonigala and pink granites were consistent each other taking their α_{95} values into consideration. In the paleomagnetic reconnaissance of Sri Lanka (Funaki et al., 1989), the NRM directions of many granites and gneisses showed (Cluster A) toward the same directions to these granites in this study. Therefore it seems that they were acquired NRM at almost same time. However, as the age of Tonigala granite (Hölzl and Köhler, 1987) was determined directly using the samples which are collected from a same outcrop for our sampling site, the paleomagnetic data of Tonigala granite is adopted for the representative data of late Cambrian to middle Ordovician of Sri Lanka in this study.

Age of Gallodai dolerite has been reported as 152.6±7.6 and 143.3±7.2ma by K/Ar of total rock by Yoshida et al., 1989. It indicated that the dolerite was magnetized at the latest Jurassic or the earliest Triassic. The NRM direction I=33.6°, D=88.3° and α_{95}=6.4° is essentially consistent with the previous result of Gallodai dolerite (I=24.6°, D=67.5° and α_{95}=21.7°).

Funaki and Wasilewski (1986) reported a VGP position of hornblende gneiss, amphibolite and granite from Ongul Island in Lützow-Holm Bay as Lat=20.2°S, Lon=20.7°E and α_{95}=4.5°. These rocks were estimated to be remagnetized or intruded at Cambro-Ordovician. On the other hand, many Jurassic VGP positions have been reported from Ferrar dolerite along the Transantarctic Mountains. One of them is Lat=45.3°S, Lon=152.0°W and α_{95}=2.4° for Wright Valley (Funaki, 1983). Sri Lanka has been estimated to be a Gondwana fragment connected with Lützow-Holm Bay (e.g. Barron et al., 1978). Therefore the reconstruction of Sri Lanka and Lützow-Holm Bay is available using the Cambrian to Ordovician VGP positions from Tonigala granite and Ongul Island, and Jurassic ones from Gallodai dolerite and Ferrar dolerite.

The VGP positions calculated from Tonigala and pink granites and Gallodai dolerite were rotated with respect to East Antarctica referred a rotation point Lat=5.3°S Lon=23.8°E and an angle (ω)=-100.5° (counterclockwise). The rotation point and ω were determined by fitting VGPs of Tonigala granite and Ongul Island and those of Gallodai dolerite and Ferrar dolerite. The latitude and longitude of the VGPs after the rotation are listed in Table 1. When Sri Lanka is rotated according to that rotation, it situates at offing of eastern Queen Maud Land. This result supports the hypothesis that Sri Lanka connected to the east Gunners Bank in Lützow-Holm Bay taking their α_{95} value consideration. Figure 5 shows a plausible reconstruction models of Lützow-Holm Bay and Sri Lanka based on the declination of NRM and its 95% probability for Tonigala granite and the

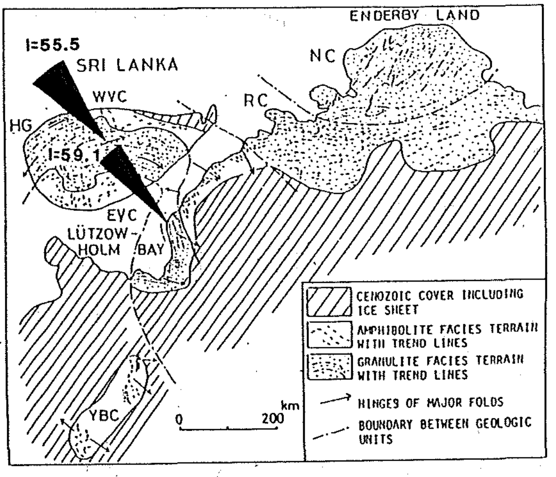

Fig. 5
A plausible reconstruction modle for Sri Lanka and Lützow-Holm Bay proposed by NRM directions of Tonigala granite and Ongul Island.

result of Ongul Island; Sri Lanka is rotated to Lützow-Holm Bay adjusting the declination of Tonigala granite to that of Ongul Island. The NRM inclinations of Tonigala granite and Ongul Island are consistent each other, as I=56.8° and I=59.1° respectively, suggesting higher possibility of this reconstruction model. This model has no discrepancy with recent reconstruction models being considered by geology, geochronology, and 2000m isobath.

5. Conclusions

Tonigala and pink granite have stable NRM carried by magnetite, and the stable NRM was magnetized at late Cambrian to middle Ordovician. Gallodai dolerite was magnetized at late Jurassic, although magnetic minerals (low titanium titanomagnetite) have been oxidized partially. These results are consistent with previous paleomagnetic study for Sri Lanka. Biotite gneiss along Gallodai dolerite was remagnetized by the dolerite intrusion at late Jurassic. However other gneiss, migmatite and pegmatite did not make a significant cluster of NRM directions.

Sri Lanka was rotated to East Antarctica referred VGPs of Tonigala granite, Gallodai dolerite, Ongul Island and Ferrar dolerite. Consequently, Sri Lanka is situated at offing of eastern Queen Maud Land including Lützow-Holm Bay. The most reliable reconstruction of Sri Lanka and Lützow-Holm Bay was proposed based on the NRM directions.

References

Barron, E.J., Harrison, C.G.A. and Hay, W.W.(1978): Ame. Geophys. Union, Trans. 59(5),436-449.

Collerson, K.D. and Sheraton, J.W. (1986): In J. Pickard (Editor), Antarctic Oasis, Academic Press, Sydny, pp21-62.

Hölzl, S. and Köhler, H. (1987): Abstract, Geol. Survey Dep. of Sri Lanak, Spec. Publ. IGCP 236.

Funaki, M., Yoshida, M. and Vitanage, P.W. (1989): Geological Journal of Sri Lanka. in contribute.

Grew, E.S.and Manton, W.I. (1979): Science, 206,443-444.

Kröner, A., Williams, I.S., Compton, W., Baur, N., Vitanage, P.W. and Perera, L.R.K. (1987): J. Geol., 95,775-791.

Yoshida, M. and Funaki, M. (1987): Abstract, Geol. Survey Dep. of Sri Lanka, Spec. Publ. IGCP 236.

Yoshida, M., Funaki, M. and Vitanage, P.W. (1989): J. Geol. Soc. of India, 33(1), 71-75.

Rock Magnetism and Paleogeophysics

Permuted Index for Volumes 1-16

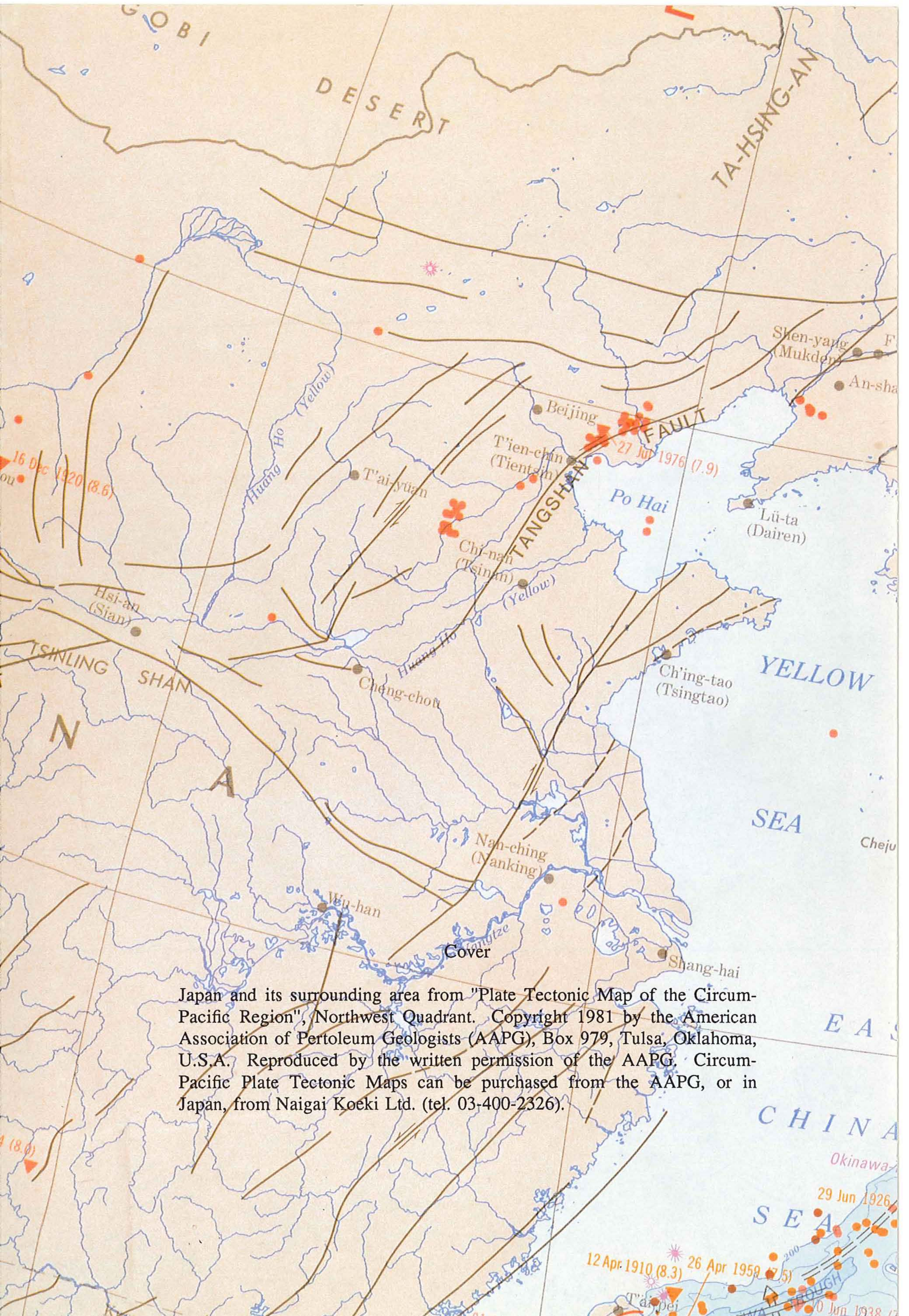

Cover

Japan and its surrounding area from "Plate Tectonic Map of the Circum-Pacific Region", Northwest Quadrant. Copyright 1981 by the American Association of Pertoleum Geologists (AAPG), Box 979, Tulsa, Oklahoma, U.S.A. Reproduced by the written permission of the AAPG. Circum-Pacific Plate Tectonic Maps can be purchased from the AAPG, or in Japan, from Naigai Koeki Ltd. (tel. 03-400-2326).